Electrochemistry of Hemoglobin I from *Lucina pectinata* immobilized on a modified gold electrode with cysteine or 3-mercaptopropionic acid: Electrochemical activity for hydrogen sulfide

By

Mario E. Ortega Núñez

A dissertation submitted in partial fulfillment of the requirements for the degree of
DOCTOR OF PHILOSOPHY
In
Applied Chemistry
(Biophysics)

UNIVERSITY OF PUERTO RICO
MAYAGÜEZ CAMPUS
2012

Approved by:

Mayra E. Cádiz, PhD. Member, Graduate Committee	Date
Rolando Tremont, PhD. Member, Graduate Committee	Date
Juan López Garriga, PhD. Member, Graduate Committee	Date
Carmen Vega Olivencia, PhD President, Graduate Committee	Date
Nilda E. Aponte, PhD. Representative, Graduate Studies	Date
René Vieta, PhD. Chairperson, Chemistry Department	Date

ABSTRACT

The extraordinary affinity of recombinant hemoglobin I from *Lucina pectinata* (rHbI) for hydrogen sulfide (H_2S) allow to postulate it as substrate for the preparation of the hydrogen sulfide sensors. The modification of a gold surface with recombinant hemoglobin I, electrochemical characterization of H_2S and electrochemical kinetics parameters were reported. The first sensor model was prepared using cysteine. This system allowed studying how the protein was immobilized on the gold surface and its response to H_2S. The second sensor model, using 3-MPA, was an exploration of another linker to try to improve the robustness of the sensor signal in the quantification of H_2S. This model provided information about the electrokinetic and electrochemical parameters of the hemoglobin, as well as their response to H_2S. Cyclic Voltammetry (CV) and X-ray photoelectron spectroscopy (XPS) were employed to characterize the electrodes modification process, while FTIR was used to verify the presence of hemoglobin on the surface. In CV a pair of well-defined redox peaks for rHbIFe(III)–rHbIFe(II) at 0.213 V (with Cys) and 0.190 V (with 3-MPA) vs. Ag/AgCl were obtained. Electrochemical parameters of immobilized hemoglobin I as formal potential ($E^{o'}$), charge transfer coefficient (α) and apparent heterogeneous electron transfer rate constant (k_s) were estimated by cyclic voltammetry data. The high-resolution XPS from S2p and C1s regions provide further evidence that cysteine and 3-mercaptopropionic acid are adsorbed to gold surface. Also, it confirms the presence of nickel ion in the Ni2p region when the monolayer Lnk/Au is treated with the solution of $NiCl_2$. The electrochemical response of rHbI-electrode in presence of hydrogen sulfide (H_2S) was studied, obtaining changes in oxidation and reduction current peaks from

the voltammograms. The amperometric response of the rHbI-(Cys)-electrode to H_2S was linear in the range from 90 to 400 nM (n = 7, r^2 = 0.993), while rHbI-(3-MPA)-electrode was linear from 40 to 600 nM with a correlation coefficient of 0.998 (n = 16). This method provides an alternative procedure of surface modification for immobilization of histidine-tag proteins or enzymes for sensors preparation.

RESUMEN

La extraordinaria afinidad de la hemoglobina I *Lucina pectinata* (rHbI) por el sulfuro de hidrógeno (H_2S) permite postularla como sustrato adecuado para la preparación de sensores de H_2S. En este trabajo se reporta la modificación de una superficie de oro con la hemoglobina I recombinante, la caracterización electroquímica de H_2S, así como los parámetros electrocinéticos de la proteína. El primer modelo de sensor se preparó usando cisteína. Este sistema permitió estudiar cómo la proteína se inmoviliza sobre la superficie de oro y su respuesta a H_2S. El segundo modelo de sensor, usando 3-MPA, fue una exploración de otro "linker" para tratar de mejorar la robustez de la señal del sensor en la cuantificación de H_2S. Este modelo proporcionó información acerca de los parámetros electrocinéticos y electroquímicos de la hemoglobina I, así como su respuesta a sulfuro de hidrógeno. Voltametría cíclica (CV) y espectroscopia de rayos X de fotoelectrones (XPS) se emplearon para caracterizar el proceso de modificación de electrodos, mientras que FTIR se utilizó para verificar la presencia de hemoglobina en la superficie. Por voltametria cíclica se pudo observar un par de picos redox bien definidos para rHbIFe (III)-rHbIFe (II) a 0,213 V (con Cys) y 0,190 V (con 3-MPA) vs Ag/AgCl. Los parámetros electroquímicos de hemoglobina I inmovilizada como el potencial formal ($E^{o'}$), coeficiente de transferencia de carga (α) y la constante heterogénea de transferencia electrónica aparente (k_s) se estimaron con datos obtenidos de la voltametría cíclica. Los espectros XPS de alta resolución en las regiones S2p y C1s proporcionaron evidencia adicional de que la cisteína y el ácido 3-mercaptopropiónico se adsorben a la superficie de oro. Además, se confirma la presencia de iones de níquel en la región Ni2p cuando la monocapa Lnk/Au se trata con la

solución de $NiCl_2$. La respuesta electroquímica del electrodo de rHbI en presencia de sulfuro de hidrógeno (H_2S) se estudió, obteniéndose cambios en las corrientes de los picos de oxidación y de reducción en los voltamogramas. La respuesta amperométrica hacia H_2S del rHbI-(Cys)-electrodo fue lineal en el intervalo de 90 a 400 nM (n = 7, r^2 = 0,993), mientras que el rHbI-(3-MPA)-electrodo fue lineal de 40 a 600 nM con un coeficiente de correlación de 0,998 (n = 16). Este método proporciona un procedimiento alternativo de modificación de superficies metálicas para la inmovilización de proteínas o enzimas "histidine-tag" para la preparación de sensores.

To *Mateo*

ACKNOWLEDGEMENTS

It is so hard to express in these lines the infinite gratitude to all those who contributed to the completion of this work. Among all these people, I would like to thank Dr. Carmen Vega for being the guide in my doctoral formation, for your friendship and your unconditional support, for showing me another side of the sciences. Similarly I want to thank Dr. Juan Lopez Garriga for being the core of this work, for his vision, his philosophies, friendship and help. Dr. Mayra Cadiz for taking the time and be available when it was necessary. I would like to thank Dr. Rolando Tremont and Dr. Rosa Brito for being unconditionals, for the friendship and help in all aspects throughout this process. I also would like to thank Ángel Antonio, Ingrid, Tamara and Ramonita for being there and supporting me at all times. I would like to acknowledge my labs partners and the people from Science on Wheels for giving me the opportunity to improve as a scientist and as a teacher. Also, all those who work administratively in the Department of Chemistry and the majority of teachers; apart from the academic relationship, now I can tell we have develop a friendship. I would like to acknowledge Dr. Carlos Cabrera and his excellent laboratory group at UPR Rio Piedras for allowing me perform most of the analyzes and make time for it..

The National Science Foundation (MCB-0843608) is acknowledged for the financial support in part to this work.

Table of Contents

List of Symbols and Abbreviations

3-MPA	3-mercaptopropionic acid
3MST	3-mercaptopyruvate sulfurtransferase
AD	Alzheimer's disease
ATR	Attenuated total reflectance
CBS	Cystathionine β-synthase
CD	Circular dichroism
CNS	Central Nervous System
CNT	Carbon nanotubes
CSE	Cystathionine γ-lyase
CV	Cyclic voltammetry
Cys	Cysteine
DEPD	Diethyl-p-phenylenediamine
FTIR	Fourier Transform Infrared Spectroscopy
H_2S	Hydrogen sulfide
Hb	Hemoglobin
HbI	*Lucina pectinata* Hemoglobin I
HbII	*Lucina pectinata* Hemoglobin II
HbIII	*Lucina pectinata* Hemoglobin III
HbO_2	Oxy hemoglobin
His	Histidine
HRP	Horseradish peroxidase

k_{off}	Kinetic rate constant for dissociation
k_{on}	Kinetic rate constant for association
L. pectinata	*Lucina pectinata*
Lnk	Linker
LSV	Linear sweep voltammetry
Mb	Myoglobin
MPTP	1-methyl-4-phenyl-1,2,3,6-tetrahydropyridine
NHE	Normal hydrogen electrode
NMDA	N-methyl-D-aspartate
NO	Nitric oxide
NTA	Nitriloacetic acid
PG	Pyrolytic graphite
PS	Polystyrene
rHbI	Recombinant Hemoglobin I
SAM	Self-assembled monolayer
SEM	Scanning electron microscopy
TCA	Trichloroacetic acid
XPS	X-ray photoelectron spectroscopy

List of Figures

List of Tables

1. INTRODUCTION

1.1. Motivation

Hydrogen sulfide is considered a broad-spectrum poison, meaning that it can poison several different systems in the body, although the nervous system is most affected. The toxicity of H_2S is comparable with that of hydrogen cyanide; it forms a complex bond with iron in the mitochondrial cytochrome c enzymes, thereby blocking oxygen from binding and stopping cellular respiration (Nicholls & Kim, 1982). It acts as a vasodilator and is also active in the brain, where it increases the response of the N-methyl-D-aspartate (NMDA) and facilitates long term potentiation, which is involved in the formation of memory, acting as neuromodulator and neuroprotector smooth muscle relaxant (Whiteman *et al.*, 2004; Kimura *et al.*, 2005; Benavides *et al.,* 2007; Kabil *et al.*, 2010).

Current evidence suggests that under physiological conditions, H_2S plays a role in promoting cell survival directly by its neuroprotective effects on both neurons and glia in the Central Nervous System (CNS) (Warencya *et al.*, 1989). Combining the fact that H_2S has a short half life and that most molecules activated or inhibited by H_2S are messenger molecules or ion channels, it suggests a primary messenger i.e. 'switch' role in the CNS to activate downstream molecules that would propagate the action of H_2S post-decay (Tan *et al.*, 2010). This gas is produced endogenously in various parts of the body such as the heart (Geng *et al.*, 2004), blood (*Zhao et al.*, 2001) and the central nervous system (CNS); (Warenycia *et al.*, 1989). The endogenous production of H_2S in the human body is controlled by two pyridoxal-5'-phosphate (PLP)-dependent enzymes, namely cystathionine β-synthase (CBS) (Fig. 1.1A) and cystathionine γ-lyase (CSE) (Fig. 1.1B) (Erickson *et al.*, 1990; Griffith, 1987; Stipanuk and Beck, 1982; Swaroop *et al.*, 1992; Sun *et al.,* 2009) and

a new identified enzyme, 3-mercaptopyruvate sulfurtransferase (3MST) (Fig. 1.1C) (Shibuya *et al.*, 2009; Kalberg *et al.,* 2010). In the CNS, CBS was found highly expressed in the hippocampus and the cerebellum (Abe and Kimura, 1996). CBS is mainly localized to astrocytes (Enokido *et al.*, 2005; Ichinohe *et al.*, 2005) and microglial cells (Hu *et al.*, 2007). CSE is mainly expressed in cardiovascular system, but was also found in microglial cells (Lee *et al.*, 2006), spinal cord (Distrutti *et al.*, 2006) and cerebellar granule neurons (Garcia-Bereguiain *et al.*, 2008). 3MST is localized in neurons (Shibuya *et al.*, 2009). By comparing the production of H_2S in different brain cells, Lee *et al.* found that H_2S production in astrocytes is 7.9-fold higher than in cultured microglial cells, 9.7-fold higher than in NT-2 cells and 11.5-fold higher than in SH-SY5Y cells (Lee *et al.*, 2009). These data suggest that astrocytes may be the main brain cells to produce H_2S.

That is why H_2S has been extensively studied in the evolution of nervous diseases. The levels of H_2S are severely decreased in the brains of Alzheimer's disease (AD) patients compared with the brains of the age matched normal individuals. Previous findings showed that S-adenosyl-l-methionine, a CBS activator, is much reduced in AD brain and that homocysteine accumulates in the serum of AD patients. These observations suggest that CBS activity is reduced in AD brains and the decrease in H_2S may be involved in some aspects of the cognitive decline in AD (Eto *et al.*, 2002). In Parkinson's disease, testing on mouse model of Parkinson's disease induced by the neurotoxin 1-methyl-4-phenyl-1,2,3,6-tetrahydropyridine (MPTP), showed that inhaled H_2S prevent neurodegeneration via upregulation of antioxidant defense mechanisms and inhibition of inflammation and apoptosis in the brain (Kida *et al.,* 2011)

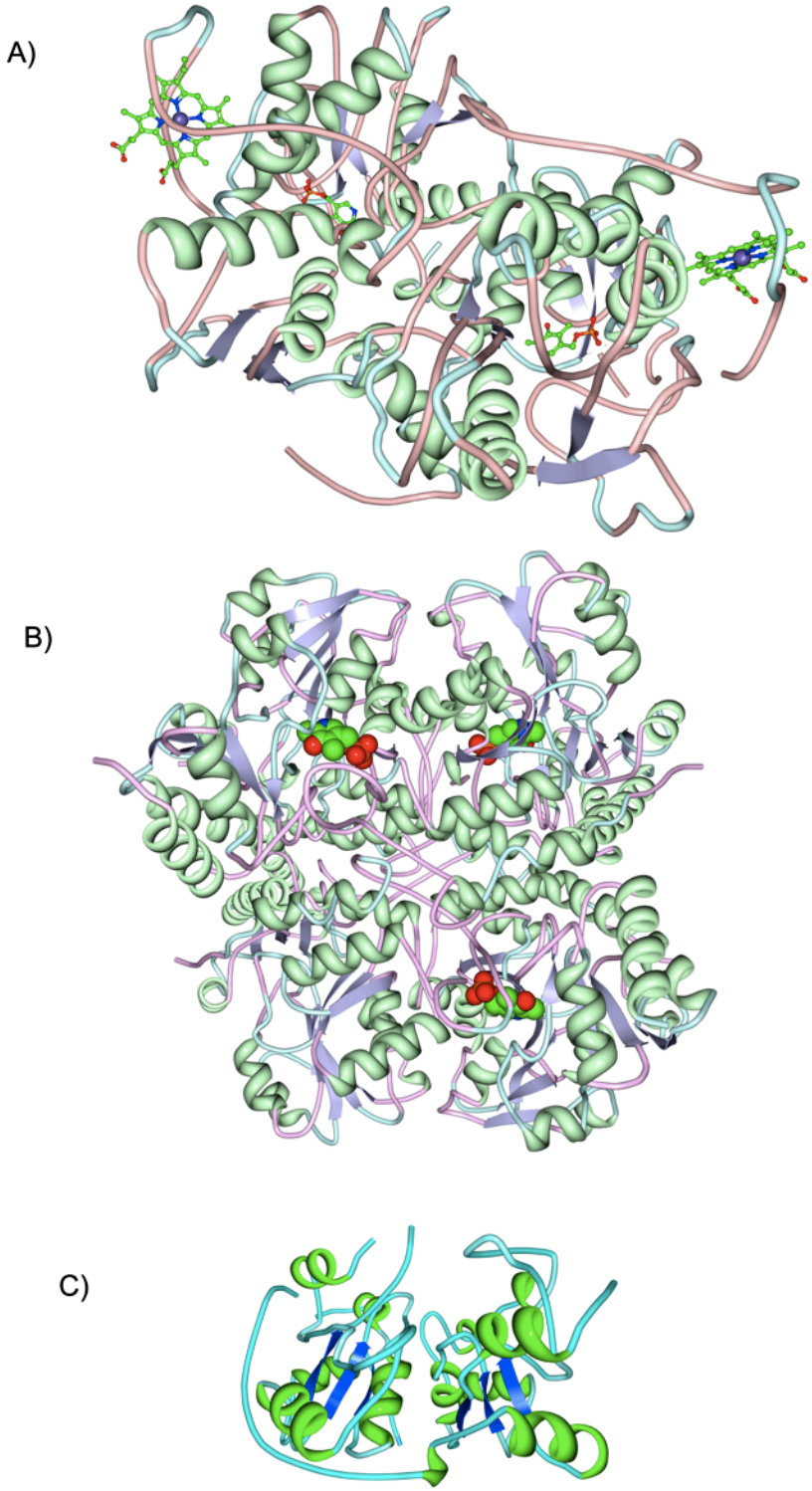

Figure 1.1. Two pyridoxal-5'-phosphate (PLP)-dependent enzymes A) cystathionine β-synthase (PDB ID: 1M54), B) cystathionine γ-lyase (PDB ID: 2NMP), and C) 3-mercaptopyruvate sulfurtransferase (PDB ID: 3OLH).

Additionally, H_2S has been attributed the property of inducing hibernation. It has been demonstrated that mice can be put into a state of suspended animation by applying a low dosage of hydrogen sulfide (80 ppm H_2S) in the air. The mice survived this procedure for 6 hours and afterwards showed no negative health consequences. If the H_2S-induced hibernation can be made to work in humans, it could be useful in the emergency management of severely injured patients, and in the conservation of donated organs Hydrogen sulfide binds to cytochrome oxidase and thereby prevents oxygen from binding, which apparently leads to the dramatic slowdown of metabolism. Animals and humans naturally produce some hydrogen sulfide in their body; it has been proposed that this gas is used to regulate metabolic activity and body temperature, which would explain the above findings (Roth, 2007).

For all the above, the detection of hydrogen sulfide has gained significant importance within analytical and biomedical communities. Many techniques such as Chronoamperometry (Lawrence *et al.*, 2004; Doeller *et al.,* 2005), UV-vis (Hawkins *et al.*, 1998; Rodríguez *et al.*, 2002; Niranjan *et al.*, 2002; Bouzaza *et al.*, 2004; Wallace *et al.*, 2007), Fluorescence (Wolfbeis *et al.*, 1987; Choi *et al.*, 1997; Choi *et al.*, 2003; Bramanti *et al.*, 2006; Blunden *et al.*, 2008; Xu *et al.*, 2010; Strianese *et al.*, 2011), Ion Chromatography (Ubuka *et al.*, 2001), Capillary Electrophoresis (Font *et al.*, 1996), Inductively Coupled Plasma (Colón *et al.*, 2008), GC-Chromatography (Tangerman *et al.*, 2009), and others not less important, have been commonly used for its analysis (Pandey *et al.*, 2012). Some of these methods and techniques reported variable concentrations of H_2S on the same biological samples due to the lack of standardization of methods between laboratories (Whiteman *et al*., 2011). Moreover, it is difficult to get them sufficiently stable for exposing them directly to real samples due to decomposition of electroactive substances

or instability of the formed complexes (short time of life) and fouling of the electrode surface and slow removal of substrates from the surface.

The high affinity for hydrogen sulfide in *Lucina pectinata* hemoglobin I, allow us to use as the active material in the preparation of a sensor. Electrochemical data presented here suggest that the protein immobilized on a surface responds to the presence of hydrogen sulfide by current changes. These data support the possibility of designing new models of electrochemical biosensors using hemoglobin I, in order to improve the response to hydrogen sulfide.

1.2. Electrochemistry of hemeproteins

Many years after the first publication describing the direct electrochemistry of Hb more than 100 papers have been published. However, many aspects of the electron transfer are still not understood. Only a few papers describe a behavior at the electrode which is consistent with the physiological function: the redox potential is around –70 mV vs. SCE and the electron transfer rate is low, an almost irreversible process. On the other hand, entrapment within a polymeric matrix causes drastic structural changes reflected by a fast electron transfer and a cathodic shift of the formal potential by more than 200 mV as compared with the redox potential. Therefore these investigations do not contribute to the understanding of the physiological processes, but they are suited for analytical applications, i.e., the measurement of Hb concentrations or NO (Scheller *et al.*, 2005).

In search of the explanation of the heme group function in the hemeproteins was characterized the electrochemical properties of a *de novo* heme protein, S824C, a protein four-helix bundle derived from a library of sequences that was designed by binary

patterning of polar and nonpolar amino acids. Protein S824C was immobilized on a gold electrode and the formal potential of heme-protein complex was studied as a function of pH and ionic strength. The response of heme/S824C to ligands imidazole or pyridine was then compared to the response of isolated heme (without protein) to the same ligands. The observed shifts in potential depended on both the concentration and the structure of the added ligand. Further, it was observed that the electrochemical response of the buried heme in heme/S824C differed significantly from that of isolated heme. These studies demonstrate that the structure S824C protein modulates the binding of N-donor ligands to heme (Das *et al.*, 2006).

Secondary, tertiary or quaternary structural changes in hemoglobin (Fig. 1.2C) during an electroreduction process were studied by in situ circular dichroism (CD) spectroelectrochemistry (Shaojun *et al*., 2002). CD spectra in the Soret band show a R → T transition of two quaternary structural components, induced by electroreduction of the heme, which changes the redox states of the center ion from Fe^{3+} to Fe^{2+} and the coordination number from 6 to 5. In the same way, the heme iron coordination of unfolded ferric and ferrous cytochrome c in the presence of 7–9 M urea at different pH values was determined. In 7–9 M urea at neutral pH, ferric cytochrome c (Fig. 1.2A) is found to be predominantly low spin bis–His-ligated heme center. In acidic 9 M urea solutions is formed a high spin His/H_2O complex. The pKa for the neutral to acidic conversion is 5.2. In 9 M urea, ferrous cytochrome c is shown to retain its native ligation structure at pH 7. Formation of a five-coordinate high spin complex in equilibrium with the native form of ferrous cytochrome c takes place below the pKa 4.8.

The formal redox potential of the His/H_2O complex of cytochrome c in 9 M urea at pH 3 was estimated to be –0.13 V, ca. 100 mV more positive than $E^{\circ'}$ estimated for the bis–His complex of cytochrome c in urea solution at pH 7 (Milan *et al.*, 2004).

With respect to the myoglobin analysis, an amperometric immunosensor for the rapid detection of myoglobin in whole blood have been developed. Due to its rapid kinetics, myoglobin (Fig. 1.2B) is a useful biochemical marker for the early assessment of acute myocardial infarction (AMI). The overall performance of the sensor, rapid analysis time, wide working range, good precision and specificity demonstrate its potential usefulness for early assessment of AMI (Ciara *et al.*, 2002). In addition, a stable film of myoglobin (Mb) or horseradish peroxidase (HRP) layer-by-layer with clay nanoparticles on various solid substrates was assembled by alternate adsorption of negatively charged clay platelets from their aqueous dispersions and positively charged heme proteins from their buffers at the appropriate pH. Cyclic voltammetry (CV), the quartz crystal microbalance (QCM), and UV/vis spectroscopy were used to monitor the film growth. CV of $\{\text{clay} \mid \text{protein}\}_n$ films on pyrolytic graphite (PG) electrodes showed a pair of well-defined, nearly reversible peaks at around –0.20 V vs. Ag/AgCl at pH 5.5, characteristic of the heme Fe(III)/Fe(II) redox couples. The Soret adsorption band of Mb in $\{\text{clay} \mid \text{Mb}\}_6$ films showed that Mb kept the conformation similar to its native state in the medium pH range (Li & Hu, 2003).

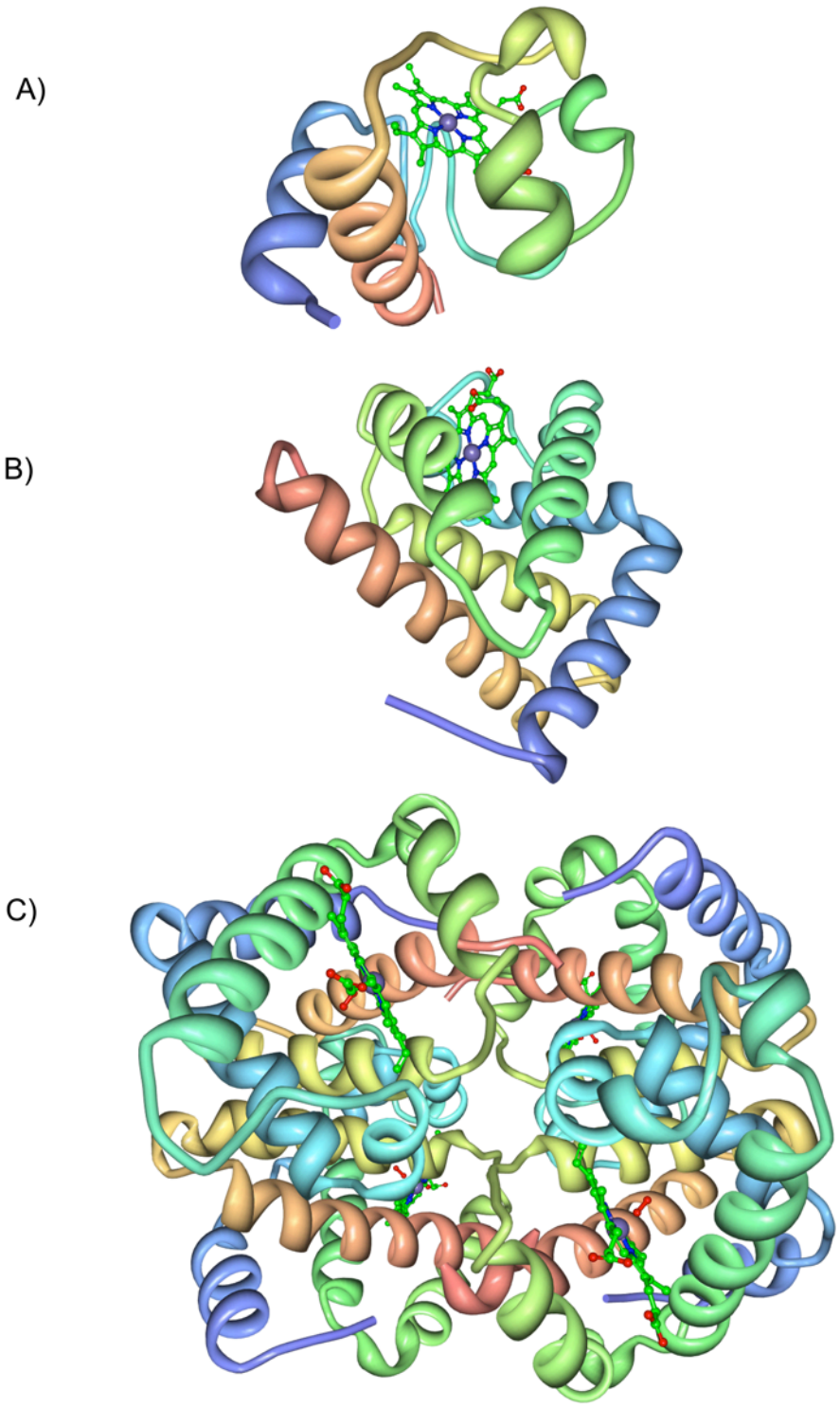

Figure 1.2. The most common hemeproteins: A) Cytochrome c horse heart (PDB ID: 1HRC); B) Human myoglobin (PDB ID: 1TES); C) Human oxy-hemoglobin (PDB ID: 1HHO).

1.3. Basic principles of electrochemical biosensors

The field of electrochemical biosensors has grown rapidly in the past few years because they may provide fast, simple and low-cost detection capabilities for biological binding events. Biosensors are devices for the detection of an analyte that combines a biological component with a detector. These devices use the specificity that is inherent to biological molecules to sense one particular analyte or set of analytes in a complex sample. In principle, biosensors can sensitively and selectively detect analytes without any separation or preconcentration of the sample (Runge and Saavedara, 2003). Biosensors in which the detection is based on the transduction of an electrochemical signal are called electrochemical biosensors. The electrochemical signal can be a change in the current, potential, or capacitance at the electrode surface. There are many different molecular architectures that can be used to create a sensitive and selective biosensor of this type (Zhang *et al.*, 2000). In what is referred to as "third generation" electrochemical biosensors (Gordon *et al.*, 1999; Zhang and Li, 2004), a redox-active protein is used to impart selectivity to the electrode surface on which it is immobilized (either by adsorption, covalent tethering, or biospecific binding). Research in this field has focused on novel sensing strategies and was supported by a large number of publications about the enhancement of specificity, sensitivity, and response time.

The technical importance, performance, techniques, advantages, and disadvantages of biosensors in general and electrochemical biosensors in particular are described (Mehrvar & Abdi, 2004). A review of applications of amperometric biosensors with different enzymes and whole cells include the determination of vitamins and amino acids (Alaejos *et al.*, 2004), third-generation electrochemical biosensors based on the direct

electron transfer of proteins, specially addressed the topic of protein film voltammetry (Zhang & Li, 2004) and different designs of electrochemical biosensors based on gold nanoparticles, enzyme-based electrodes, immunosensors and DNA sensors (Hart *et al*, 2004; Yañez & Pingarrón, 2005; Sánchez and Cabrera, 2007).

Previously, human hemoglobin has been used like electroactive components in biosensors. Nitric oxide biosensor based on hemoglobin (Hb) was prepared by means of direct electrochemistry of a hemoglobin solution. Spectroscopic studies show that Hb maintains most of its three-dimensional structure in the film, and keep its reactivity with NO; the peak current related to NO is linearly proportional to its concentration and it can detect traces of NO as low as 2.9mM (Li *et al.*, 2000). However, in order to quantify the reaction of NO with Hb, a sensitive (nanomolar concentration range) electrochemical assay was developed to selectively measure HbNO and –SNOHb (*S*-nitrosothiols-Hb). This assay allows the monitoring of free NO during the reaction with human Fe(III)Hb and Fe(II)HbO_2 (Carlo *et al.*, 2004).

Direct electrochemistry and electrocatalysis of hemoglobin (Hb), myoglobin (Mb), and horseradish peroxidase (HRP), incorporated in gluten biopolymer films cast on pyrolytic graphite (PG) electrodes, were studied by voltammetry and amperometry. Positions of soret absorption band of protein-gluten films suggested that the heme proteins kept their secondary structure similar to their native state in the films in the medium pH range. The voltammetric or amperometric responses of H_2O_2 at the protein-gluten film electrodes could be used to determine the concentration of H_2O_2 in aqueous solution (Hongyun & Hu, 2003). In the same way, hemoglobin entrapped in a titania sol–gel matrix was prepared and used a mimetic peroxidase to construct a novel amperometric biosensor for hydrogen peroxide. The Hb entrapped titania sol–gel film was obtained with a vapor

deposition method, which simplified the traditional sol–gel process for protein immobilization, and the morphologies of both titania sol–gel and the Hb films were characterized using scanning electron microscopy (SEM). H_2O_2 could be reduced by the catalysis of the entrapped hemoglobin at −300mV vs. SCE without any mediator. The reagentless H_2O_2 sensor exhibited a fast response, good sensitivity and a linear range for H_2O_2 determination with a detection limit of 1.2×10^{-7} M (Jiuhong *et al.*, 2003). Conversely, the hemoglobin in polystyrene (PS) catalyze electrochemical reduction of various substrates such as trichloroacetic acid (TCA), nitrite, oxygen and hydrogen peroxide. A sensor based on hemoglobin (Hb)-coated polystyrene (PS) latex bead film deposited on pyrolytic graphite (PG) electrode surface and Hb-PS film electrodes exhibited a pair of well-defined, quasi-reversible cyclic voltammetric (CV) peaks at around –0.36 V vs. SCE in pH 7.0 buffers, characteristic of Hb heme Fe(III)/Fe(II) redox couples. Positions of soret absorption bands of Hb-PS films suggest that Hb retains its near-native structure in the films in its dry form and in solution at medium pH (Sun & Hu, 2004). On the other hand, Hb was immobilized on nanometer-sized gold colloid particles associated with a cysteamine monolayer on a gold electrode surface, and it kept its biological activity well. Direct electron transfer (eT) between Hb and the modified electrode was achieved without the aid of any electron mediator and the immobilized Hb displayed the features of a peroxidase and gave an excellent electrocatalytic response to the reduction of H_2O_2 (Gu *et al.*, 2001).

There are very few reports in the literature that describe methods to determine hydrogen sulfide in solutions using enzymes or heme-proteins. Carbon nanotube (CNT) modified glassy carbon electrode exhibiting strong and stable electrocatalytic responses towards hydrogen sulfide was studied. The CNT-coated electrodes allow highly sensitive,

low potential (+0.1 V) and stable amperometric sensing. A wide linear dynamic range (1.25 – 112.5 μM) was achieved with a detection limit of 0.3 μM (Lawrence, 2004). On the other hand, a spectrophotometric method for the determination of the H_2S concentration was reported. This method, based on the reaction between H_2S and the ferric derivative of hemoglobin I (HbI) from *Lucina pectinata*, allows the quantitative determination of H_2S dissolved in a given solution even at concentrations as low as 1 μM (Boffi *et al.*, 2000).

All the studies previously mentioned demonstrate that heme-proteins present high promise as active substances in electrochemical biosensors. The specificity and the selectivity of these biomolecules, as well as the stability of the redox couple Fe(II)/Fe(III) makes suitable for the study.

1.4. Hydrogen sulfide sensors

Previously, various techniques used in the analysis of H_2S were mentioned. The measures performed by most of these techniques are based on the response obtained from a sensor. Most of these sensors vary by method (how they interact with H_2S), operational criteria (e.g., response time, range of concentrations and stability) and applicability in different environments. Here are some of the most common sensors that are currently used for the analysis of H_2S.

1.4.1. Semiconducting oxides

- *Y_2O_3-stabilized zirconia (YSZ)*: An electrochemical sensor that combines Y_2O_3-stabilized zirconia with an oxide layer of WO_3 was prepared. This sensor detects 0.2-25 ppm H_2S in air at 400 °C, but the response was hardly affected by CO_2 and water vapor (Miura *et al.*, 1996).

- *SnO_2-Ag nanocomposite*: A hydrogen sulfide gas sensor was developed fabricating thin film SnO_2-Ag nanocomposite, which shows sensing characteristics upon exposure to H_2S as low as 1 ppm at working temperature as low as 70°C. This sensor also shows higher sensitivity to H_2S under various humidity conditions, in comparing to commercialized H_2S sensors as well as published data. The results show that this sensor has a good selectivity due to its less sensitive to common interference gases like Cl_2, HCl, SO_2, C_6H_{14}, CH_4, CO, C_3H_8, etc. (Gong *et al.*, 2006).
- *Copper oxide on tin oxide films*: Sensors based in CuO deposited on SnO_2 films or composites for sensing H_2S were prepared by different research groups (Manorama *et al*, 1994; Esfandyarpour *et al*., 2004; Lee *et al.*, 2005; Patil *et al.*, 2006). They observed changes in conductivity as a principle for determining the concentrations of hydrogen sulfide, and the sensors working in concentration ranges from 0.01-3 ppm (CuO-SnO_2 composite), 1-300 ppm (CuO on SnO_2 films) and 0.1-10 ppm (CuO-SnO_2 micro sensor).
- *Lanthanum alloy nanocrystalline*: Nanocrystalline $La_{0.7}Pb_{0.3}Fe_{0.4}Ni_{0.6}O_3$ sensor was prepared by a sol-gel citrate method. The gas sensing properties were studied for different reducing gases such as H_2S, ethanol, CO and LPG. The $La_{0.7}Pb_{0.3}Fe_{0.4}Ni_{0.6}O_3$ powder showed large response to H_2S gas when 0.5 wt% Pd to $La_{0.7}Pb_{0.3}Fe_{0.4}Ni_{0.6}O_3$ was added. The sensor showed a good response to 150 ppm H_2S gas at an operating temperature 200°C (Jagtap *et al.*, 2008).
- *Cadmium-indium oxide sensor*: $CdIn_2O_4$ sensor for H_2S gas was synthesized by using sol–gel technique. When $CdIn_2O_4$ thick films are doped with cobalt

concentrations the response is improved. This sensor exhibits high response and selectivity toward H_2S for 10 wt.% Co doped $CdIn_2O_4$ thick films. The current–voltage characteristics of 10 wt.% Co doped $CdIn_2O_4$ calcined at 650°C shows one order increase in current with change in the bias voltage at an operating temperature of 200°C for 1000 ppm H_2S gas (Chaudhari *et al.*, 2012).

1.4.2. Conducting polymers

- *Polyaniline nanowires-gold nanoparticles*: A chemiresistive sensor using polyaniline nanowires-gold nanoparticles hybrid network was reported (Shirsat *et al.*, 2009). Polyaniline nanowires with a diameter of 250-320 nm were synthesized by templateless electrochemical polymerization, and then electrochemically functionalized with gold nanoparticles using cyclic voltammetry technique. This sensor shows a limit of detection (0.1 ppb), and wide analysis range (0.1–100 ppb).
- *Polyaniline-copper sensor*: A printable polyaniline-copper (II) chloride sensor [PAN-$CuCl_2$] for the detection of hydrogen sulfide gas was prepared. The sensing device is composed of screen-printed silver interdigitated electrode (IDE) on a flexible PET substrate with inkjet printed layers of polyaniline and copper (II) chloride. The sensor is used as a chemiresistor, with changes in measured current being correlated with concentration. On exposure to hydrogen sulfide, 2.5 ppmv (parts per million by volume) is clearly detectable with a linear relationship between measured current and concentration over the 10-100 ppmv region. A disadvantage associated with this sensor is that the free copper and silver in the film is converted to sulfides, and the sensor response diminishes. Also, humidity interferes in the

response (Crowley *et al.*, 2010). Figure 1.3 shows changes of the PAN-$CuCl_2$ before and after treatment with H_2S.

1.4.3. Optical sensors

- *CdSe/CdS quantum dots on poly(dimethylsiloxane) films*: The fluorescence quenching of CdSe/CdS quantum dots (QDs) by hydrogen sulfide in dichloromethane is reported, embedded QDs in films of poly(dimethylsiloxane) (PDMS). After exposing the film to 10 ppm of hydrogen sulfide, the film loses its fluorescence within 1 min. The fluorescence recovers completely after the film is left in the open air for 2 h (Xu *et al.,* 2010). Fig. 1.4 shows fluorescent images of CdSe/CdS QDs in dichloromethane under the excitation of 365 nm UV, to study the fluorescence-quenching phenomenon. In (Fig. 1.4B–F), the dichloromethane is also mixed with 100 ppm H_2S, water, hexane, 1-butylamine and 1-heptanol.

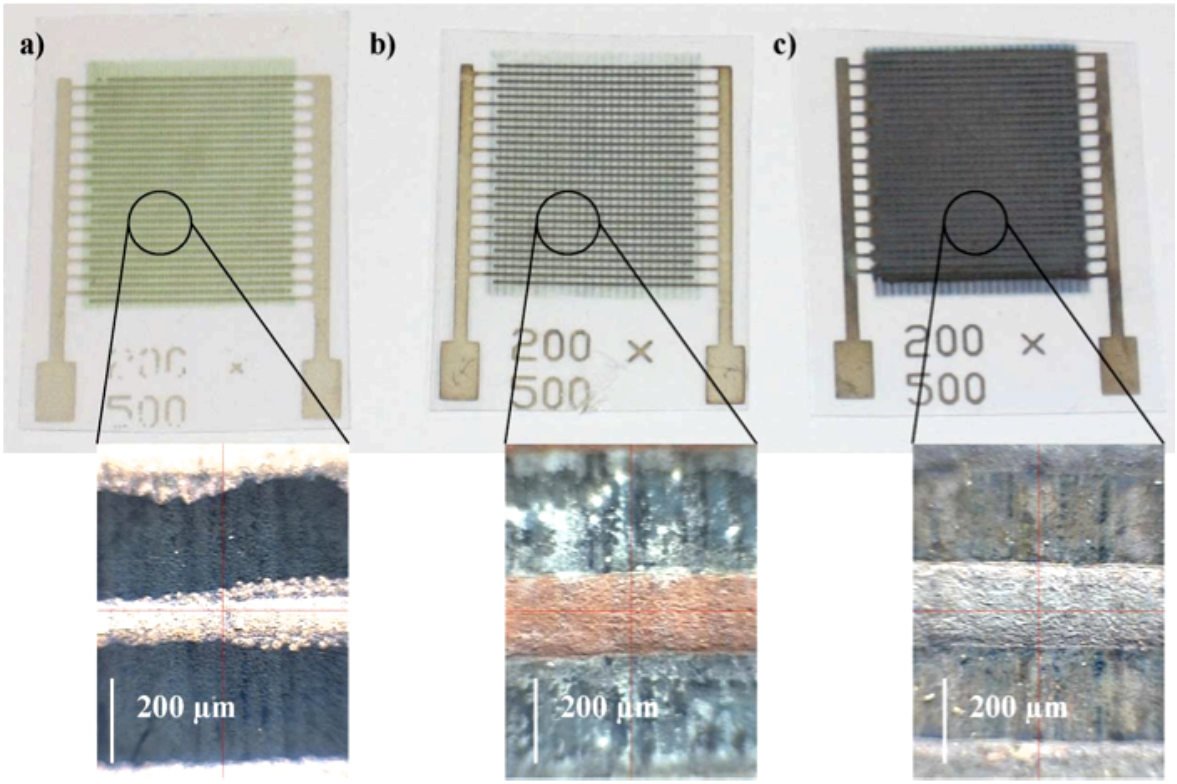

Figure 1.3. Interdigitated electrodes with inkjet printed films of (a) PANI, (b) PANI-CuCl2 (pre H_2S exposure), and (c) PANI-CuCl2 (post H_2S exposure). Insets compare optical microscopy of the electrode digits and sensor films (Crowley *et al.*, 2010).

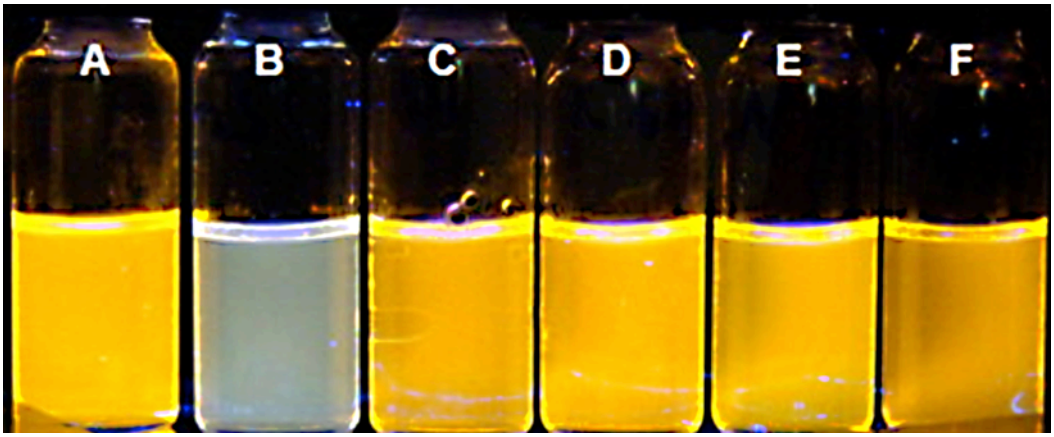

Figure 1.4. Fluorescent images of CdSe/CdS QDs in dichloromethane under the 365 nm UV excitation. To study the fluorescence quenching phenomenon. In (B–F), the dichloromethane is also mixed with (B) 100 ppm H_2S, (C) 10 µL of water, (D) 2 µL of hexane, (E) 2 µL of 1-butylamine and (F) 2 µL of 1-heptanol (Xu *et al.*, 2010)

- *Fluorescent Proteins*: A fluorescent protein (FP) modified with the sulfide-reactive azide functional group was genetically encoded in *E. coli* and mammalian cells. These structurally modified FP-chromophores were selectively reduced by H_2S, resulting in sensitive fluorescence enhancement detectable by spectroscopic and microscopic techniques, responding to a concentration not greater than 50 μM NaHS (Chen *et al.*, 2012).

1.4.4. Electrochemical sensors

- *Cell Clark type*: An electrochemical cell design of the Clark type (Fig. 1.5.a) including a thin layer of electrolyte in contact with a microelectrode has been applied for the determination of sulfide utilizing an electrochemically initiated reaction (Fig. 1.5.b) with aqueous diethyl-p-phenylenediamine (DEPD). Linear Sweep Voltammetry (LSV) was used to determine the current increases by addition of 0.05 M sodium sulfide solution. The response was linear over a range of the hydrogen sulfide concentrations of 10-100 μM (Lawrence *et al.*, 2003).

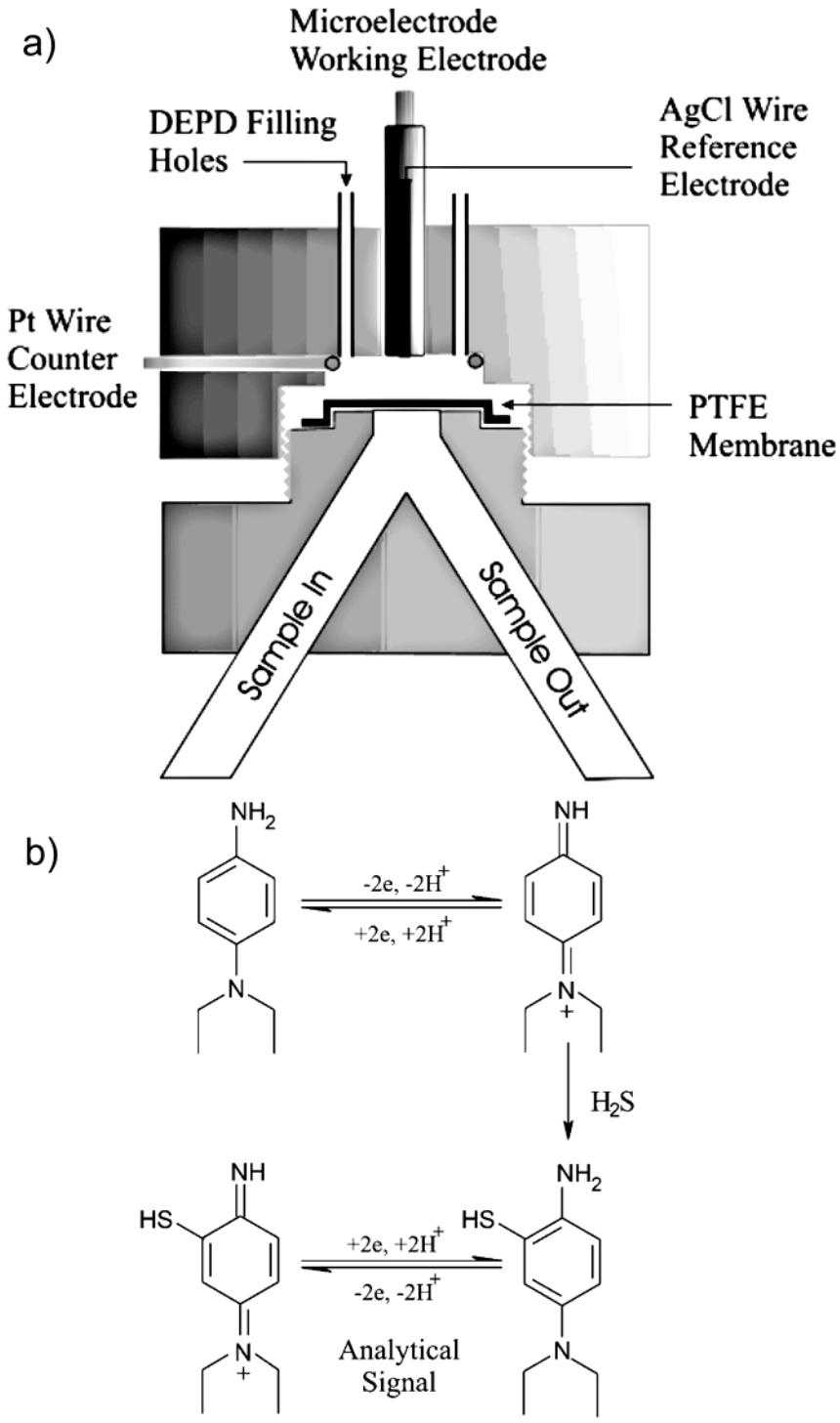

Figure 1.5. a) Cell Clark type design; b) Mechanism of the reaction electrochemically initialized using diethyl-p-phenylenediamine for the H_2S detection.

- *Polarographic sensor*: Currently most H_2S analysis are performed using selective membrane electrodes by polarographic techniques based on the specific electrochemical reaction of HS^- ion formed in the first dissociation of H_2S gas dissolved in water with the redox couple $Fe(CN)_6^{3+}/Fe(CN)_6^{4+}$ (Doeller *et al.*, 2005). Fig. 1.6.a shows the main parts that comprise this sensor. This polarographic hydrogen sulfide sensor (PHSS), background current resulting from electrolytic conduction of current from cathode to anode occurs as ferricyanide is reduced at the cathode and oxidized at the anode. Hydrogen sulfide diffusion through the membrane initiates the reduction of ferricyanide to ferrocyanide, which donates electrons to the anode, creating a current proportional to the sample sulfide concentration (Fig. 1.6.b). Ferricyanide reduction at the cathode contributes to the background current, which is much less than that due to hydrogen sulfide. Because the cathode potential is not as negative as the equilibrium potential of HS^-, the ferricyanide reduction rate is less than the signal current resulting from sample H_2S. The current signal is linear against H_2S concentration between 10 nM to 80 μM. Some of the disadvantages of this system are: a) the time resolved of the analysis and signal stabilization are extremely large, b) analyte measurements are achieved indirectly by HS^- ion detection, c) weak and fragile membrane, and d) the large size equipment required.

Finally, Padley *et al.* (2011) conducted a detailed analysis of most existing sensors for the analysis of H_2S. A summary of most of the sensors listed there and others from literature are summarized in Fig. 1.7.

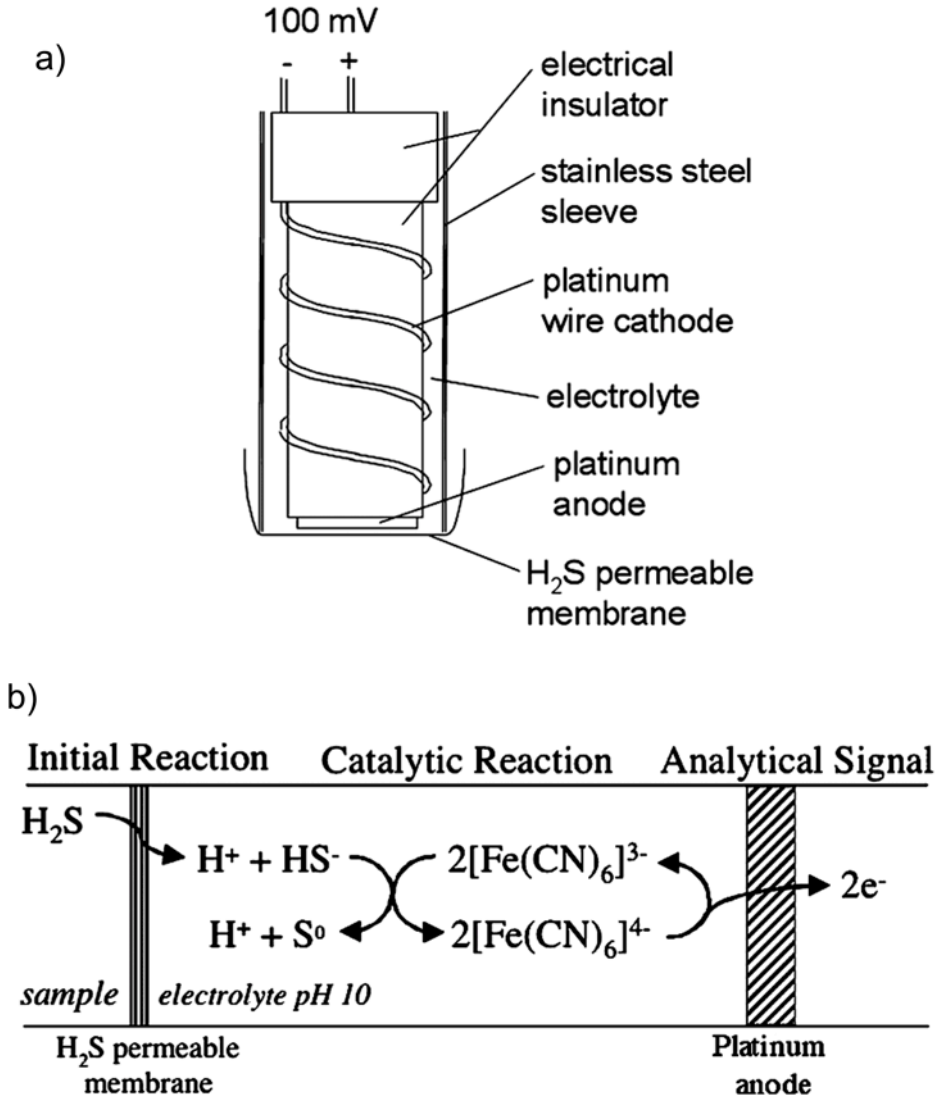

Figure 1.6. a) The PHSS is approximately 5 mm long and has a 2-mm outside diameter working at 100 mV. b) PHSS electrolyte redox chemistry. The PHSS electrolyte is 0.05 M $K_3[Fe(CN)_6]$ in 0.5 M carbonate buffer pH 10.

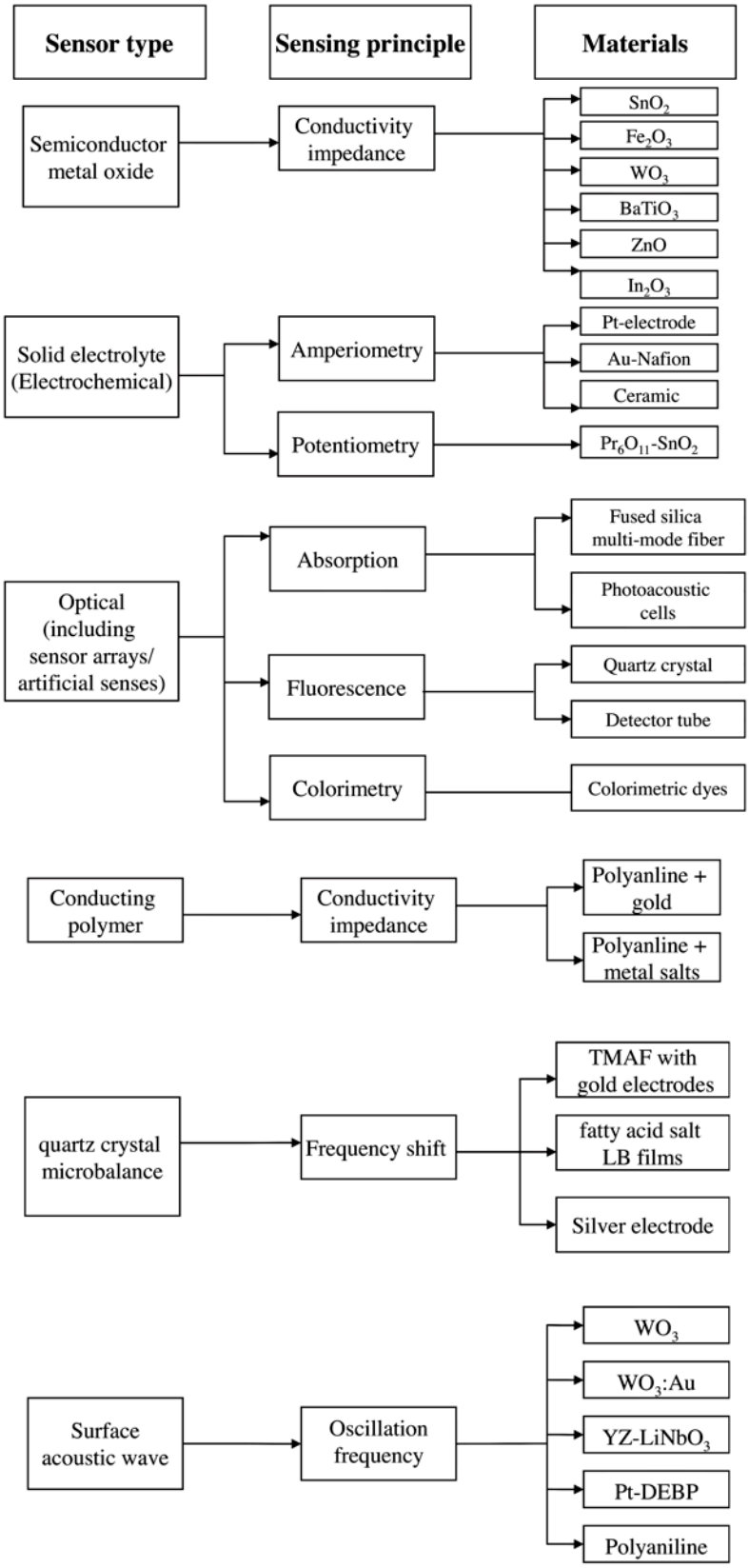

Figure 1.7. The most common sensors for the detection of hydrogen sulfide.

1.5. *Lucina pectinata* hemoglobins

Lucina pectinata is a native clam who lives in the sedimentary coasts of Puerto Rico, characterized by the low tension of oxygen or almost anoxic atmosphere. In recent years, this bivalve has been widely studied because it produces cytoplasmic hemoglobins that participate in a symbiotic process with chemoautotrophic bacteria. These bacteria occupy one-third part of the total volume of the clam. Three hemoglobins, HbI, HbII and HbIII, are in high concentrations in this clam with very specific functions. These hemoglobins provide oxygen (HbII and HbIII) to the symbiotic bacteria, and hydrogen sulfide to the clam (HbI). The oxyhemoglobin I ($HbIO_2$) is reactive to hydrogen sulfide and forms ferric hemoglobin sulfide, whereas HbII and HbIII remain oxygenated without reacting. Although HbII and HbIII have very similar amino acids composition, they differ remarkably in HbI properties. Hemoglobin I is a monomeric protein of 142 amino acid residues, having a molecular weight of 14,812.80 Dalton, which function is in its ferric state to transport hydrogen sulfide (H_2S) to the symbiotic bacteria and it is called sulfide-reactive hemoglobin (León *et al.*, 2004). Fig. 1.8.a shows the HbI X- Ray crystallography structure (Rizzi et al., 1994). HbII and HbIII are oxygen reactive hemoglobins, and they exist as monomers at low concentrations. Recently, the HbII crystal structure (Fig. 1.8.b) was resolved showing to be a homodimer at concentration ~1-2 mM (Gavira *et al.*, 2006; Gavira *et al.*, 2008) with a heme pocket more collapsed than HbI. At high concentrations (~4mM) HbII tends to form oligomers of more than 4 subunits, and HbIII tends to form a dimer (~1mM). A mixture of HbII/HbIII of ~6mM exhibits self-association and can form a non-interactive heterotetramer (Kraus & Wittenberg, 1990). It has been suggested that HbI

is used to transport the hydrogen sulfide to the bacteria while HbII and HbIII provide oxygen to the gills and to the bacterial symbionts (Rizzi et al., 1996).

Spectroscopic studies performed suggest that it is necessary a distinctive distal heme pocket arrangement to normalize the ligand binding kinetics (Pietri *et al.*, 2005). In the heme cavity, this clam has an unusual collection of amino acids. There is a glutamine (GlnE7) in the distal site of the heme pocket in the three hemoglobins instead of the classical histidine. This glutamine is also present in elephant myoglobin and shark myoglobin. The other surrounding amino acid residues are three phenylalanines (PheCD1, PheE11, PheB10) for HbI (Fig. 1.8.a), while HbII (Fig. 1.8.b) and HbIII have two phenylalanines (PheCD1, PheE11) and a tyrosine residue (TyrB10) as showed in figures 1.8.c and 1.8.d. At alkaline pH, the tyrosyl competes with a hydroxyl radical as a ligand for the heme iron. At acid pH, the tyrosyl is assumed to be protonated and water ligates to the ferric heme (Kraus & Wittenberg 1990; Pietri *et al.,* 2005). Based in this arrangement at the distal ligand-binding site, it was suggested then that this environment is responsible for the high affinity of HbI for H_2S.

The fast ligand association of H_2S to HbI, k_{on} = $2.3x10^5$ $M^{-1}s^{-1}$, and the slower ligand dissociation, k_{off} = $2.2x10^{-4}$ s^{-1} at pH 5.0, show the affinity of ferric HbI for hydrogen sulfide is 4000-fold greater than those of ferric HbII, HbIII and myoglobin (Kraus & Wittenberg, 1990). Table 1 presents the affinity constants for the reaction between ligands (O_2, CO and H_2S) and HbI, HbII and HbIII from *Lucina pectinata* and myoglobin from sperm whale (Cerda *et al.*, 1999). Fascinatingly, the development of recombinant protein expression (rHbI) and several site-directed variants of HbI from *L. pectinata* provide opportunities to study ligand-binding dynamics of this unusual hemoglobin.

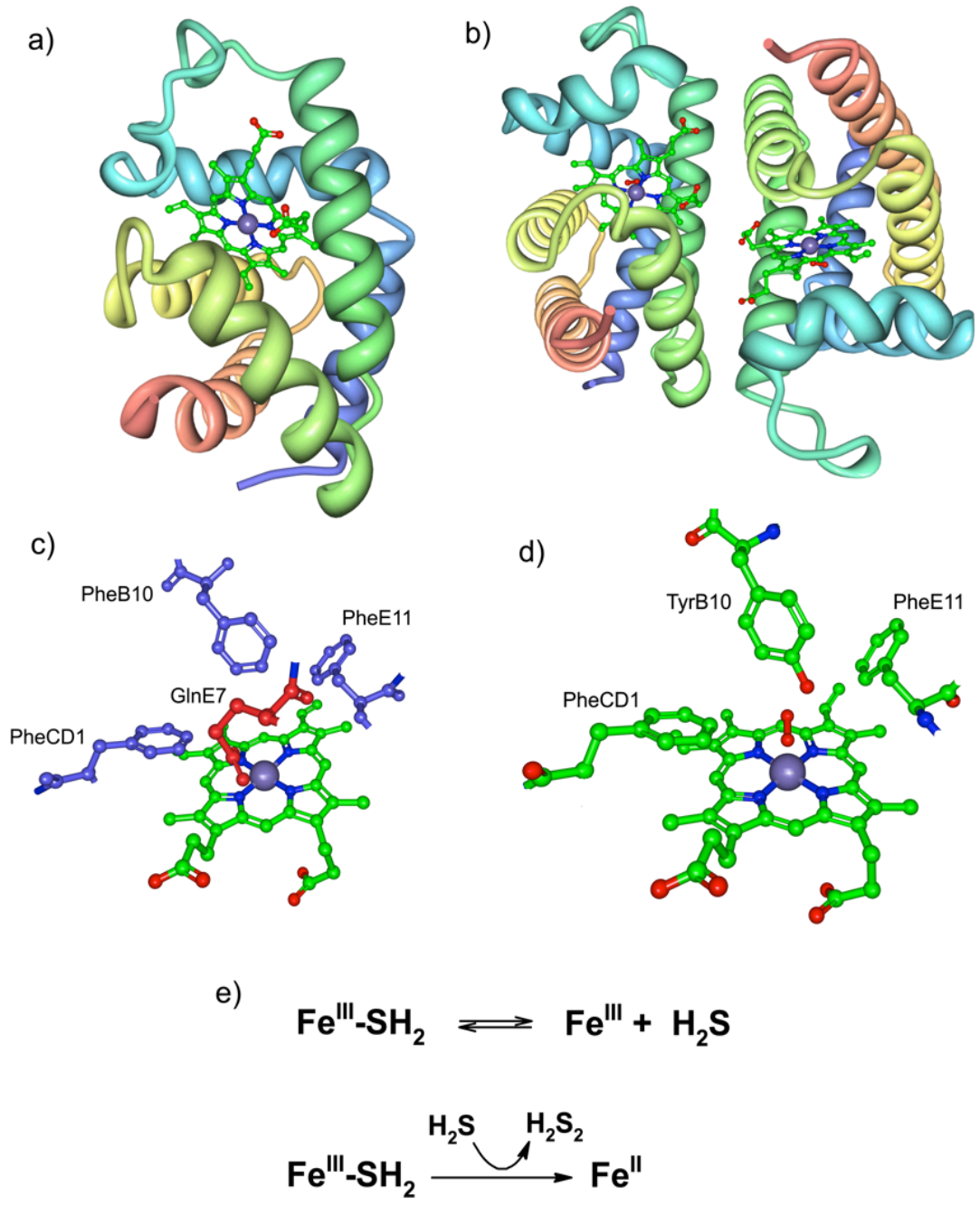

Figure 1.8. a) *Lucina pectinata* HbI crystallographic structure, PDB ID: 1FLP (Rizzi et al., 1994); b) *Lucina pectinata* HbII crystallographic structure, PDB ID: 2OLP; c) and d) Comparison of the arrangement of the amino acids in the heme pocket in HbI and HbII; e) The first reaction dominates at low H_2S concentrations and the second one at higher H_2S concentrations.

Table 1.1. Affinity constants for the reaction of *Lucina pectinata* hemoglobins and sperm whale hemoglobin with oxygen, carbon monoxide, and hydrogen sulfide.

Hemoglobin	$K_{affinity}$ x 10^6		
	O_2	CO	H_2S
HbI	1.637	54.930	1045.45
HbII	3.545	2.676	0.665
HbIII	3.840	0.673	2.606
Sperm whale Mb	1.900	23.784	0.183

Cerda *et al.,* 1999

The H_2S association rate constant, k_{on} of the WTHbI is 2.73 x 10^4 $M^{-1}s^{-1}$ comparable to the obtained for the rHbI at 2.43 x10^4 $M^{-1}s^{-1}$ both at pH 6.0 (León *et al.*, 2004). UV-Visible, ESI-MS, and kinetic studies demonstrated that rHbI and variants bind heme and they have identical binding properties as the wild type HbI (WTHbI).

Using site-directed mutagenesis, spectroscopic and theoretical approaches, Pietri *et al.* showed that hemoglobin I fluctuations are required to allow H_2S access to the rHbI distal heme site and bind rapidly to the ferric iron (Pietri *et al.*, 2009). This ligand is partially stabilized by hydrogen bonding with glutamine (Rizzi *et al.*, 1996). Hydrogen sulfide release is due to two competing processes that involve slow dissociation of H_2S from the ferric adduct (at low H_2S concentrations) and heme iron reduction followed by H_2S liberation (at high H_2S concentrations) (Pietri *et al.*, 2009). Figure 1.8.e shows the reactions represented by these processes. Heme reduction is facilitated by the hydrogen bond between glutamine and bound H_2S, and replacement of this residue by valine, which disrupts the hydrogen bond, prevents reduction. Also, since HbI mutants have proton

acceptor groups near the bound H_2S, the reduction is greatly enhanced. The mutant GlnE7His, in addition to inducing a rapid reduction, was the only one to form sulfeheme after heme reduction (Pietri *et al.*, 2009).

For the above, Pietri *et al.* concluded that (a) H_2S association is regulated by external kinetic barriers, (b) H_2S release is controlled by two competing reactions involving simple sulfide dissociation and heme reduction, (c) at high H_2S concentrations, reduction of the ferric center dominates, and (d) reduction of the heme is also enhanced in those rHbI mutants having polar distal environments (Pietri *et al.*, 2011).

1.6. Objectives

The most important challenge in the construction of a biosensor is the immobilization process of the biologically active material (enzyme, protein, DNA, etc.), without causing major changes in the material function. The purpose of this research was to immobilize the recombinant hemoglobin I from *Lucina pectinata* on a suitable surface for the preparation of an electrochemical sensor, and thus be able to obtain current changes when the hemoglobin comes into contact with the hydrogen sulfide. This was achieved under the following objectives:

a) To verify the progressive formation of the sensor using the technique of cyclic voltammetry as a tracking technique. This corresponds to the steps of:
    i. Formation of self assembled monolayer of gold-linker (Lnk/Au). The linker can be cysteine or 3-mercaptopropionic acid.
    ii. The nickel complex formation (Ni^{2+}/Lnk/Au). This is accomplished by interacting a nickel (II) solution with the Lnk/Au surface.

iii. The recombinant hemoglobin I immobilization by the nickel complex (rHbI/Ni^{2+}/Lnk/Au). The nickel (II) complex formed on the gold surface is left in a recombinant hemoglobin I solution of moderate concentration.

b) To establish the number of electrons transferred when recombinant hemoglobin I was immobilized. This was done with the purpose of determining the redox potential of immobilized hemoglobin and electrokinetic properties, i.e. constant electron transfer (k_s) and electron transfer coefficient (α). Furthermore, these properties served to evaluate the rHbI stability on the gold surface.

c) Detecting changes in voltammetric currents of immobilized protein when it interacts with H_2S by adding a Na_2S solution to a phosphate buffer solution pH 6.70.

d) To evaluate the response amperometric sensor in the absence and presence of common interferences, and plot calibration curves for determining concentrations of hydrogen sulfide by current changes.

Overall, this study provides valuable information about recombinant hemoglobin I immobilization for purposes of preparing electrochemical hydrogen sulfide sensors. In addition, the electrochemistry of the protein is studied and shows the possibility of constructing different types of sensors based on this model.

2. INSTRUMENTATION

2.1. Cyclic Voltammetry (CV)

2.1.1. Instrumentation and Principles

Cyclic voltammetry (CV) is a potential-controlled reversal electrochemical technique. A cyclic potential sweep is imposed on an electrode and the current response is measured. Analysis of the current response provides information about the thermodynamics and kinetics of electron transfer at the electrode-electrolyte interface, as well as the kinetics and mechanisms of solution chemical reactions initiated by the heterogeneous electron transfer. The primary events in most cyclic voltammetry experiments are electrode-mediated oxidation and reduction processes of electroactive species in solution. In order to react, the electroactive species has to diffuse from the bulk solution to the electrode-solution interface (Bard and Faulkner, 2001).

A potentiostat is one of the most widely used instruments in electrochemical studies and makes possible the performance of techniques such as cyclic voltammetry (CV). The potentiostat-galvanostat (Epsilon, Bioanalytical Systems, Inc.), was available to perform the cyclic voltammetry experiments presented here.

A potentiostat system sets the control parameters of the experiment. Its purpose is to impose on an electrode (the working electrode) a cyclic linear potential sweep and to output the resulting current-potential curve. This sweep is described in general by its initial (E_i), switching (E_s), final (E_f) potentials, and sweep (or scan) rate (v, in V/s). The potential as a function of time is:

$$E = Ei + vt \qquad (2.1)$$

$$E = Es - vt \qquad (2.2)$$

where (2.1) represents the forward sweep and (2.2) the reverse sweep.

The electrochemical reaction of interest takes place at the working electrode (WE). Electrical current at the WE due to electron transfer is termed faradaic current. The potentiostat operates with a three-electrode system in an analytical cell. The three-electrode system function is to maintain the potential of the working electrode at a desired level with respect to a fixed reference electrode. This goal is achieved by passing the necessary current between the working electrode and a third electrode, called the counter or auxiliary electrode (CE). The counter electrode is driven by the potentiostatic circuit to balance the faradaic process at the working electrode with an electron transfer of opposite direction (e.g. if oxidation takes place at the WE, reduction takes place at the CE). The process at the CE is not of interest, and in most experiments the small currents observed mean that the electrolytic products at the CE have no influence on the processes at the WE. The reference electrode is designed in such a way that its composition is constant over time and then its potential is fixed. Therefore, any changes in the cell are ascribed to processes occurring in the working electrode. The faradaic current at the WE is traduced to a potential output at a selected sensitivity, expressed in amperes per volts, and recorded in a digital or analog form. The cyclic voltammetry (CV) response is plotted as current versus potential (Gosser, 1993; Bard and Faulkner, 2003). Figure 2.1 shows a three-electrode cell model and electrochemical cell station.

The measured current *i* (due to the number of electrons that cross the interface) is related to the extent of the chemical reaction, and therefore, to the amount of reactant consumed and product generated.

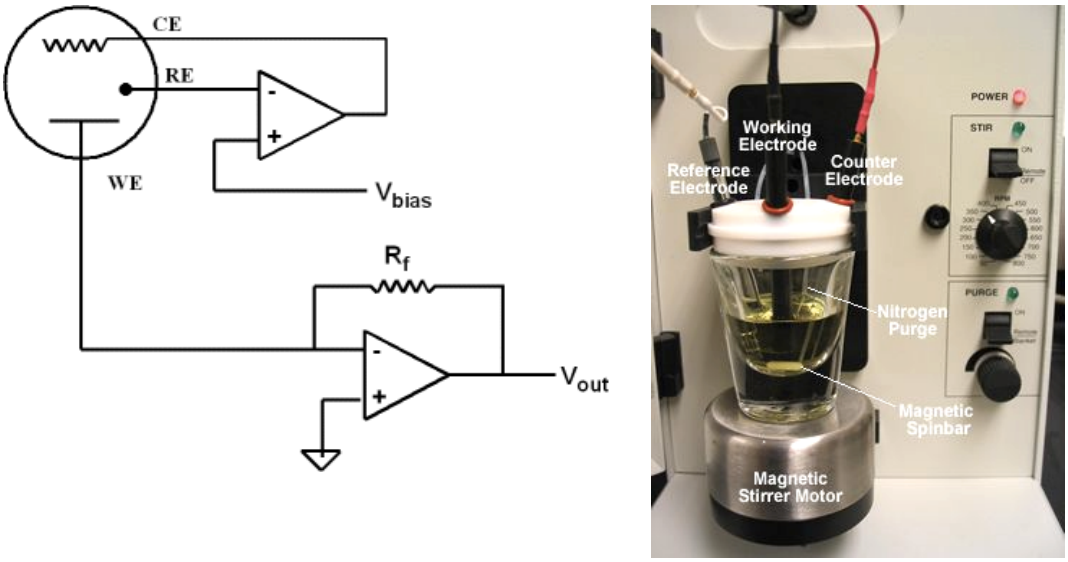

Figure 2.1. Schematic symbol of a three-electrode cell, using conventional symbols, and the electrochemical cell.

The measured current can be plotted as a function of potential to obtain the corresponding cyclic voltammogram. Figure 2.2 shows an example of (a) a cyclic potential and (b) a resulting cyclic voltammogram. The potential is changed linearly in one direction and then the potential is reverted linearly in the opposite direction. While scanning in the negative direction, at a sufficiently negative potential, a reduction peak appears corresponding to the reduction of an electroactive species in solution. This peak is often called reduction peak or cathodic peak and its area is proportional to the amount of electrons crossing the interface. Similarly, the oxidation peak (or anodic peak) is obtained at a sufficiently positive potential and the peak area is proportional to the amount of electrons that cross the interface.

The potential in which the redox process occurs is related to the standard potentials, E°, which is specific for a particular electroactive species in an electrochemical system described with an established set of experimental conditions. The voltammogram potentials where the maximum currents, i, for the oxidation and reduction processes are obtained can be designated as anodic peak potential (E_{anodic}) and cathodic peak potential ($E_{cathodic}$), respectively. An important quantity that can be calculated and provides information about the electrochemical behavior of the electroactive species is $\Delta E = |E_{cathodic} - E_{anodic}|$. Among electroactive species, there are three possible kinds of electrochemical behavior for the electrocatalized redox processes: reversible, quasi-reversible or irreversible. When an electroactive species is reversible, the oxidation and reduction processes are equally feasible. For a reversible process, ΔE lies within the range of 60 to 90mV. For a quasi-reversible process, ΔE is greater than 90mV. For an irreversible process only one of the reactions occurs oxidation or reduction. Then, in an irreversible process the electroactive species can be reduced but not oxidized or vice versa.

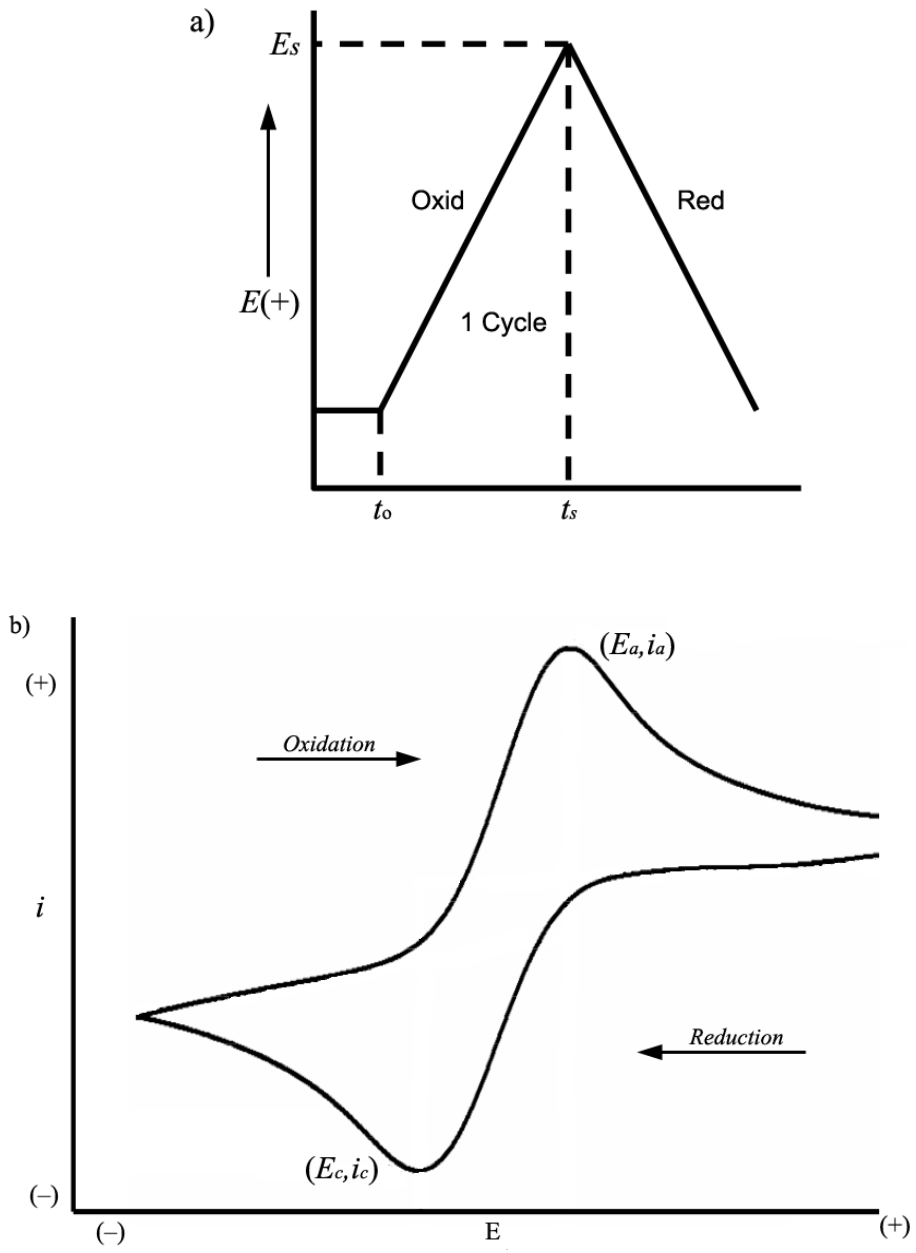

Figure 2.2. a) Linear potential sweep used in a cyclic voltammetry experiment and b) Cyclic voltammograms corresponding to a reversible redox process

For this study, electrochemical measurements were carried out in a conventional three-electrode cell previously N_2-purged for 15 min. The nitrogen atmosphere was maintained during the experiments. The measurements were performed at room temperature on a BASi Epsilon for an Electrochemistry Potentiostat/Galvanostat system with EC software, connected to a cell stand C-3 for voltammetry. The cell is equipped with a platinum wire auxiliary electrode (7.5 cm) with gold-plated connector (MW-1032), and a 7.5 cm long RE-5B Ag/AgCl reference electrode with a Vycor frit (the filling solution is aqueous 3M NaCl that has been saturated with AgCl). The software EC epsilon version 1.60.70 was used.

2.2. X-ray Photoelectron Spectroscopy (XPS)

X-ray photoelectron spectroscopy (XPS), also called electron spectroscopy for chemical analysis (ESCA), analysis provides qualitative and quantitative information for all elements present except H and He. The sample is placed in an ultrahigh vacuum chamber and then irradiated with photons from an X-ray energy source. The photoelectrons emitted from a core-level of the atoms have a specific kinetic energy (KE) and are measured by the spectrometer. XPS spectra are obtained by using the equation (2.3):

$$E_B = h\nu - KE - \Phi \qquad (2.3)$$

where E_B is the binding energy of the electron in the atom, $h\nu$ is the energy of the X-ray photons, and Φ is the work function of the spectrometer (Watts and Wolstenholme, 2003).

For each and every element, there will be a characteristic binding energy associated with each core atomic orbital ie each element will give rise to a characteristic set of peaks in the photoelectron spectrum at kinetic energies determined by the photon energy and the

respective binding energies. The presence of peaks at particular energies therefore indicates the presence of a specific element in the sample under study. Furthermore, the intensity of the peak is related to the concentration of the element within the sampled region. Thus, the technique provides a quantitative analysis of the surface composition. The exact binding energy of an electron depends not only upon the level from which photoemission is occurring, but also upon the formal oxidation state of the atom and the local chemical and physical environment, which give rise to small shifts in the peak position in the spectrum: chemical shifts. Atoms of a higher positive oxidation state exhibit a higher binding energy due to the extra coulombic interaction between the photoemitted electron and the ion core. This ability to discriminate between different oxidation states and chemical environments is one of the major strengths of the XPS technique (Grant and Briggs, 2003).

XPS was used to determine the composition of the modified gold surfaces. A PHI 5600ci spectrometer with an Al Kα monochromatic X-ray source at 15 kV and 350.0W was used to obtain a survey and multiplex XPS spectra. Spectra were recorded at a take-off angle of 45° and pass energy of 187.8 eV for the survey and 58.7 eV for the high- energy resolution studies. The binding energies were corrected using the carbon (C1s) contamination peak at 284.5 eV, as reference.

2.3. Fourier Transform Infrared Spectroscopy (FTIR)

Infrared spectroscopy (IR spectroscopy) is the spectroscopy that deals with the infrared region of the electromagnetic spectrum, that is light with a longer wavelength and lower frequency than visible light. It covers a range of techniques, mostly based on absorption spectroscopy. As with all spectroscopic techniques, it can be used to identify

and study chemicals. A common laboratory instrument that uses this technique is a Fourier transform infrared (FTIR) spectrometer.

Fourier transform infrared spectroscopy (FTIR) is a technique that is used to obtain an infrared spectrum of absorption, emission, photoconductivity or Raman scattering of a solid, liquid or gas (Griffiths and Hasseth, 2007). An FTIR spectrometer simultaneously collects spectral data in a wide spectral range. This confers a significant advantage over a dispersive spectrometer, which measures intensity over a narrow range of wavelengths at a time. The term Fourier transform infrared spectroscopy originates from the fact that a Fourier transform (a mathematical process) is required to convert the raw data into the actual spectrum.

Attenuated total reflectance (ATR) is a sampling technique used in conjunction with FTIR spectroscopy, which enables samples to be examined directly in the solid or liquid state without further preparation. ATR uses a property of total internal reflection resulting in an evanescent wave. A beam of infrared light is passed through the ATR crystal in such a way that it reflects at least once off the internal surface in contact with the sample. This reflection forms the evanescent wave, which extends into the sample. The penetration depth into the sample is typically between 0.5 and 2 μm, with the exact value being determined by the wavelength of light, the angle of incidence and the indices of refraction for the ATR crystal and the medium being probed (Mirabella, 1993). Varying the angle of incidence may vary the number of reflections. A detector then collects the beam as it exits the crystal. Most modern infrared spectrometers can be converted to characterize samples via ATR by mounting the ATR accessory in the spectrometer's sample compartment.

In our case, FTIR spectroscopy was used to corroborate the presence of the protein in the final surface. Spectrum 100 FTIR Spectrometer, from Perkin Elmer, equipped with a Universal diamont ATR (uATR) top plate accessory one refraction, was used. Software: Spectrum.

3. MATERIALS AND METHODS

3.1. Recombinant Hemoglobin I preparation

3.1.1. Large-scale expression of recombinant Hemoglobin I

The recombinant protein HbI was prepared as described by León and collaborators (León *et al.,* 2004). The *E. coli* Bli5 competent cells with the plasmid were developed at the Biomolecular Laboratory of Dr. Carmen Cadilla (University of Puerto Rico, Medical Sciences Campus), and provided in scraped Petri dishes. The large-scale expression process was performed in a 5-L BioFlo 3000 Bioreactor (New Brunswick). Briefly, colonies from the scrapped dishes were grown in a 250 mL sterilized Erlenmeyer containing 50 mL of the Terrific Brooth (TB) medium. The culture was incubated for 12 hours at 120-150 rpm, and 37°C. After 12 hours, the culture was transferred to a 2.5 L culture flask with 450 mL of the TB medium, and incubated overnight with the same conditions. The 4 L TB media for the large-expression was prepared directly inside the bioreactor vessel, and sterilized for 60 min at 121˚C. When the media reached a temperature of 37˚C, 30 µg/mL of chloramphenicol, 70 µg/mL of kanamycin, 500 µL of antifoam solution (Sigma), 0.17 M KH_2PO_4, 0.72 M K_2HPO_4, and 75 mL of the glucose (50% w/v) were added. The dissolved oxygen (dO_2) and the pH were controlled during the experiment. The media was inoculated with the overnight culture prepared before the fermentation. The cell growth was monitored measuring the optical density at 600 nm (OD_{600}). Figure 3.1 shows a typical bacterial growth curve achieved in this case by observing the growth of the *E. coli* cells transformed to express rHbI. When the OD_{600} value was between 1 or 2, adding 5 mL of 1 M IPTG solution and 33 mg/mL hemin chloride in NH_4OH induced the protein expression.

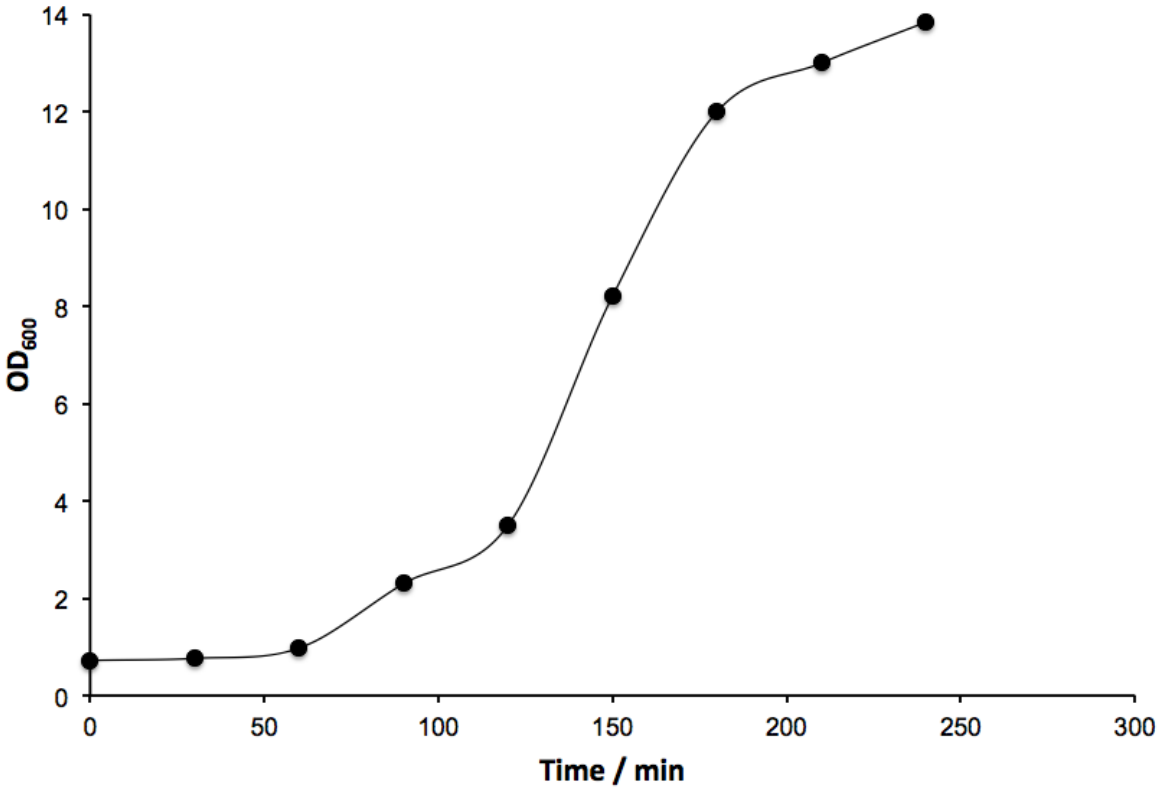

Figure 3.1. Typical bacterial growth curve for the rHbI expressed with BLi5 *E. coli* cells.

The OD_{600} was taken every 30 minutes after the induction until the *lag* phase was reached. The expression process was finished when two or three constant values of OD_{600} reading were obtained in the *lag* phase. The cell culture was centrifuged for 20 minutes at 4,000 rpm, 4˚C in a Beckman J2-HS Centrifuge. The cell pellet was stored at –56˚C for further lysis and purification procedures.

3.1.2. Affinity Chromatography of recombinant Hemoglobin I

The brown pellets were lysed by sonication using 10 mL of tris-EDTA buffer (10 mM Tris-HCl, 0.1 mM EDTA, pH of 8.0) for every 50 mL of culture centrifuge. The protein was purified by adding the lysate to a cobalt metal affinity resin (TALON, Invitrogen). This resin contains a sepharose bead bearing the tetradentate chelator of cobalt (II), which binds polyhistidine-tagged recombinant proteins. This resin is also highly selective towards polyhistidine-tagged proteins therefore offering high yields of our protein of interest. To pack the disposable column, the resin was shaken to resuspend it completely and 20 mL of the slurry solution were added into the column. The resin settled and precipitated, and then the ethanol was removed. This yielded approximately 10 mL bed volume of resin. Then, the column was equilibrated by adding 10 mL of buffer (50 mM sodium phosphate, 300 mM sodium chloride at pH 7.0) and letting it filter out of the column. This step was repeated 10 times. After the column was equilibrated, 10 mL of the lysate were added directly into the column, sealed on both ends and gently shaken to resuspend the resin. This shaking was continuous for 3-5 minutes. The cap on both ends was removed and the lysate from the resin eluted. The resin was washed with a wash buffer (50 mM sodium phosphate, 300 mM sodium chloride, and 10 mM imidazole at pH 7.0) by

adding 10 mL of the buffer and gently mixing for 5-10 min then eluting the buffer from the resin. This process was repeated several times. The resin was completely settled in the column with no air bubbles, before moving to the protein elution, and then the elution buffer (50 mM sodium phosphate, 300 mM sodium chloride, and 150 mM imidazole at pH 7.0) was slowly added. The eluent was collected until the color changed from transparent to red and continued until it got back to clear. To avoid problems of protein denaturation (precipitation), it is preferable to remove imidazole with ultrafiltration and to continue the purification process before 24 hours.

3.1.3. Size Exclusion Chromatography of recombinant HbI

The final purification step was achieved using the HiLoad 26/60 Superdex 200 preparation grade (ÄKTA FPLC, Amersham Bioscience). A small sample (~5 mL) of the crude extract was loaded onto the column using a flow rate of 4.4ml/min observing that the pressure does not exceed 0.5 MPa, and performed at room temperature. The eluted fractions were collected in a Frac-950 fraction collector (Amersham Pharmacia Biotech). The FPLC instrument has a UV-Vis lamp that monitors the presence of proteins in each fraction at 280 nm. ÄKTA FPLC software (Unicorn 4.00) monitors the entire purification process, which recorded the elution chromatogram. Careful observation of this chromatogram determines which fractions may contain the proteins of interest. The fractions were mixed and concentrated using an AMICON ultrafiltration cell with YM-10 membranes; and at the same time the salts were removed and the solvent was changed to deionized water in order to store the protein for further purification. The proteins were stored at -56˚C.

The concentration of the hemoglobin solution prior to the modification process was determined with spectral properties of the ferric state (metaquo) of the wild-type HbI

(Kraus and Wittenberg, 1990). The concentration of each sample was found using the absorption maxima (λ_{max}) in the UV-vis region, the corresponding absorptivity coefficients, and the Beer-Lambert Law. Also, before proceeding to modify the electrode, the protein was analyzed to check if it remained in the metaquo state running a UV-vis spectrum (Fig. 3.2).

3.2. Cleaning procedures and electrodes pretreatments

All the glass materials were cleaned during 15 minutes in an acidic solution made of concentrated H_2SO_4: HNO_3 (50:50), followed by a copious rinse in deionized water (18.2 MΩ·cm). The purpose of using a two-strong-acids cleaning solution is to remove adsorbed species in glass materials. Specifically, the strong acids degrade any adsorbed organic molecules on the glass walls of electrochemical cells, purging tubes, volumetric flasks, Pasteur pipets, and beakers, among other materials. Any other materials resistant to the acidic solution -such as the CTFE components that make up the cell tops and the electrode housings- were also cleaned using the H_2SO_4: HNO_3 solution.

On the other hand, the gold electrodes were rinsed with water removing any material, which is attached to the surface. It was dried using paper towels (Kimwipes®) and rinsed with methanol. Then, pads were wetted with deionized water and placed three or four drops of slurry of alumina. The polishing process was started with 1 μm alumina, then 0.3 μm and finally 0.05 μm. The electrode surface was polished rubbing gently on the pad for about 2 min, starting with the nylon pad and finish with velvety pads for polishing. The electrode was rinsed with deionized water and sonicated for 3 min. Then, it was rinsed again with deionized water and dried with nitrogen.

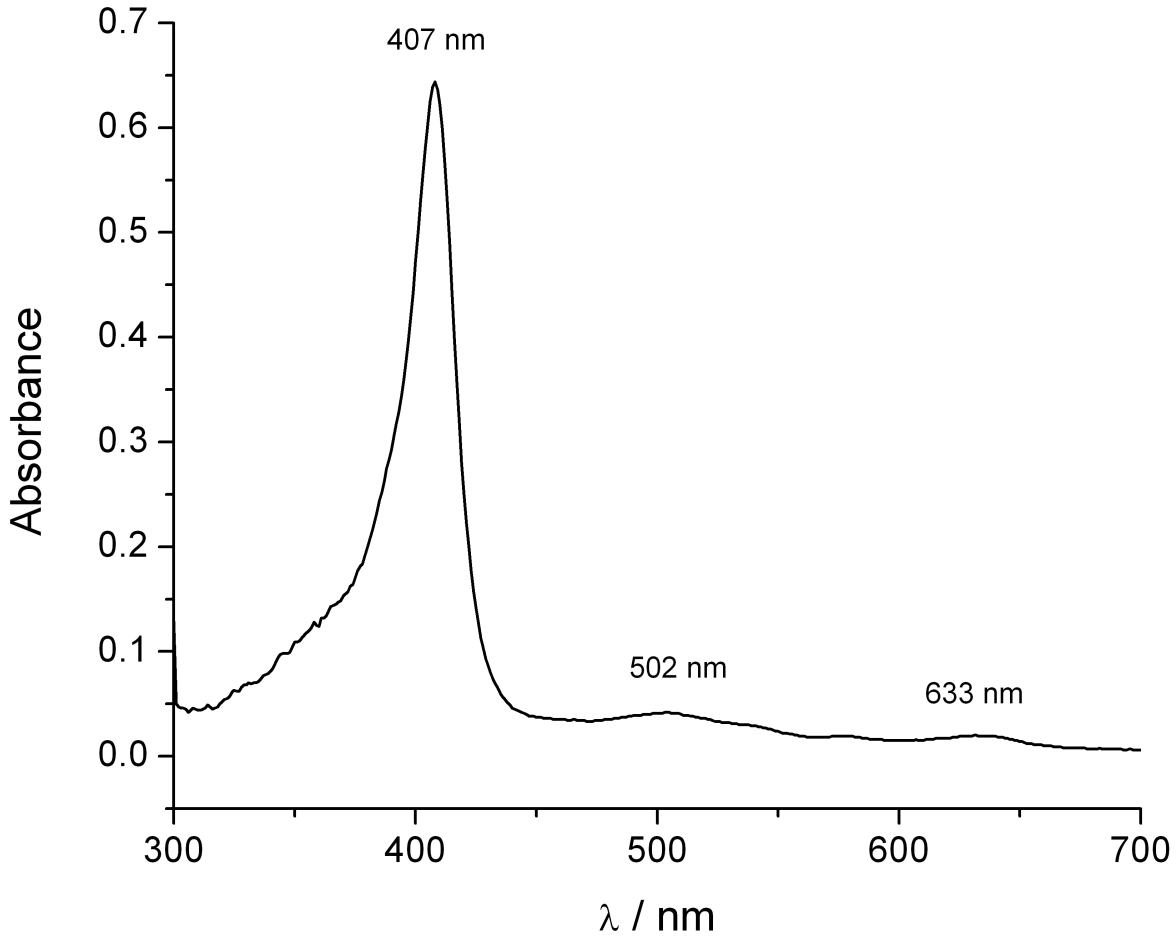

Figure 3.2. Typical UV-vis spectrum obtained for metaquo rHbI at pH 7.5. The peak at 407 nm corresponds to soret band with Q bands at 502 nm and 633 nm.

Cyclic voltammetry in 0.1 M H_2SO_4 was performed and compared with the voltammogram shown in Fig. 3.3. If it doesn't show the distinctive peaks for gold, was repeated from the cleaning procedure until the voltammogram matches.

3.3. Electrochemical measurements

Cyclic voltammetry technique was used to identify changes in current–potential shifts throughout the modification process. Also, current changes were evaluated in the modified hemoglobin-electrode when aliquots of a Na_2S solution were added in order to provide H_2S. There were two types of voltammetric analysis. First, measurement at 100 mVs^{-1} scan rate were done for each modification step in a cell containing 10 mL 0.1 M phosphate buffer solution pH 6.70 in order to confirm that the surface was modified. Second, cyclic voltammograms were obtained at the same scan rate for each addition of Na_2S solution to the 0.1 M phosphate buffer solution (deoxygenated with nitrogen), using the modified electrode rHbI modified gold electrode. The amperometric analysis was carried out by applying potential of 0.3 V vs. Ag/AgCl on a stirred cell at 25°C. The response was measured as the difference between total and residual currents.

3.4. Preparation of solutions

3.4.1. Preparation and description of the electrolyte solution

Although an ideal electrolyte does not undergo electron transfer or adsorption processes, it is an essential component of electrochemical systems. An electrolyte solution provides a high ionic strength in such a way that migration of the electroactive species from the bulk solution to the electrode surface is feasible.

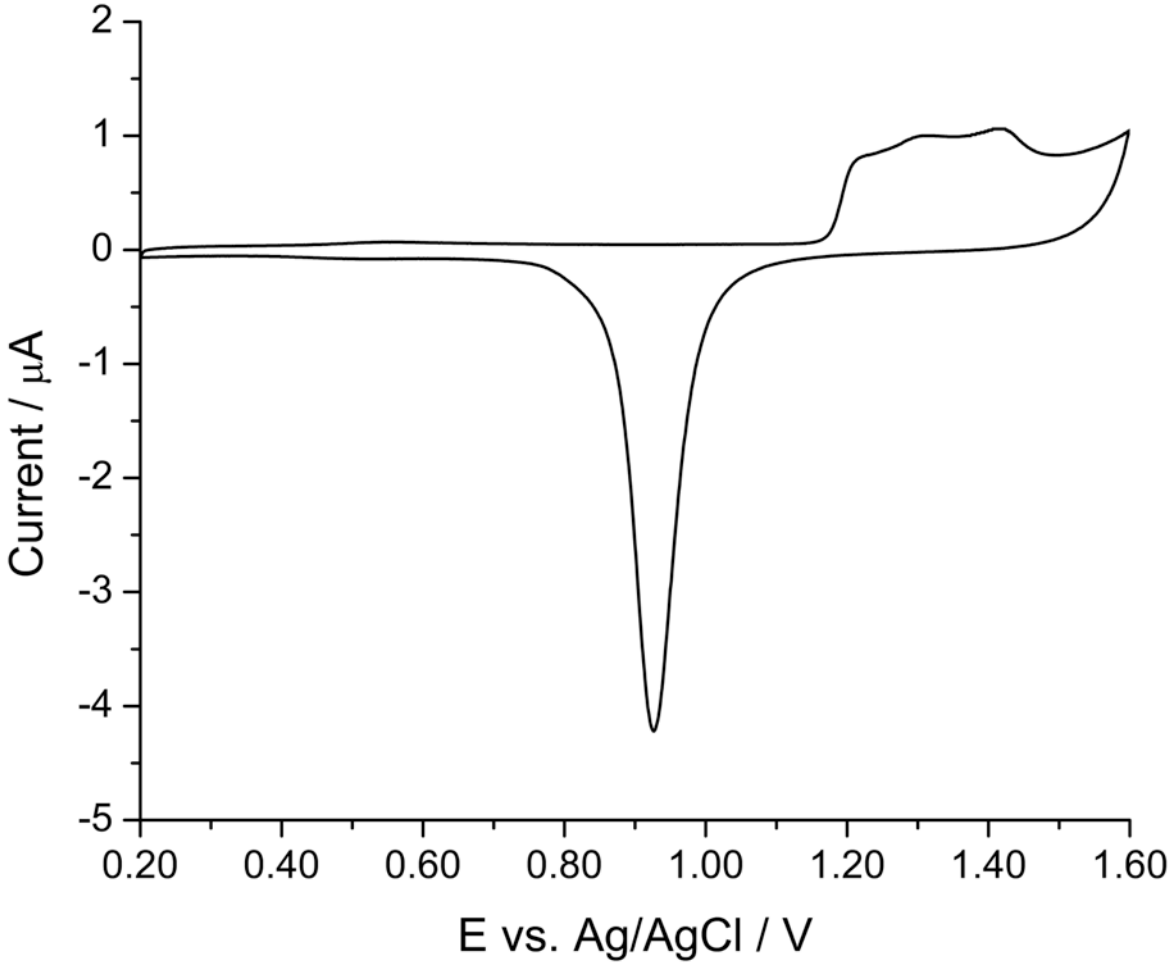

Figure 3.3. Cyclic voltammogram of clean gold electrode in 0.1 M H_2SO_4 solution at 100 mV s^{-1}

Then, the presence of the electrolyte species is required to facilitate the electrode-mediated oxidation and reduction processes of electroactive species in solution.

The support electrolyte solution used to perform the cyclic voltammetry experiments was a 0.1 M phosphate buffer pH 6.70. This solution was prepared by dissolving 6.880 g Na_2HPO_4 (Sigma, S7907) and 6.180 g NaH_2PO_4 (Sigma, S8282) in deionized water in a 1 L volumetric flask. A pH meter was used to verify the pH 6.70, and if adjustment was needed, NaOH or HCl 3 M was added.

3.4.2. Preparation and description of linkers' solutions

The linker substances used in this study were cysteine and 3-mercaptopropionic acid. These substances are structurally similar, but differ by the absence of the amino group in 3-mercaptopropionic acid. These compounds form ordered structures (assembly) on the gold surface in layers establishing the main link connection between the protein and the metal surface.

Self-assembly is a natural process whereby molecules spontaneously adsorb, and with sufficient time form ordered structures at the surface of the electrode. In particular, thiols (as well as disulfides), will form very strong sulfur-gold bonds, and are often used as the anchor for further molecular modifications. The self-assembly process is most commonly achieved by incubating the gold surface in a thiol or disulfide solution for approximately 24 hours. This extended period permits not only the binding to the substrate, but ample time for molecular re-organization on the surface as well. However, the use of different techniques to evaluate SAM formation, suggest that the process requires time on the order of 100-800 seconds to hours (Bensebaa *et al.*, 1997). Alternatively, SAMs may be

formed under electrochemical potential control (Ma and Lennox, 2000). It has been suggested that electrochemically-prepared SAMs have the same quality as those prepared by several hours of incubation. High quality SAMs have been achieved much faster using electrochemical deposition of long chain thiols.

Self-Assembled Monolayers (SAMs) formed from short-chain alkanethiols have predominantly been utilized in the fabrication of biosensors (Baldrich *et al.*, 2008; Ferreira *et al.*, 2005; Shervedani *et al.*, 2006). However, unlike their long-chain counterparts, these monolayers are not as densely packed, and consequently do not offer low capacitance values. Yet, these SAMs are still effectively employed for biosensor development. Likely the most common utilized modifier or linker is cysteine (Hager and Brolo, 2003). Cys SAMs are particularly suited to biological applications such as: selective detection of cytochrome *c* in the presence of cytochrome *b*5 (Qian *et al.*, 1998), evaluating the electron transfer of promoter-protein complexes (Zhang *et al.*, 2004), and chiral discrimination of 3,4-dihydroxyphenylalanine (Matsunaga *et al.*, 2007).

Cysteine (Cys, $HSCH_2CHNH_2COOH$) is a non-essential amino acid. The thiol group facilitates binding to gold substrates, whereas either the amino or carboxylic moieties are oriented away from the surface. Cys further contains a chiral carbon, and is thus available as both L and D isomers. The designation of L and D is based on the derivation of the species in relation to glyceraldehyde (since these are biological molecules, a biological standard is used), with L being the biologically relevant isomer.

The 3-mercaptopropionic acid (3-MPA, $SHCH_2CH_2COOH$) was also used in this study. This molecule is structurally related to Cys without the amino group. Therefore comparisons of the two species through relation of the similar structures should provide further insights into the immobilization process and the protein electrochemical behavior.

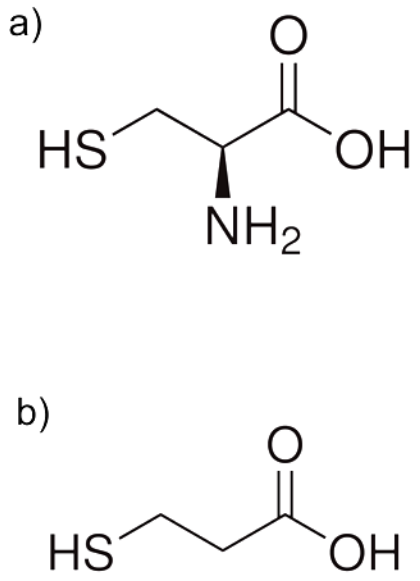

Figure 3.4. Linkers used in this study, a) L-Cysteine and b) 3-mercaptopropionic acid

The cysteine (L-Cys, Sigma W326305) and 3-mercaptopropionic acid (Sigma M5801) solutions were prepared using anhydrous ethanol as solvent. The approximate concentrations of both were 50 μM.

3.4.3. Nickel (II) Chloride solution preparation

Recombinant hemoglobin I from *Lucina pectinata* possesses a histidine-tag added by directed mutagenesis techniques, containing imidazole rings of high electron density that are used for purposes of purification.

Immobilized-Metal Affinity Chromatography (IMAC) is a separation technique that uses covalently bound chelating compounds on solid chromatographic supports to entrap metal ions, which serve as affinity ligands for various proteins, making use of coordinative binding of some amino acid residues exposed on the surface. In IMAC the adsorption of proteins is based on the coordination between an immobilized metal ion and electron donor groups from the protein surface. Most commonly used are the transition-metal ions Cu(II), Ni(II), Zn(II), Co(II), Fe(III), which are electron-pair acceptors and can be considered as Lewis acids. Electron-donor atoms (N, S, O) present in the chelating compounds that are attached to the chromatographic support are capable of coordinating metal ions and forming metal chelates, which can be bidentate, tridentate, etc., depending on the number of occupied coordination bonds. The remaining metal coordination sites are normally occupied by water molecules and can be exchanged with suitable electron-donor groups from the protein. In addition to the amino terminus, some amino acids are especially suitable for binding due to electron donor atoms in their side chains. Many residues, such as Glu, Asp, Tyr, Cys, His, Arg, Lys and Met, can participate in binding (Gaberc-Porekar and Menart, 2001; Arnold, 1991; Sulkowski, 1989).

In our case, we have a surface "multidentate" due to the large number of cysteine or 3-mercaptopropionic acid molecules that are present with carboxyl (and amino groups in Cys) outward surface. In general, tetradentate ligands, such as nitriloacetic acid (NTA) and TALON (trade name for carboxymethylated aspartic acid: CM-Asp), have higher affinities for metal ions than the tridentate chelator iminodiacteic acid (IDA). Putative structures of metal ion complexes with an octahedral arrangement around a divalent metal are shown in Fig. 3.5.

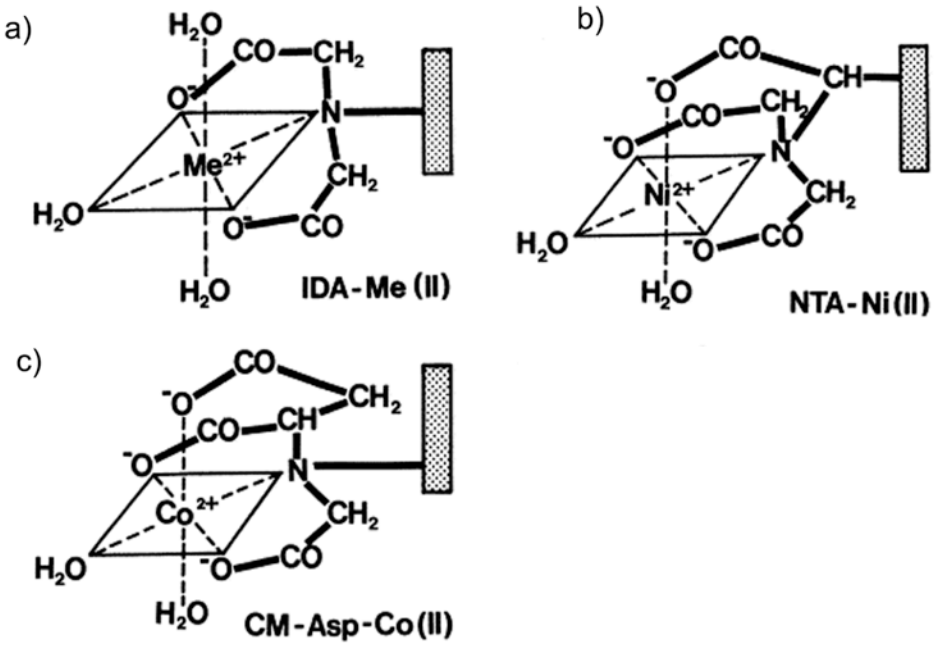

Figure 3.5. Structures of some representative chelators in complex with usually used metal ions: IDA–Me(II), NTA–Ni(II), CM–Asp–Co(II), TED–Me(II). Me(II) stands for Cu(II), Ni(II), Zn(II) or Co(II). Spacers to the solid support are not specified, but may vary in length and chemical structure. Water molecules can be replaced by other ligands, usually histidines exposed on the protein surface. (This figure is a modification of Gaberc-Porekar and Menart, 2001)

The 50 mM $NiCl_2$ solution was prepared by dissolving 1.188 g $NiCl_2.6H_2O$ (Sigma 31462) in deionized water in a 100 mL volumetric flask.

3.5. Preparation of recombinant Hemoglobin I electrode

3.5.1. Preparation of Linker Self-Assembled Monolayer

Self-assembly of linkers (Cysteine or 3-mercaptopropionic acid) were done on gold surfaces using MAXTEK® gold substrates and commercial Au disk electrodes (BASi) of 1.6 mm of diameter. These monolayers were prepared by immersing a clean gold electrode in a vial containing 0.5 mL of an ethanolic solution of 50 μM of linker for 24 h. Nitrogen was used for degassing the solutions, and the vials were sealed and left unperturbed during the modification period. Afterward, the substrates obtained were washed with ethanol, dried under a nitrogen flow and maintained in a desiccator for further characterization. The surfaces are described as Cys/Au or 3-MPA/Au for the cysteine or 3-mercaptopropionic acid modifications on gold surfaces in the rest of the manuscript, respectively.

3.5.2. Recombinant Hemoglobin I modified electrode preparation

The surfaces Lnk/Au were immersed into 50 mM $NiCl_2$ aqueous solution for 2 h. Then, the surfaces were rinsed with deionized water and dried under nitrogen flow for further analysis. After, the modified electrodes (Ni^{2+}/Lnk/Au) were left into a 100 μM rHbI aqueous solution for 72 h to obtain the hemoglobin I modified gold surface. The electrodes were stored in phosphate buffer pH 6.70 at 4°C until electrochemical analysis, and the modified surfaces corresponding to quartz-polycrystalline gold plates in a desiccator for surface examination. All the modification process is depicted in Scheme 3.1.

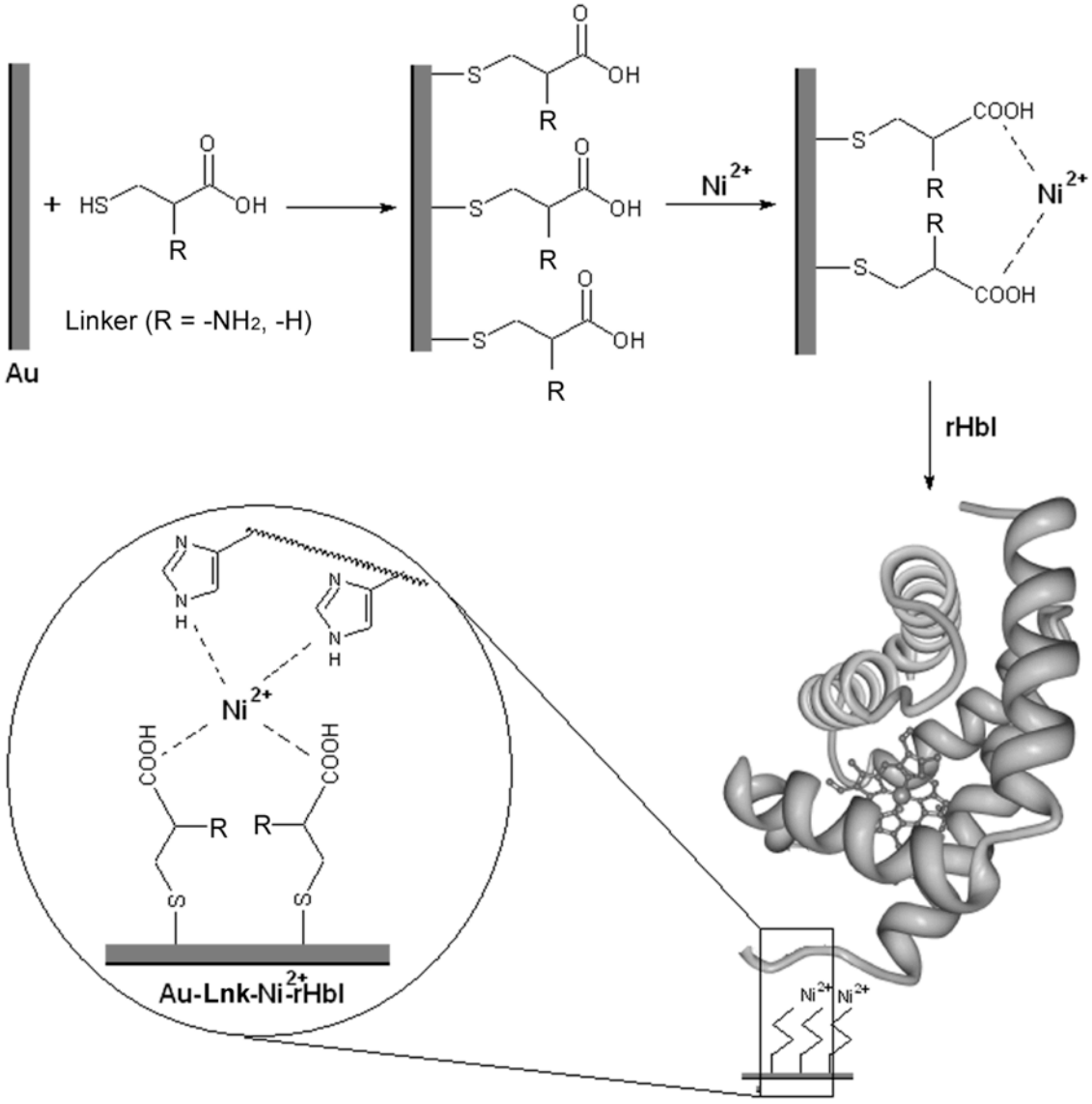

Scheme 3.1. Representation of the modification process of the gold electrode with the linker (Cys or 3-MPA), nickel ion and recombinant hemoglobin I.

4. CYSTEINE-GOLD ELECTRODE MODIFIED WITH HEMOGLOBIN I AND H_2S QUANTIFICATION

4.1. Introduction

Hydrogen sulfide, H_2S, is a colorless, toxic, flammable gas that is responsible for the foul odor of rotten eggs. It often results when bacteria break down organic matter in the absence of oxygen, such as in swamps, and sewers. It also occurs in volcanic gases, natural gas and some well waters (Giggenbach, 1971). Is considered a broad-spectrum poison, do to the fact that it can poison several different systems in the human body, although the nervous system is most affected.

The detection of hydrogen sulfide has gained significant importance within analytical and biomedical communities as a consequence of its toxicity and the corresponding risk associated. Many techniques have been commonly used for its analysis, but it is difficult to get sensors sufficiently stable for exposing them directly to real samples due to decomposition of the electroactive substances, or instability of the formed complexes. Other inconveniences are the poisoning of the electrode surface and the slow removal of modifiers from the surface. Another problem encountered is the commercial unavailability of some modifiers, which limits their extensive application (Bakker and Qin, 2006). Currently most H_2S analysis are performed using selective membrane electrodes by polarographic techniques based on the specific electrochemical reaction of HS^- ion formed in the first dissociation of H_2S gas dissolved in water with the redox couple $Fe(CN)_6^{3+}/Fe(CN)_6^{4+}$. This polarographic hydrogen sulfide sensor, background current resulting from electrolytic conduction of current from cathode to anode occurs as ferricyanide is reduced at the cathode and oxidized at the anode. Because the cathode

potential is not as negative as the equilibrium potential of HS^{-}, the ferricyanide reduction rate is less than the signal current resulting from sample H_2S (Doeller *et al.*, 2005). Some of the disadvantages of this system are: the time resolved of the analysis and signal stabilization are extremely large, analyte measurements are achieved indirectly by HS^{-} ion detection, weak and fragile membrane, and the large size equipment required.

On the other hand, short-chain alkanethiols, has been widely used where cysteine is one of the most common linker used for the manufacture of commercial biosensors. Cysteine (Cys) is a non-essential amino acid where the thiol group provides the bond to gold surfaces where the amino and carboxyl moieties are oriented away from the surface of the electrode (Hager and Brolo, 2003). Some of the most relevant applications where gold-cysteine surface is involved are the detection of cytochrome c (Qian and Zhuang, 1998), chiral discrimination between 3,4-dihydroxyphenylalanine isomers (Zhang *et al.*, 2004) and studies of electron transfer involving protein-promoter complexes (Matsunaga *et al.*, 2007). Also cysteine has a thiol group that is excellent for bonding to gold surfaces, leaving the carboxyl and amino groups exposed to coordinate with metal ions (Arrigan and Bihan, 1999; Zen and Kumar, 2001). Immunoproteins have been assembled and immobilized on gold-cysteine surfaces by using these free amino and carboxyl groups (Baldrich *et al.*, 2008).

From this previous information, we can deduce that it is possible to immobilize some biomolecules in order to prepare new sensors. This suggests that several proteins can be linked and immobilized to a surface or support through the formation of covalent bonds between one or more amino acids of the biomolecule with the surface. We also can attach an intermediate linker that has one extreme bonded tightly to the metal surface and the other extreme of the linker to the protein molecule. Generally, these proteins have groups of

high electron density allowing them to establish such links. Recombinant hemoglobin I from *Lucina pectinata* possesses a histidine-tag added by directed mutagenesis techniques, containing imidazole rings of high electron density that are used for purposes of purification. The nickel or cobalt ions present in commercial resins are responsible for the binding process to these proteins. Complexing the nickel ions to the gold-cysteine surfaces allow to bind the hemoglobin by the histidine-tag. This special characteristic of rHbI allows us to postulate it as a protein for the design of a potential biosensor in the quantification of H_2S. This study presents the modification of a gold surface with cysteine, nickel ion (Ni^{2+}) and recombinant hemoglobin rHbI using spectroscopic and electrochemical techniques. Hemoglobin rHbI was used because it contains the histidine-tag, required for the bond formation between the nickel ion and the protein, in contrast to HbI wild type that does not have it. The cyclic voltammetry was used to confirm the modification process, and the electrochemical response of the electrode according to hydrogen sulfide concentration.

4.2. Characterization of Cysteine-Gold electrode with Hemoglobin I

4.2.1. XPS characterization

X-ray photoelectron spectroscopy (XPS) was used to characterize the monolayer Cys/Au when the gold surface was exposed to a cysteine solution in anhydrous ethanol for 24 hours. Similarly, this technique was used to establish the presence of Ni^{2+} ion and formation of the surface Ni^{2+}/Cys/Au when the monolayer was placed in a solution of $NiCl_2$ to form the complex between cysteine and Ni^{2+} ions. The XPS binding energy spectra of the (a) clean gold and (b) treated with 50 mM cysteine in ethanol are shown in Fig. 4.1.

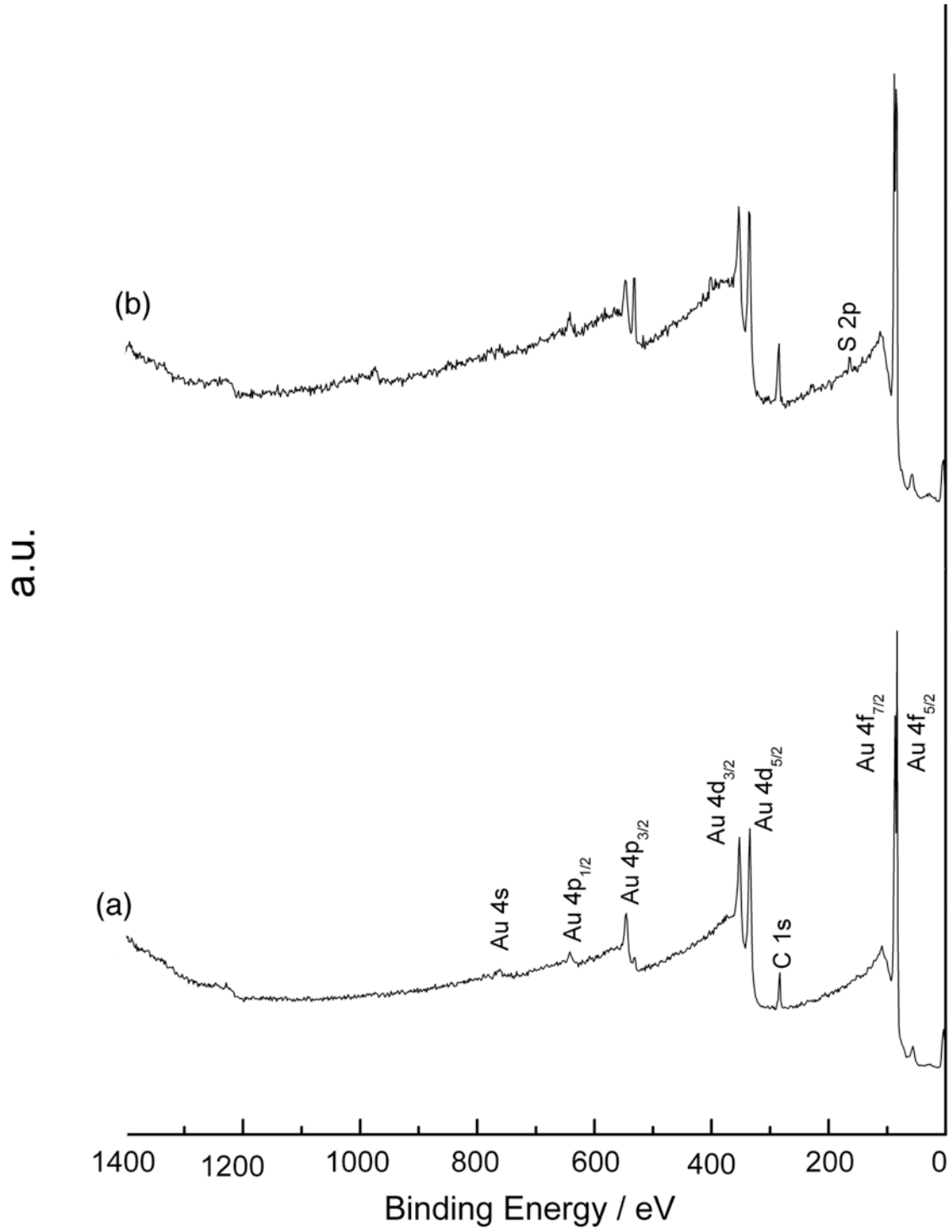

Figure 4.1. Wide-scan XPS spectra for the (a) clean gold and (b) Cys/Au electrode systems.

The spectrum in Fig. 4.1b presents the binding energy peaks that were attributed to Au4f, C1s, O1s, S2p, which are present in the gold surfaces treated with the Cys solution. The XPS spectrum in Fig. 4.1a, has the same XPS signals as that presented for the Cys/Au modified surface, with the exception of the S signal. The S binding energy peaks confirm the modification of the gold surface with Cys. This is typically observed when the compound is adsorbed at the Au surface through the thiol group. Figure 4.1a shows that the C1s signal corresponding to the clean gold is present, and this is possibly due to the contamination of the environment with organic compounds, which can have the same or higher number of carbon atoms compared with cysteine (Ratner, 1997). Also, Fig. 4.2(I) shows a HRXPS comparison between (a) Au and (b) Cys/Au in the S2p region, denoting the difference in signal for both spectra due to appearance of a broad peaks centered approximately at 163 eV in Cys/Au spectrum, corresponding to one doublet ($S2p_{3/2}$ and $S2p_{1/2}$) with a peak separation of 1.2 eV and area ratio 2:1. These peaks may deconvolution while maintaining the above characteristics in terms of splitting and area ratio, using Gaussian curves. This doublet consists of two components, S1 and S2, where the main component S1 occurs at 161.2 eV while the minor one, S2, is found at 163.3 eV (Fig. 4.2(II)). The main component S1 is attributed to Cys molecules chemisorbed on gold and indicates the formation of a thiolate species. This component is characteristic of organosulfur compounds on gold reported for cysteine (Dodero *et al.*, 2000; Cavalleri *et al.*, 2001) and for thiols with unsubstituted alkyl chains and with chains containing aromatic moieties. The second component S2, located near 164.0 eV could be assigned to Cys molecules not bound to gold, that is, physisorbed molecules forming a partially occupied upper layer (Yang and Fan, 2002). In addition, Fig. 4.2(III) shows a HRXPS comparison for (a) Au and (b) Cys/Au surfaces in C1s region.

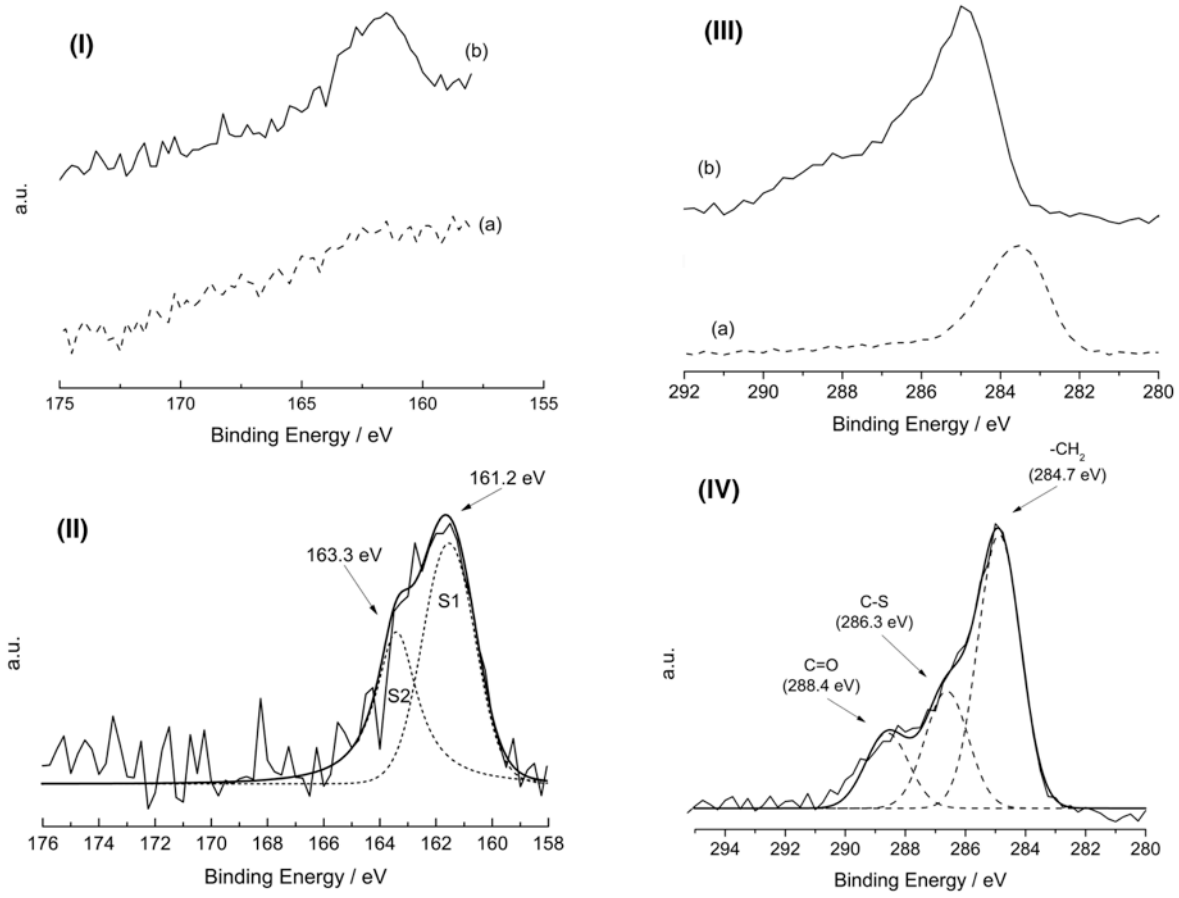

Figure 4.2. XPS spectra of the (a) clean gold and (b) Cys/Au in S2p and C1s binding energy regions. (I) and (III): High-resolution X-ray photoelectron spectra for unmodified (dash line) and Cys modified gold (solid line) surface at S2p and C1s binding energy regions, respectively. (II) and (IV): Curve fitted high-resolution X-ray photoelectron spectra for S2p and C1s binding energy regions for Cys/Au surface, respectively.

In Cys/Au spectrums, it is observed the formation of several overlapping peaks that are not present in clean gold. Fig. 4.2(IV) shows the deconvolution to the peaks present in the signal in the region C1s, and it is evidence the presence of characteristic peaks for the -CH_2 groups (284.8 eV), C-S (286.3 eV) and C=O (288.4 eV) (Dodero *et al.*, 2000; Cavalleri *et al.*, 2001). This definitely confirms the adsorption of the cysteine on the gold surface. Furthermore, to confirm clearly the presence of Cys on the gold surface in Cys/Au assembly, a high resolution spectra in Au4f and O1s regions were performed. Fig. 4.3(A) shows the comparison between the spectra in the region Au4f for (a) Cys/Au surface and (b) clean gold. The spectrum corresponding to Cys/Au surface (a) shows a well-defined doublet with a peak separation of 3.6 eV and a half-width of 1.6 eV. The peak $Au4f_{7/2}$ shows a binding energy of 84.0 eV which is the typical value expected when thiolate forms self-assembled monolayers on Au surfaces. Furthermore, decrease on the peak height and area is an indication that these compounds are adsorbed on the gold surface blocking the XPS detection of Au4f photoelectrons. The high resolution XPS spectrum for O1s region in Fig. 4.3(B) shows a slightly asymmetric broad peak centered about at 532 eV for Cys/Au surface. This peak can be formed by the contribution of the oxygen of the carboxyl and -OH groups, previously reported in the literature (Aryal *et al.*, 2006). In addition, this slight asymmetry may be is due to the presence of water molecules coadsorbed by the surfaces. The oxygen (O1s) and carbon (C1s) signals, which appear on the clean gold surface, correspond to contaminants from the air, from the cleaning process, or from handling of the substrate (Ratner, 1997). Moreover, the surface modification obtained between Cys/Au surface with Ni^{2+} ions was followed by XPS.

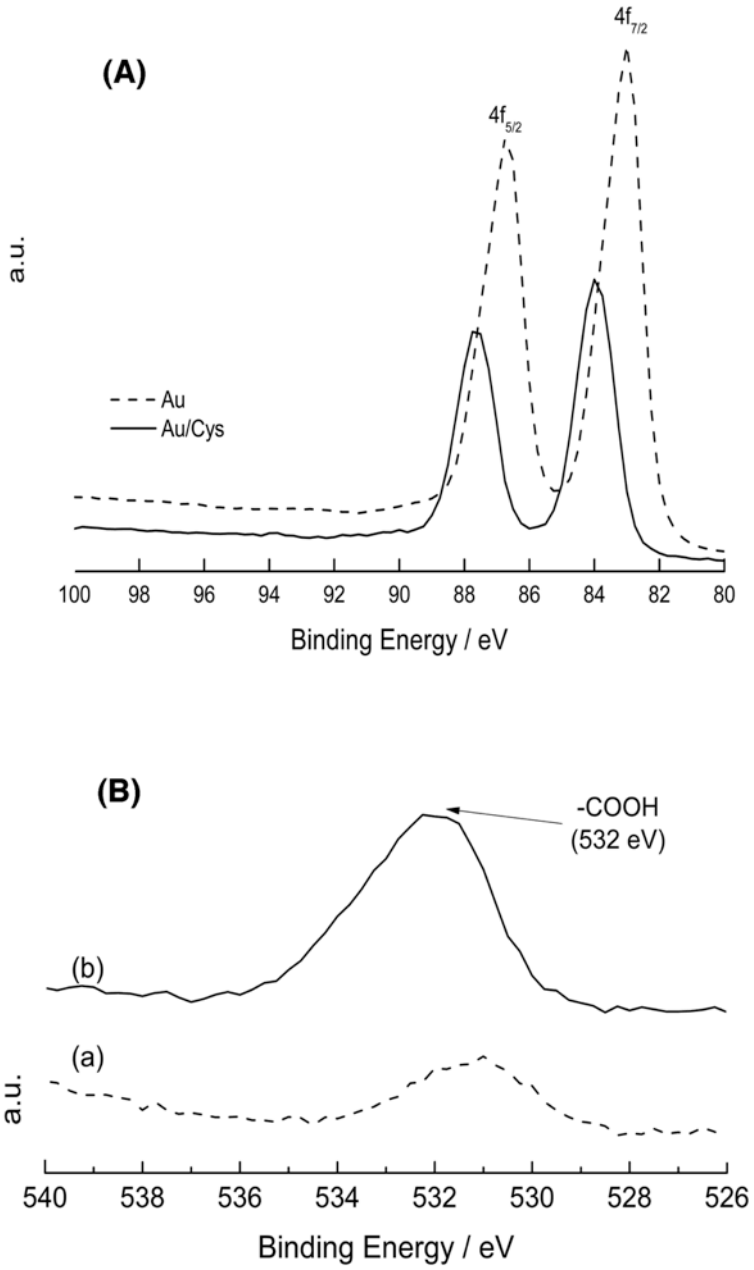

Figure 4.3. XPS spectra of the clean gold and Cys/Au in (A) Au4f and (B) O1s binding energy regions.

Fig. 4.4 presents the curve-fitted HRXPS spectrum for the binding energy region of Ni2p in the modified surface Ni^{2+}/Cys/Au. The Ni2p peaks appear at binding energies of 856 eV (Ni–O) and 861 eV (satellite peak) consistent with previously reported in the literature (Nesbitt *et al.*, 2000), indicating the presence of a Ni–O bond on the modified Cys/Au surface.

For hemoglobin-modified surface rHbI/Ni^{2+}/Cys/Au, was not possible to detect either the presence of Ni^{2+} ions from a Ni^{2+}–N (histidines) bond or the presence of iron from the porphyrin under these analysis conditions. Eventually, the body volume of the hemoglobin may interfere with the penetration of X-rays, acting as a multilayer composite where bonds cannot be observed in lower layers. This surface was analyzed with different take-off angles and the results were similar.

4.2.2. Cyclic Voltammetry and amperometric studies

Figure 4.5 shows the differences between the voltammograms for gold electrode modified with cysteine (dashed line), nickel ion (dotted line) and hemoglobin I (solid line) in phosphate buffer solution pH 6.70. In Cys/Au assembly a progressive oxidation current increase from 400 to 600 V vs. Ag/AgCl is observed when compared with the gold bear, suggesting the presence of cysteine on the metal surface. Previous work has already recognized and characterized this kind of surfaces (Brito *et al.*, 2004; Laiho *et al.*, 2003). When this surface interacts with the nickel ions, are observed broad oxidation and reduction peaks, which possibly can be attributed to the strong interaction between the carboxyl groups with nickel ions.

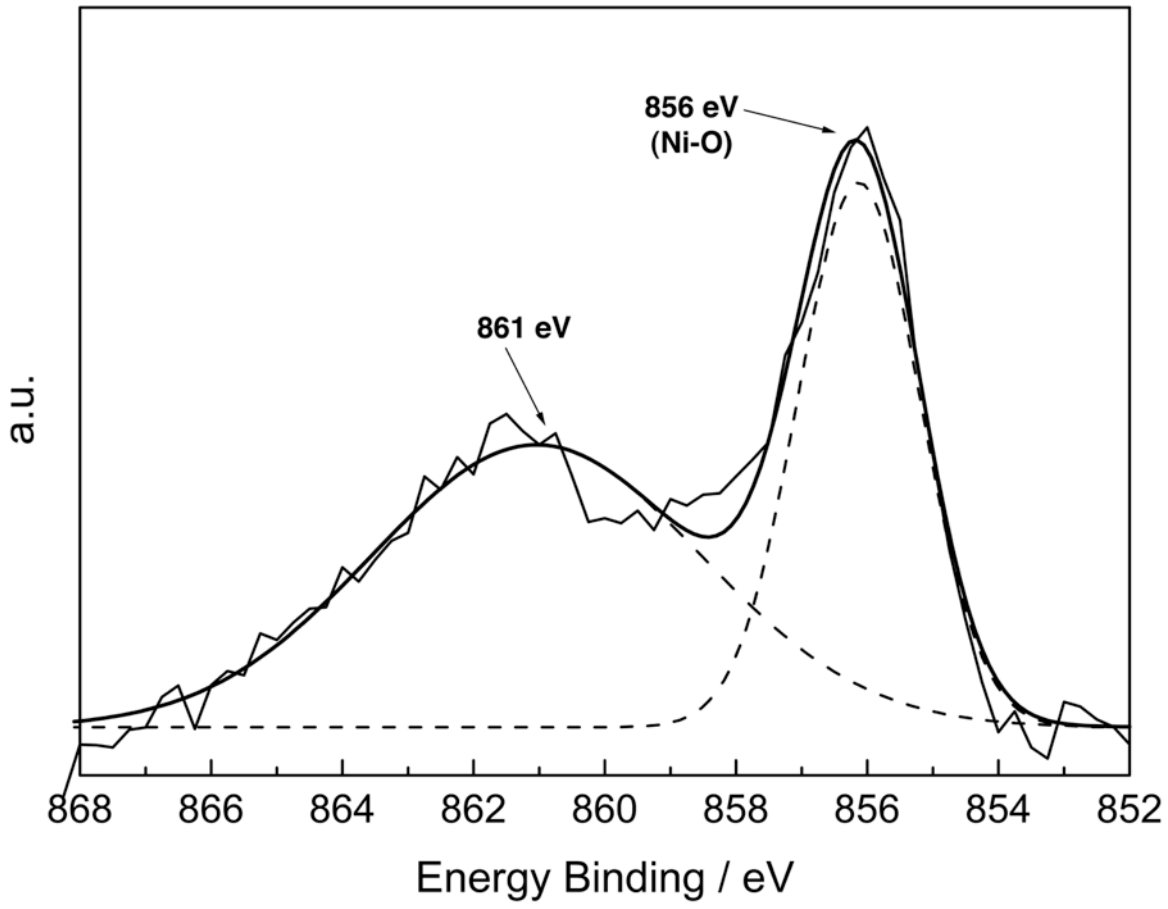

Figure 4.4. Curve-fitted high-resolution XPS spectrum Ni2p region in Ni^{2+}/Cys/Au surface. The binding energy assigned to Ni-O bond is at 855 eV and a satellite peak observed at 861 eV, characteristic of the species containing Ni-O bond.

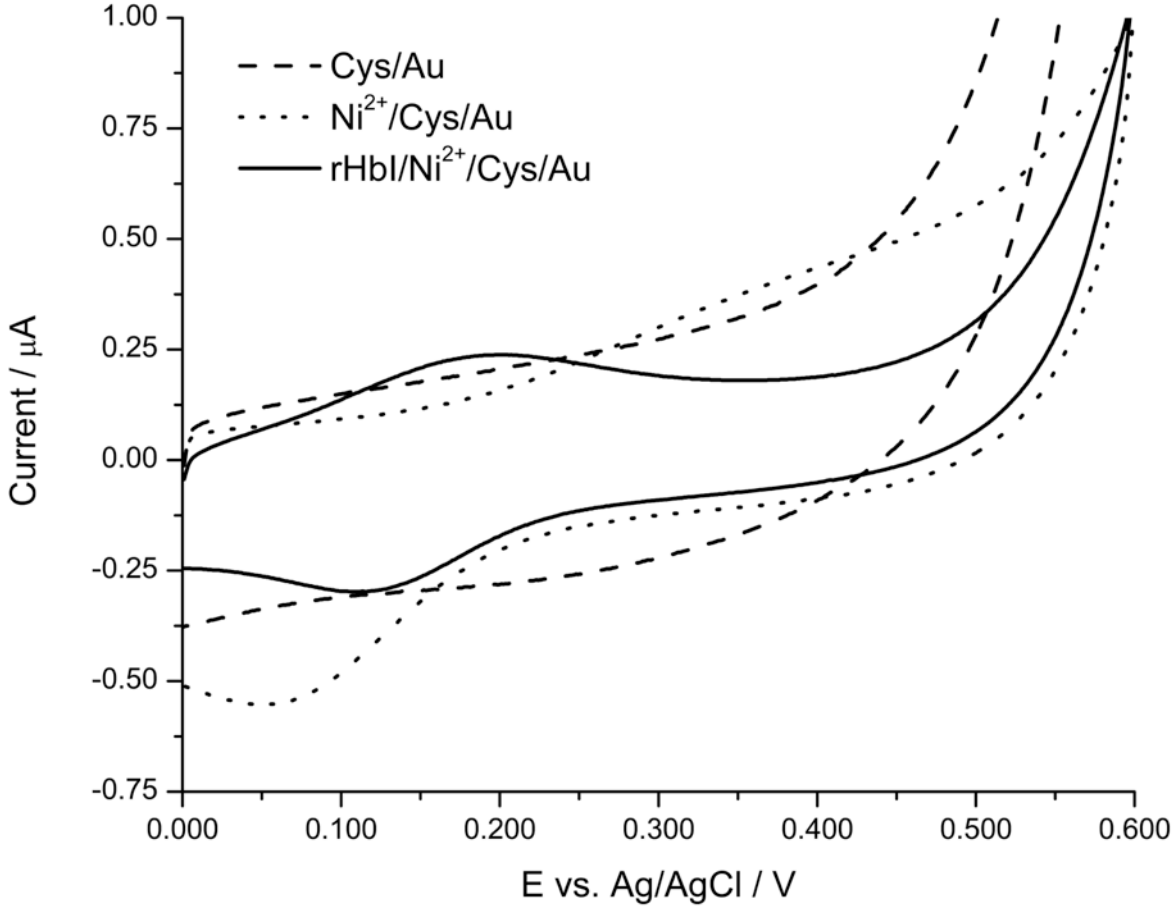

Figure 4.5. Cyclic voltammograms of Cys/Au (dashed line), Ni^{2+}/Cys/Au (dotted line) and rHbI/ Ni^{2+}/Cys/Au (solid line) electrodes in phosphate buffer solution pH 6.70 at scan rate 100 mVs^{-1}.

It is well established that the complex formation concerning proteins histidine-tagged with resins containing nickel or cobalt ions can be used for purposes of purification (Hemdan and Porath, 1985; Bush *et al.*, 1991). Histidines exhibit highly selective coordination with nickel and cobalt ions and under physiological pH conditions, bind by non-bonding electron pairs of the imidazole nitrogens with the half empty orbitals of these ions. Originally, the modification of Ni^{2+}/Cys/Au with rHbI was more convenient to be done at weakly basic pH (at 7.50) to favor the formation of a covalent bond between the imidazoles of histidine-tag of recombined hemoglobin and nickel ion-cysteine complexes. Then, this structure was exposed to recombinant hemoglobin for 72 h, producing a drastic change in the voltammogram (Fig. 4.5, solid line) showing a redox couple. The half wave potential ($E_{1/2}$), calculated from the average value of the anodic (E_{ox} = 0.177 V vs. Ag/AgCl) and cathodic peak (E_{red} = 0.250 V vs. Ag/AgCl) potentials, is 0.213 V vs. Ag/AgCl ($E_{1/2}$ = 0.004 V vs. NHE). In the literature there is diverse data about different redox potentials of heme proteins when used in different media. As reference hemeprotein we used myoglobin, because they are structurally similar. Table 4.1 summarizes some of the redox potentials found for myoglobin in different media surfaces. The potential obtained for rHbI is close to values reported in the table 4.1. It is noted that the potentials vary between the different forms of immobilization of myoglobin, and that it is due to changes in the environment where they are analyzed and the different media used. Hemoglobin I from *Lucina pectinata* and myoglobin are monomeric and globular hemoproteins having similarities in their amino acid sequence, and both proteins in the metaquo form (ferric state) have similar spectral properties. Although these proteins are structurally very similar, they differ in the internal amino acids composition around the heme group.

Table 1. Redox potential of myoglobin immobilized on some supports or surfaces.

Myoglobin supports	**$E^{\circ\prime}$ (V) vs. NHE**
Nanoporous ZnO[a]	–0.053
Myoglobin-Au-ITO[b]	–0.007
Colloidal gold nanoparticles[c]	–0.131
Ni/NiO[d]	0.0895
Sol-gel[e]	–0.099

[a]Zhao *et al.*, 2006; [b]Zhang and Oyama, 2005; [c]Yang *et al.*, 2006; [d]Ganjali *et al.* 2008; [e]Gongxuan *et al.*, 2004

On the other hand, this rHbI-electrode achieved good response when the sodium sulfide solution is added. Fig. 4.6 shows the cyclic voltammetric behavior of the rHbI/Ni^{2+}/Cys/Au electrode observing a decrease of anodic and cathodic currents. Previous works have shown that rHbI has the ability to bind hydrogen sulfide obtained from a sodium sulfide solution. When Na_2S is added to a buffer solution pH<6.9, hydrogen sulfide is released (Pietri *et al.*, 2009). The H_2S concentrations were calculated based on the H_2S dissolved in the solution, which is only one component of the total sulfide equilibrium. The equation involved in the calculation corresponding to the total sulfide equilibrium system is $[H_2S] = [Na_2S] / \{1+(K_1/[H^+])+(K_1K_2/[H^+])\}$, where $pK_1 = 6.89$ and $pK_2 = 19$ (Giggenbach, 1971). In our case, the equilibrium of H_2S system from sodium sulfide is shifted toward the formation of H_2S because the pH of the solution is less than pK_1.

The decreasing in anodic and cathodic currents during consecutives voltammetric cycles as consequence of the addition of sodium sulfide is an indication of the interaction of the hemoglobin molecules on the modified surface with the hydrogen sulfide produced in solution.

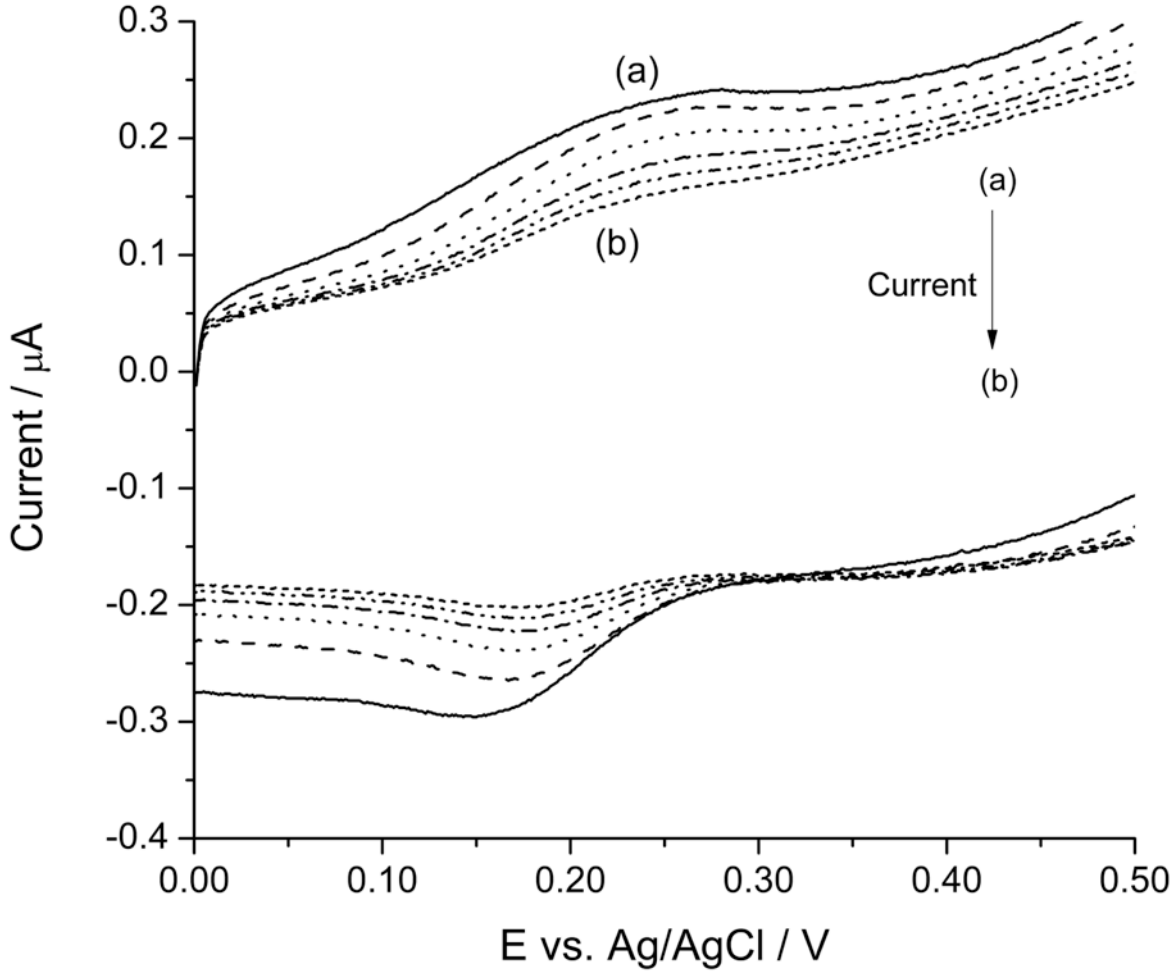

Figure 4.6. Cyclic voltammetric behavior of the rHbI/Ni^{2+}/Cys/Au electrode when 20 μM Na_2S solution is added to 0.1 M phosphate buffer solution pH 6.70 at 100 mV/s, producing H_2S concentrations of (a) 0 nM to (b) 400 nM.

As the concentration of hydrogen sulfide increases with the successive addition of sodium sulfide to the weakly acid buffer solution, the voltammograms reaches constant waves. This behavior suggests that the heme pocket for hemoglobin molecules are binding hydrogen sulfide molecules, reaching saturation. It is well known that hemoglobin molecules are associated with hydrogen sulfide to form the complex rHbI-H_2S (Pietri *et al.*, 2009):

$$\text{rHbIFe(III)} + H_2S \leftrightarrows \text{rHbIFe(III)}{-}H_2S$$

Likewise, this behavior indicated that the rHbI kept its native structure capable to bind H_2S after being immobilized onto the electrode. Due to the fact that there is a change in the amplitude of the signal but there is no change in the potential range of the wave, we conclude that the oxidation number of hemoglobin remains constant. The form in which hemoglobin I is associated to H_2S has been studied previously (Kraus and Wittenberg, 1990; Rizzi *et al.*, 1996; Pietri, *et al.*, 2009), where it has been shown that the porphyrin preserves its oxidation state (rHbI metaquo, Fe^{+3}) when it interacts with H_2S. When an H_2S molecule binds to the hemoglobin-Fe^{3+}, forming the species rHbIFe(III)–H_2S, it apparently prevents it from performing the redox process $rHbIFe^{3+}$/$rHbIFe^{2+}$, because the link established between the ferric hemoglobin and hydrogen sulfide is stable. Therefore, this entails a decrease in hemoglobin concentration on the surface every time an H_2S molecule enters, this behavior being observed in the reduction of voltammetric wave currents.

Furthermore, the amperometric response of rHbI/Ni^{2+}/Cys/Au with successive additions of Na_2S to 0.1M phosphate buffer solution pH 6.70 is shown in Fig. 4.7. The linear response range of H_2S concentration was from 90 nM to 400 nM with a correlation coefficient of 0.993 (n = 7).

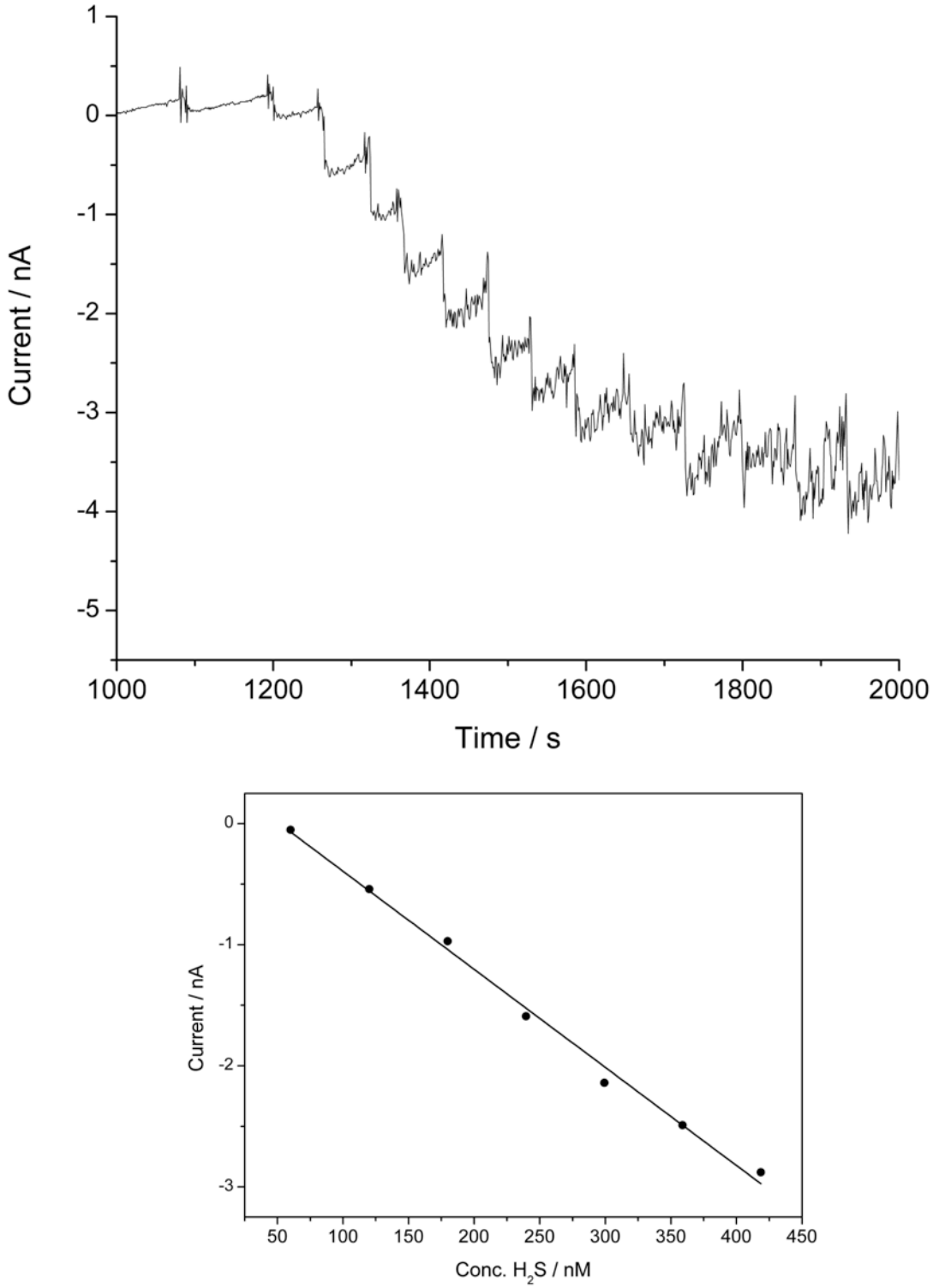

Figure 4.7. Top: Amperometric response of the rHbI/Ni^{2+}/Cys/Au in 0.1M phosphate buffer solution pH 6.70. Bottom: Calibration curve of current vs. H_2S concentration from the amperometric data.

From the slope of -0.0081 nA/nM, the lower limit of detection was estimated to be 27 nM at a signal to noise ratio of 3, and the lower limit of quantification of 89 nM. This electrode can be reused when is placed in a phosphate buffer solution pH 6.70 at 0.00 V vs. Ag/AgCl for 1 h or until the current stabilizes. Moreover, this electrode lost only 6% of its initial activity after more than four successive measurements and when it is stored in 0.1M phosphate buffer solution pH 6.70 at 4 °C, when not in use. Also, its relative response current was examined by checking periodically. The hemoglobin-modified electrode retained 95% of activity within a storage period of 30 days under these conditions, but after a storage period of 90 days the sensor showed loss of activity for H_2S. Also, the rHbI-electrode holds good response to a mixture of ions 1 mM Ca^{2+}, Na^{+}, K^{+}, NH_4^{+}, NO_3^{-}, SO_4^{2-}, Cl^{-}, Br^{-}, I^{-} and 100 mM PO_4^{-3} (from buffer). It should be emphasized that the higher the concentrations of these ions the more significant will be the loss of electrode activity. It is possible that hemoglobin has been denatured by high salinity. On the other hand, erratic response is observed when a small aliquot of a solution 1 mM CN^{-} was added to the buffer solution. Cyanide is a ligand that binds strongly to ferric ion forming a very stable complex with hemoglobin, and cannot be displaced by ligands such as O_2, NO or H_2S. Some publications in hemeproteins functionality and dynamic confirm this fact (Antonini and Brunori, 1971). On the other hand, when a small aliquot of 1 mM H_2O_2 is added to a phosphate buffer solution, a similar behavior is observed. Several recent studies demonstrate that monomeric hemeproteins similar to rHbI, may be associated with the ferric ion of the porphyrin (Griebenow *et al.*, 2011), but as the peroxide concentration increases, it could interact with any part of the assembly structure, showing an erratic response of the electrode. In conclusion, for the analysis of H_2S it is recommended that hydrogen peroxide and cyanide is removed from the solution, both of which can greatly

interfere with the analysis. The problem is that the iron from the porphyrin in these hemeproteins binds to these ligands in the ferric state, and the oxidation state does not change.

5. ELECTROCHEMISTRY OF HEMOGLOBIN I IMMOBILIZED ON A MODIFIED GOLD ELECTRODE WITH 3-MERCAPTOPROPIONIC ACID

5.1. Introduction

Self-assembled monolayers are arrangements of organic compounds on the surface of a solid. These monolayers are formed by the interaction between terminal functional groups and a surface, which can form the basis for nanoelectronic applications and biosensors. It has a particular interest for those molecules that show a dual chemical functionality for the formation of these monolayers. These molecules have a functional attaching group with high affinity for the substrate which forms a covalent bond; a hydrocarbon chain that acts as a bridge between the surface and the species of interest, and a terminal functional group that binds or interacts with the chemical species and determines the monolayer surface properties.

Several studies have detailed behavior of monolayers based on alkanethiols on gold surfaces formed by absorption from the solution. In these works it is presented that short-chain monolayers are less packed and less insulating than their counterparts long-chain, that are highly ordered and densely packed (Nuzzo *et al.*, 1987; Bain *et al.*, 1989; Porter *et al.*, 1987). On the other hand, many investigations have been focused on the immobilization of biomolecules using thiol monolayers on gold in order to construct devices to measure properties or chemical activity of biomolecules (Zhang *et al.*, 2004; Matsunaga *et al.*, 2007). In some cases, molecules such as enzymes or proteins are immobilized because of Au-thiol SAMs complexing properties for metal ions (Zen *et al.*, 2001; Arrigan and Bihan, 1999). After forming complexes with the monolayer, these metal ions have the ability to

coordinate with electron-rich groups that are found in proteins or enzymes (Baldrich *et al.*, 2008). In previous works the high affinity of metal complexes for amino groups from lysine or histidine of the proteins or enzymes have been demonstrated (Aravinda *et al.,* 2009; Johnson and Martin, 2005).

Because hemoglobin I from *Lucina pectinata* presents high affinity for hydrogen sulfide, it was used as the species that binds H_2S in our electrode. Apart from the results obtained for the electrode modified with recombinant hemoglobin I using cysteine as linker, a gold electrode modified with 3-mercaptopropionic acid as linker was prepared. The intention of this change in the linker was to observe if the electrochemical response of the electrode changed, and to perform the electrokinetic analysis that allow us to learn more about the electrochemistry of the hemoglobin immobilized and evaluate the stability of the sensor during operation. Furthermore, the H_2S response using this modified electrode (3-MPA/rHbI) was evaluated and compared with the cysteine/rHbI electrode.

5.2. Analysis of 3-MPA/Au electrode with rHbI

5.2.1. XPS Characterization

In order to characterize the binding mode 3-MPA molecules on the Au surface, an XPS study of the layer formed after 24 h of modification from the ethanolic solutions of this substrate was performed. In addition, the formation of metal complexes between 3-MPA with Ni^{2+} ions when the modified surface (3-MPA/Au) was left in a 50 mM $NiCl_2$ solution for 24 h, obtaining Ni^{2+}/3-MPA/Au surface was studied. Figure 5.1 shows the comparison of the spectra between (a) 3-MPA modified surface and (b) clean gold, in regions S2p and C1s.

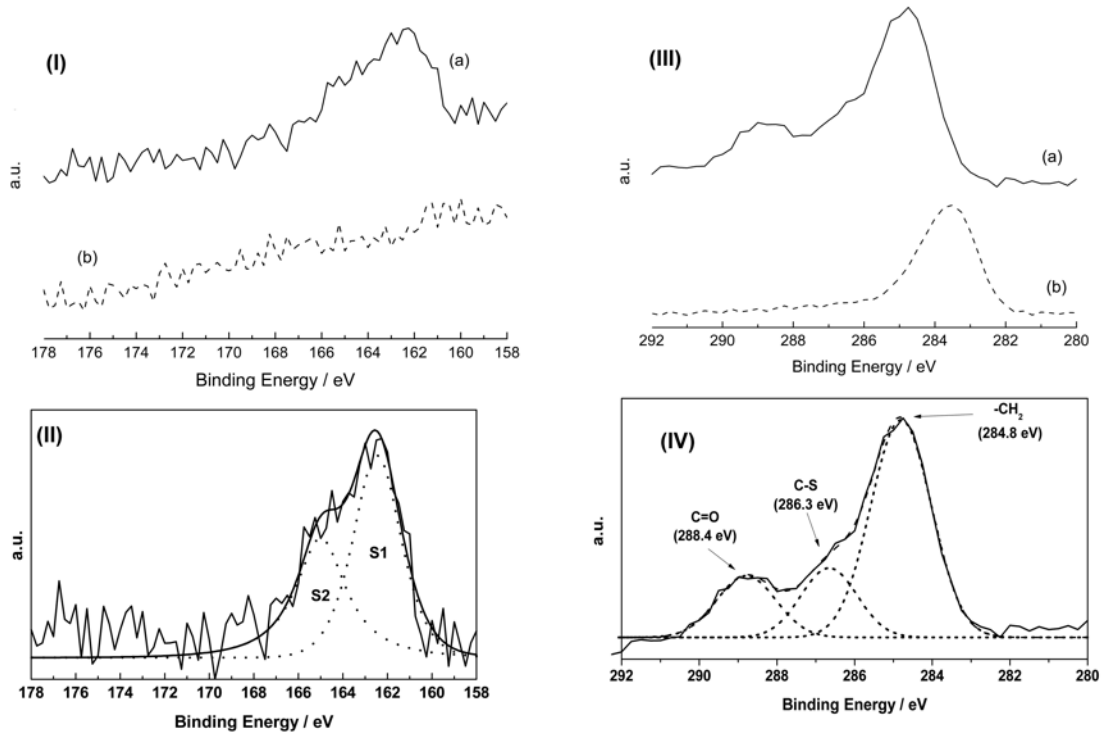

Figure 5.1. XPS spectra of the (a) 3-MPA/Au and (b) clean gold in S2p and C1s binding energy regions. Inset (I) and (III): High-resolution X-ray photoelectron spectra for unmodified (dash line) and 3-MPA modified gold (solid line) surface at S2p and C1s binding energy regions. Inset (II) and (IV): Curve fitted high-resolution X-ray photoelectron spectra for S2p and C1s binding energy regions for 3-MPA/Au surface. Inset (I) y (II) corresponds to S2p energy region and Inset (III) and (IV) corresponds to C1s energy region."

In inset (I) in Figure 5.1 shows the difference in signals between Au and 3-MPA/Au, due to appearance of a broad peaks centered at approximately 163 eV in 3-MPA/Au spectrum, corresponding to one doublet ($S2p_{3/2}$ and $S2p_{1/2}$) with a peak separation of 1.2 eV and area ratio 2:1. These peaks may deconvolution while maintaining the above characteristics in terms of splitting and area ratio, using Gaussian curves. This doublet consists of two components, S1 and S2, where the main component S1 occurs at 162.3 eV while the minor one, S2, is found at 164.2 eV (Inset II, Fig. 5.1). The S1 component is attributed to 3-MPA molecules chemisorbed on gold and indicates the formation of a thiolate species. This component is characteristic of organosulfur compounds on gold reported for cysteine (Dodero *et al.*, 2000; Cavalleri *et al.*, 2001) and for thiols with unsubstituted alkyl chains and with chains containing aromatic moieties. The S2 component, located at 164.0 eV could be assigned to molecules not bound to gold, that is, physisorbed molecules forming a partially occupied upper layer (Yan and Fan, 2002).

Inset III in Fig. 5.1 shows the comparison of HRXPS spectra of C1s region for the Au and 3-MPA/Au surfaces. In 3-MPA/Au spectrums, it is observed the formation of several overlapping peaks that are not present in clean gold. Inset IV in Fig. 5.1 shows the deconvolution to the peaks present in the signal in the region C1s. It is evidence the presence of characteristic peaks for the $-CH_2$ groups (284.8 eV), C-S (286.3 eV) and C=O (288.4 eV) (Abdureyim *et al.*, 1999; Whelan *et al.*, 1999). This confirms the adsorption of the 3-MPA on the gold surface.

Furthermore, to confirm clearly the presence of 3-MPA on the gold surface in 3-MPA/Au assembly, a high resolution spectra in Au4f and O1s regions were performed. Inset I in Fig. 5.2 shows the comparison between the spectra in the region Au4f for (a) 3-MPA/Au surface and (b) clean gold.

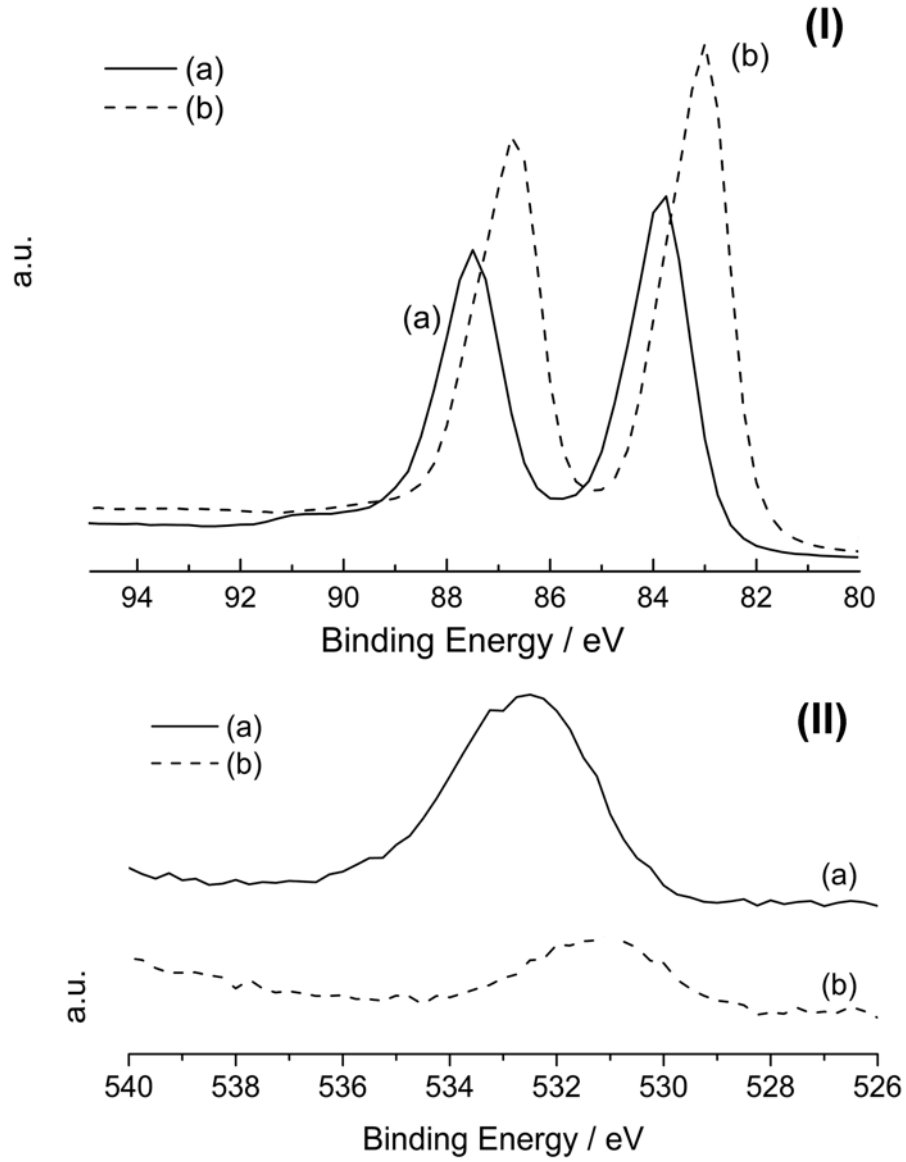

Figure 5.2. XPS spectra of the (a) 3-MPA/Au and (b) clean gold in Au4f and O1s binding energy regions. Inset (I): Au4f. Inset (II): O1s.

The spectrum corresponding to 3-MPA/Au surface (a) shows a well-defined doublet with a peak separation of 3.6 eV and a half-width of 1.6 eV. The peak $Au4f_{7/2}$ shows a binding energy of 84.0 eV which is the typical value expected when thiolate form self-assembled monolayers on Au surfaces. Furthermore, a decrease on the peak height and area is an indication that these compounds are adsorbed on the gold surface blocking the XPS detection of Au4f photoelectrons. The high resolution XPS spectrum for O1s region (Inset II in Fig. 5.2) shows a slightly asymmetric broad peak centered about at 532 eV for 3-MPA/Au surface. This peak can be formed by the contribution of the oxygen of the carboxyl and -OH groups, previously reported in the literature (Cavalleri *et al.*, 2001; Abdureyim *et al.*, 1999). In addition, this slight asymmetry may be is due to the presence of water molecules coadsorbed by the surfaces. The oxygen (O1s) and carbon (C1s) signals, which appear on the clean gold surface, correspond to contaminants from the air, from the cleaning process, or from handling of the substrate (Ratner, 1997).

Similarly, the bond formation between Ni^{2+} and 3-MPA/Au was followed by XPS analysis in the Ni2p region (Fig. 5.3). The Ni2p peaks appear at binding energies of 856 eV (Ni–O) and 861 eV (satellite peak) consistent with previously reported in the literature (Nesbitt *et al.*, 2000). This observation indicates the presence of a Ni–O bond on the both modified surfaces.

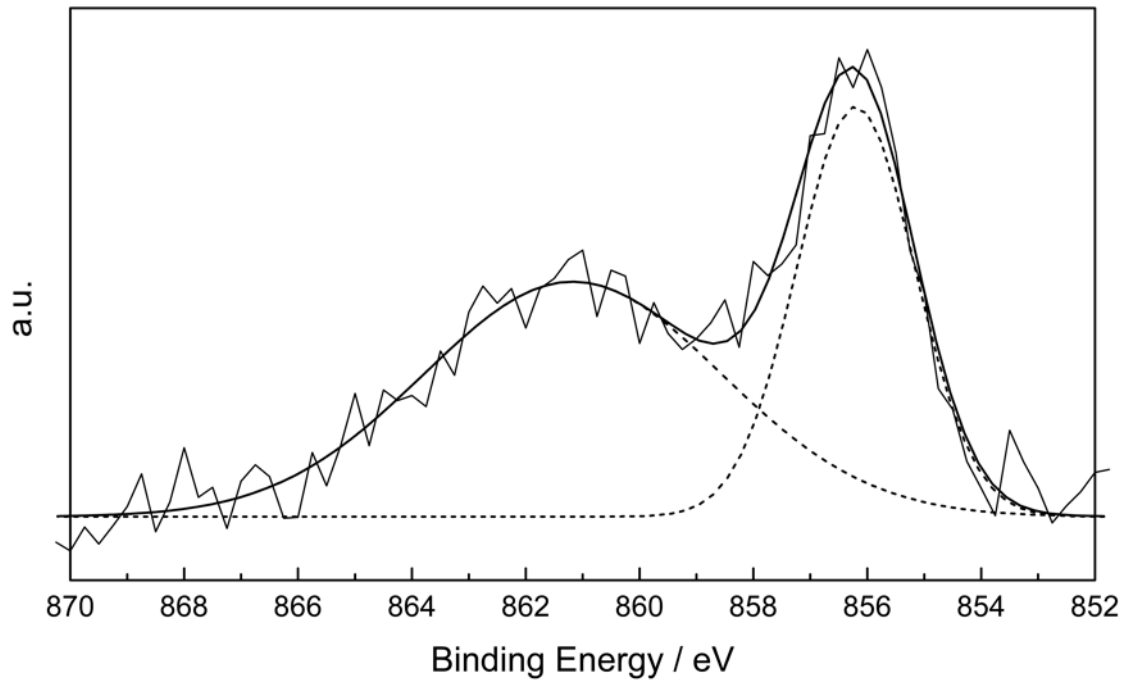

Figure 5.3. Curve-fitted high-resolution XPS spectrum Ni2p region in Ni^{2+}/3-MPA/Au surface. The binding energy assigned to Ni-O bond is at 855 eV and a satellite peak observed at 861 eV, characteristic of the species containing Ni-O bond (dashed lines correspond to the peaks deconvolution).

For the hemoglobin-modified surface rHbI/Ni^{2+}/3-MPA/Au, it was not possible to detect the presence of Ni^{2+} ions from a Ni^{2+}–N (histidines) bond or the presence of iron from the porphyrin under these analysis conditions. Eventually, the body volume of the hemoglobin may interfere with the penetration of X-rays, acting as a multilayer composite where bonds cannot be observed in lower layers. These surfaces were analyzed with different take-off angles and the results were similar.

5.2.2. FTIR analysis of the rHbI modified surface

FTIR analysis was conducted with the aim to verify the presence of the protein on the surface. The stages prior to hemoglobin-modified surface have already been extensively characterized by XPS, but due to the difficulty to obtain reasonable data for rHbI-modified surface by this technique, it was required to identify the amide bands (vibrational modes for $–COO^–$ and –NH) characteristic of hemoglobin by FTIR.

Fig. 5.4 shows the FTIR spectrum of rHbI-modified surface (rHbI/Ni^{2+}/3-MPA/Au). The peak near 1650 cm^{-1} is attributed to the amide I band of the protein as result from the C=O stretching vibrations of the peptide bond. Similarly, the peak at 1537 cm^{-1} (N-H bending vibration/C-N stretching vibration) corresponds to the amide II band of the protein. The peak near 3300 cm^{-1} is considered to be N-H bending vibration and the peak near 1400 cm^{-1} is from protein side-chain COO^-. This information confirms the presence of hemoglobin in the final stage of surface modification.

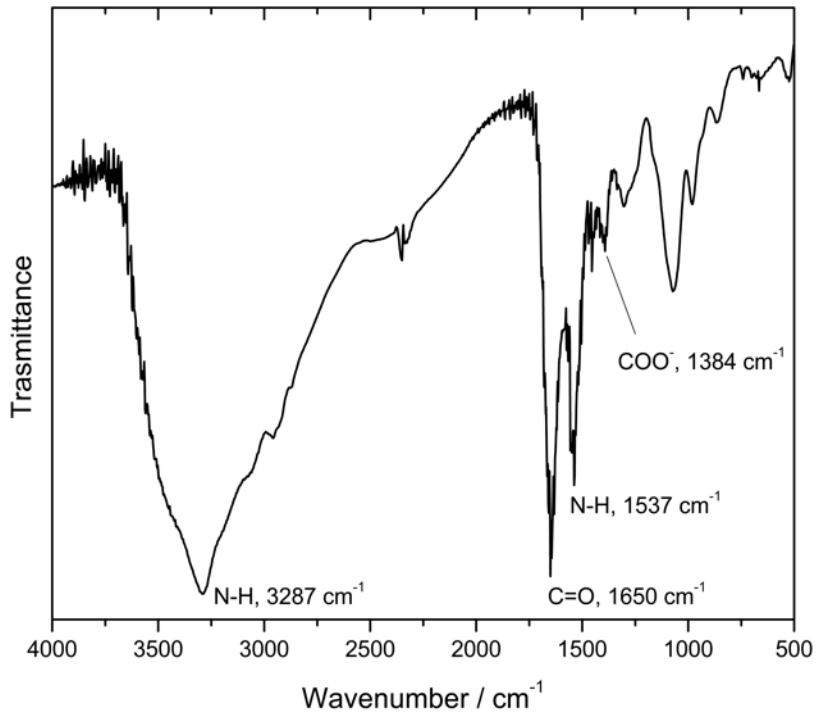

Figure 5.4. FTIR spectrum of rHbI/Ni^{2+}/3-MPA/Au surface. The bands observed at 1650 cm^{-1} and 1537 cm^{-1} corresponding to C=O (amide I band) and N-H (amide II band) of the protein, respectively.

5.2.3. rHbI immobilization on Ni^{2+}/3-MPA modified gold electrode

To establish the formation of the surface-modified hemoglobin comparative voltammograms of 3-MPA/Au (gold surface modified with 3-mercaptopropionic acid), Ni^{2+}/3-MPA/Au (3-MPA/Au modified with nickel ions) and rHbI/Ni^{2+}/3-MPA/Au (gold surface modified with the protein) were carried out. Voltammograms are shown in Figure 5.5.

It can be established that in this potential window, voltammetric signal is not observed for clean gold electrode. However, the 3-MPA/Au assembly shows a weak signal of a redox couple, which may be attributed to a rearrangement process on the surface by protonation of carboxyl groups, which may be interacting with the gold surface. This may occur when ethanol (used as solvent in the modification of gold surface) is removed causing an increase in the concentration of mercaptopropionic acid and inducing an interaction of the carboxyl groups with the gold surface. When this surface interacts with the nickel ions, it causes a decrease in the voltammetric current, possibly by the formation of a strong interaction between the carboxyl groups with the nickel ions. Then, this structure was exposed to recombinant hemoglobin for 72 h, producing a drastic change in the voltammogram showing a redox couple with an oxidation and reduction peaks at 0.229 V and 0.150 V vs. Ag/AgCl, respectively, at 100 mV/s. The difference between the two peaks is 79 mV, where the simplified equation for the electrochemical reduction of rHbI can be expressed as:

$$\text{rHbIFe(III)} + e^- \leftrightarrows \text{rHbIFe(II)}$$

The calculated formal potential is of 0.190 V vs. Ag / AgCl (–0.029V vs. NHE), comparable with other myoglobin-modified surfaces (Table 1).

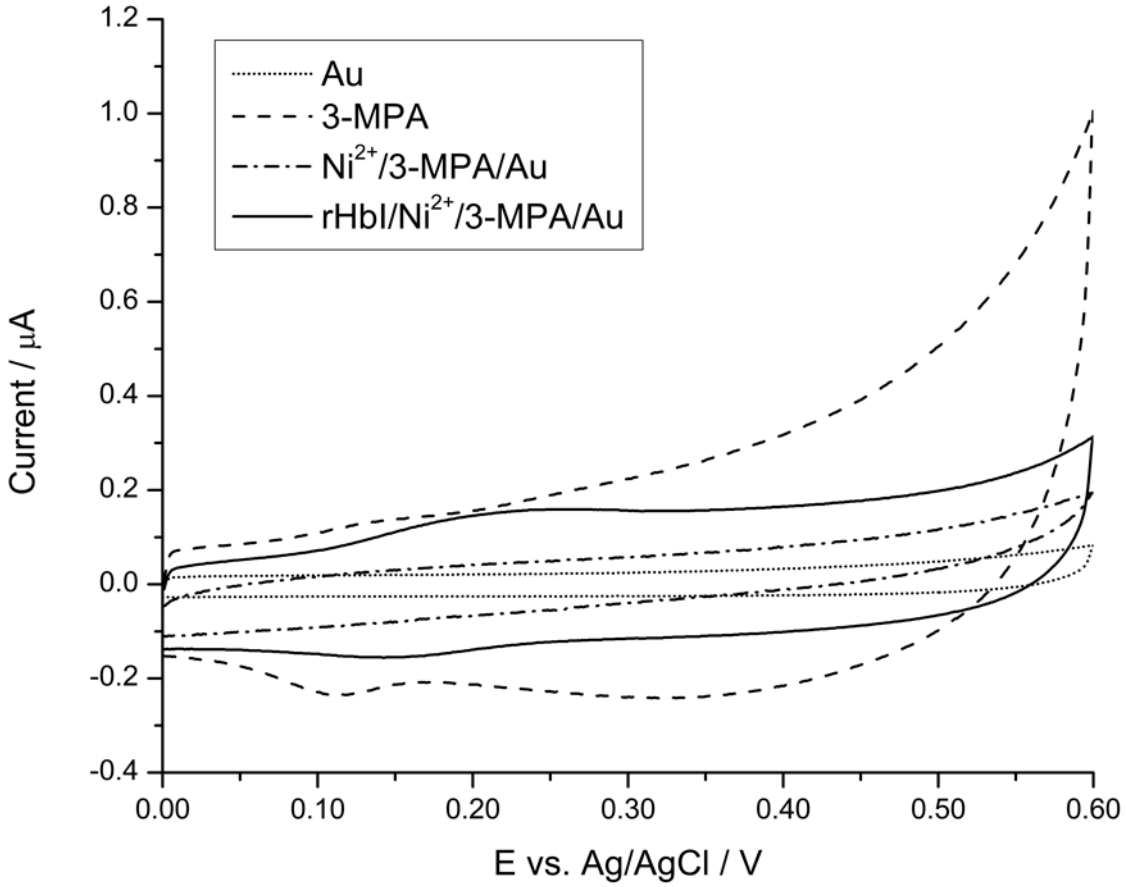

Figure 5.5. Cyclic voltammograms in 0.1 M phosphate buffer solution at pH 6.70 of gold electrode (dotted line), 3-MPA/Au (dashed line), Ni^{2+}/3-MPA/Au (dash-dotted line) and rHbI/Ni^{2+}/3-MPA/Au (solid line) modified electrodes at 100 mVs^{-1}.

Table 5.1. Comparison of the formal redox potential of myoglobin immobilized on various supports.

Myoglobin supports	***$E^{\circ'}$ (V) vs. NHE***
Nanoporous ZnO[a]	–0.053
Myoglobin-Au-ITO[b]	–0.007
Colloidal gold nanoparticles[c]	–0.131
Ni/NiO[d]	0.0895
Sol-gel[e]	–0.099
Carbon Nanotubes[f]	–0.007

[a]Zhao *et al.*, 2010; [b]Zhang *et al.*, 2005; [c]Yang *et al*., 2006; [d]Ganjali *et al.*, 2008; [e]Gongxuan *et al.*, 2004; [f]Zhao *et al.*, 2003

The potential obtained for rHbI is close to the values reported in table 1. It is noticed that potentials vary between the different forms of myoglobin immobilization, and this is due to changes in the environment as well as the different support electrolyte used. Hemoglobin I from *Lucina pectinata* and myoglobin are monomeric and globular hemoproteins having similarities in their amino acid sequence; both proteins in the metaquo form (ferric state) have similar spectral properties. In this research, a different value for myoglobin was obtained. Although these proteins are structurally very similar, they differ in the internal amino acids composition around the heme group.

Evidently, hemoglobin I is bound to the assembly Ni^{2+}/3-MPA/Au. The binding between histidine-tagged proteins with nickel or cobalt ions is known, and is the principle of the purification method of these kinds of proteins (Hemdan *et al.*, 1985; Bush *et al.*, 1991). Histidines exhibit highly selective coordination with nickel ions and bind by non-bonding electron pairs of imidazole nitrogens to the half empty orbitals of these ions. Figure 5 (solid line) suggests that the protein is adsorbed to the surface since a significant change on the voltammetric behavior with respect to the previous stage is observed, and the formation of a redox couple is attributable to the iron porphyrin.

5.2.4. Voltammetric behavior of rHbI modified electrode

The challenge of the biomolecules immobilization for biosensors preparation is to ensure that these compounds do not lose their biological activity, either in a catalytic process as performed by enzymes or some proteins, or any other substrate that fulfills a specific biological function. In this case, a stability analysis of the hemoglobin-surface by

measuring kinetic parameters was performed, studying the effect of the scan rate on immobilized protein.

Voltammetric analysis of modified surfaces was performed in a 1mM ferricyanide solution to evaluate the blocking effect on the electron transfer when the surface is modified with the protein. The cyclic voltammograms for bare gold (Fig. 6a) show an anodic peak at approximately 236 mV and a cathodic peak at around 195 mV corresponding to reversible redox couple $Fe(CN)_6^{4-}/Fe(CN)_6^{3-}$. After modification with 3-mercaptopropionic acid (Fig. 6b) and rHbI (Fig. 6c) the expected peak separation and a decrease in current response due to restricted access of the electroactive species from solution to the electrode surface was observed.[37]

In order to investigate the hemoglobin I characteristics at the rHbI-electrode, the effect of scan rates on the hemoglobin voltammetric behavior was studied in detail and the kinetic parameters were acquired. Figure 7 shows representative cyclic voltammograms of the hemoglobin-modified electrode in phosphate buffer pH 6.70 at different scan rates. The cyclic voltammograms show a linear increment of anodic and cathodic currents when the scan rate is increased (inset Fig. 7). In the case of the anodic current a linear behavior was obtained expressed by $I_{pa} = 1.417 \times 10^{-6}\nu + 4.679 \times 10^{-8}$ with a correlation coefficient of 0.998, and the cathodic current for $I_{pc} = -1.475 \times 10^{-6}\nu - 6.039 \times 10^{-8}$ and correlation coefficient 0.997, suggesting that the protein is stable at the surface and the modification was successful.

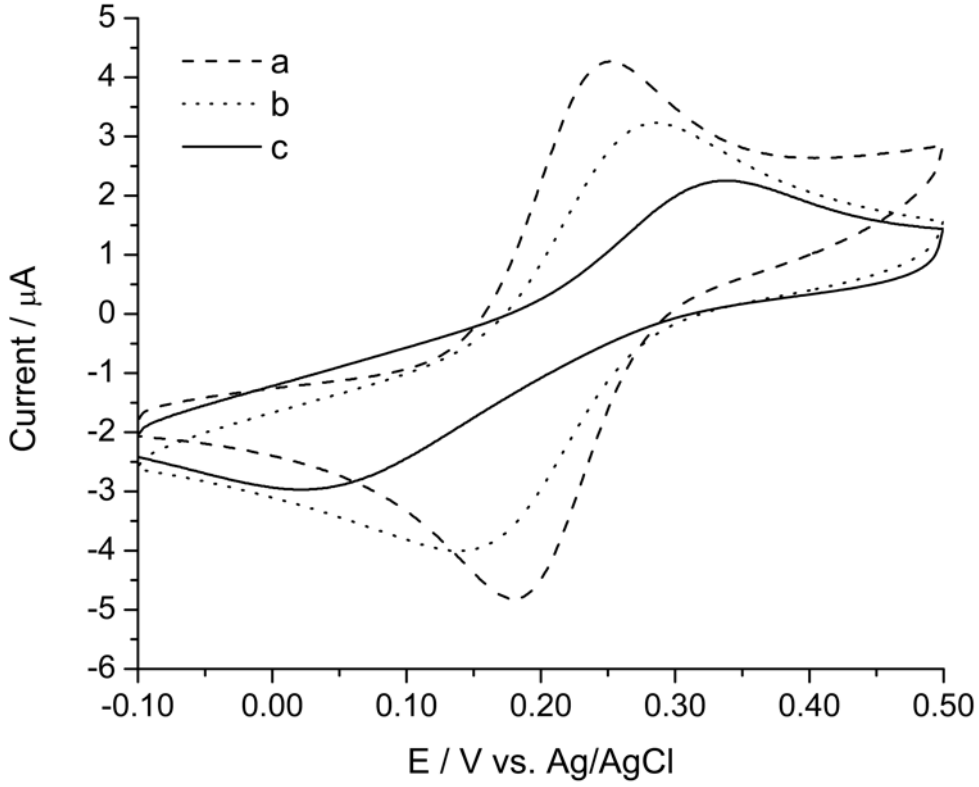

Figure 5.6. Cyclic voltammograms of 2.5 mM $Fe(CN)_6^{3-}$ in 0.1 M KCl solution at (a) a gold electrode and (b) a 3-MPA/Au electrode and (c) a rHbI-modified gold electrode. Scan rate 100 mVs^{-1}.

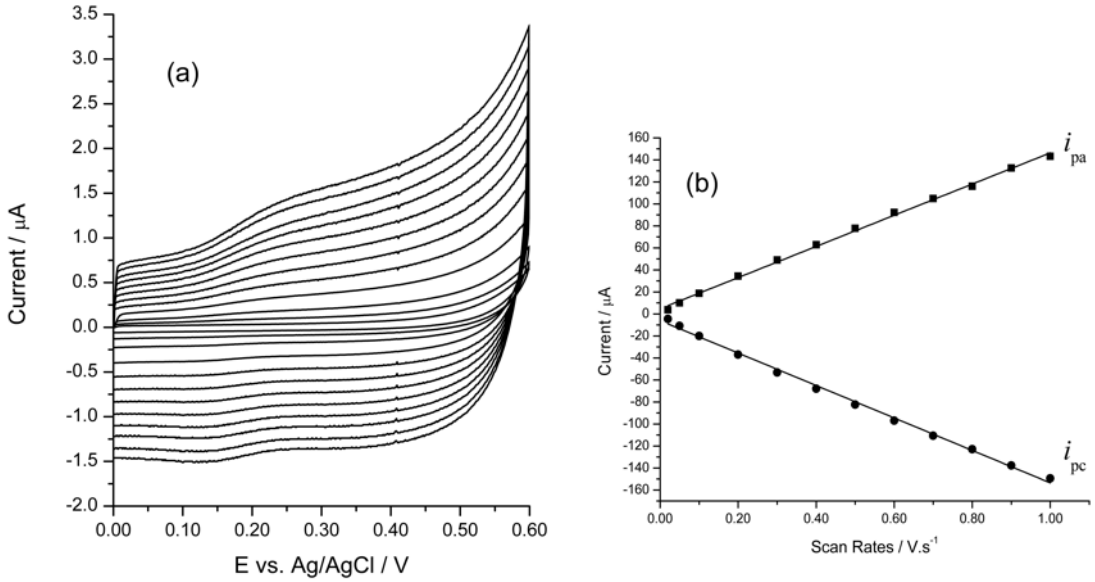

Figure 5.7. (a) Cyclic voltammograms for gold surface modified rHbI/Ni^{2+}/3-MPA/Au with scan rate from 20, 50, 100, 150, 200, 300, 300, 400, 500, 600, 700, 800, 900 and 1000 mV/s in 0.1 M phosphate buffer at pH 6.70. (b) The plot of peak currents vs. scan rates.

An estimate of the charge transfer coefficient (α) and the heterogeneous electron transfer rate constant k_s was performed using the Laviron method (Laviron, 1974).

In 1974 Laviron published the mathematical treatment for using linear sweep voltammetry to determine the electron transfer rate constant (k_{ET}) based on the Butler–Volmer approach, and the only experimental data required to use in this method are the overpotentials (Eq. 5.1).

$$\eta = E_p - E^{\circ'} \qquad (5.1)$$

where η is the overpotential, E_p the peak potential and $E^{\circ'}$ the formal potential of the system.

The Laviron method is widely used for determining the electron transfer rate constant, however, it is subject to a number of constraints that limit its application (Bush *et al.*, 1991). First, this method relies on α, the transfer coefficient, which is a measure of the symmetry of the energy barrier of the redox reaction. Ideally, $\alpha = 0.5$ for all overpotentials, however in many cases α deviates from 0.5. Therefore, determination of α is crucial to finding k_{ET}. To determine α, the peak potential E_p is plotted vs. log ν (Nassar *et al.*, 1997). E_{pa} and E_{pc} are plotted separately in this way to give two branches. At higher scan rates where $\eta > 100$ mV, the data should be a straight line where the slope of the line is given in Eq. 5.2.

$$slope = -\frac{2.3RT}{\alpha nF} \qquad (5.2)$$

R is the universal gas constant (8.314 J/molK), T is the temperature in Kelvin, *n* is the number of electrons transferred and *F* is the Faraday's constant (96487 C/mol). The k_{ET} can be determined by applying the constraint of $\eta = 0$ to Eq. (5.3) which reduces to Eq. (5.4).

Determining the x-intercepts of the lines for the anodic and the cathodic branches provide νa and νc, respectively, values that are used in Eq. (5.4) to determine k_{ET}.

$$\log k_s = \alpha \log(1-\alpha) + (1-\alpha)\log\alpha - \log\left(\frac{RT}{nF\nu}\right) - \frac{\alpha(1-\alpha)nF\eta}{2.3RT} \qquad (5.3)$$

$$k_{ET} = \frac{\alpha nF\nu_c}{RT} = (1-\alpha)\frac{nF\nu_a}{RT} \qquad (5.4)$$

As a result of this model, deducting from equations 5.1, 5.3 and 5.4, the charge transfer coefficient can be estimated by equation 5.5:

$$E_{pa} = E^{o'} - \frac{RT}{(1-\alpha)nF} + \frac{RT}{(1-\alpha)}\ln\nu \qquad (5.5)$$

where α is the coefficient of electron transfer, $E^{\circ'}$ is the formal potential, *n* is the number of electrons, R is the universal gas constant, T is the absolute temperature and F is Faraday's constant. Subsequently, this method is a measure of the symmetry of the energy barrier of the redox reaction and it is expected that the value of α is ideally 0.5, but in most cases the value of α varies slightly, considered valid when $0.3 < \alpha < 0.7$ (Ganjali *et al.*, 2008). In this case, when $n = 1$, $\alpha = 0.65$, which indicates a single reversible electron transfer process. For calculation of the heterogeneous electron transfer rate constant (k_s), the equation 5.3 was used.

The calculated value of the constant was 0.84 s^{-1}, which is comparable with Mb/nanoporous ZnO/graphite (Zhao *et al.*, 2006) and lower than for other supports (Table 2), except for NiNP (Ganjali *et al.*, 2008).

Table 2. Heterogeneous electron transfer rate constants for myoglobin in different supports

Myoglobin supports	k_s (s^{-1})
Mb/$2C_{12}N^{+}Br^{-}$ [(a)]	31
Myoglobin/polyacrylamide[b]	86
Mb/hydrated poly(ester sulfonic acid)[c]	52
Mb/MWNTs[d]	5.4
Mb/nanoporous ZnO/graphite[e]	1.0
Mb/arylhydroxylamine[f]	51
Mb/agarose[g]	47
Mb/NiNP[h]	0.34
Mb/Cys/Au[i]	1.66

[a]Nassar *et al*., 1997; [b]Shen *et al.*, 2002; [c]Hu *et al.*, 1997; [d]Zhao *et al.*, 2003; [e]Zhao *et al.*, 2006; [f]Ashok-Kumar and Chen S, 2007; [g]Liu *et al.*, 2004; [h]Ganjali *et al.*, 2008; [i]Paulo *et al.*, 2011

5.2.5. Hydrogen sulfide association with recombinant Hemoglobin I

For the H_2S association with hemoglobin I analysis, a solution of sodium sulfide was used. Clearly, when sodium sulfide was added to the buffer, hydrogen sulfide is released (Pietri *et al.*, 2009; Pietri *et al.*, 2011) and the voltammetric behavior of the modified electrode changed decreasing its reduction and oxidation peak currents. This indicates that the electrode rHbI/Ni^{2+}/3-MPA/Au is able to bind H_2S. Figure 5.8 shows the voltammograms obtained in phosphate buffer at pH 6.70 when concentrations of hydrogen sulfide from 0 nM (a) to 600 nM (b) are added.

This behavior suggests that the heme pocket for each hemoglobin molecule is binding to hydrogen sulfide, until the hemoglobin-surface is saturated. It is well known that hemoglobin I molecules react with hydrogen sulfide to form the complex rHbI-H_2S according to Eq. 5.6 (Pietri *et al.*, 2011):

$$rHbIFe(III)–H_2O + H_2S \leftrightarrows rHbIFe(III)–H_2S + H_2O \qquad (5.6)$$

Likewise, is important to mention that this behavior indicated that the rHbI kept its native structure capable of binding H_2S after being immobilized onto the electrode, where most of the adsorbed protein is active. Furthermore, due to the fact that there is a change in the amplitude of the signal but there is no change in the potential range of the wave, it can be concluded that the oxidation number of hemoglobin remains constant. The form in which hemoglobin I is associated to H_2S shows that iron from the porphyrin preserves its oxidation state (rHbI-Fe^{+3}). Hemeproteins with a low-polarity distal environment in the vicinity of the iron in the porphyrin will react with H_2S according to equation 4, and the sulfide release is dictated by slow H_2S dissociation without inducing significant reduction (Pietri *et al.*, 2009; Pietri *et al.*, 2011).

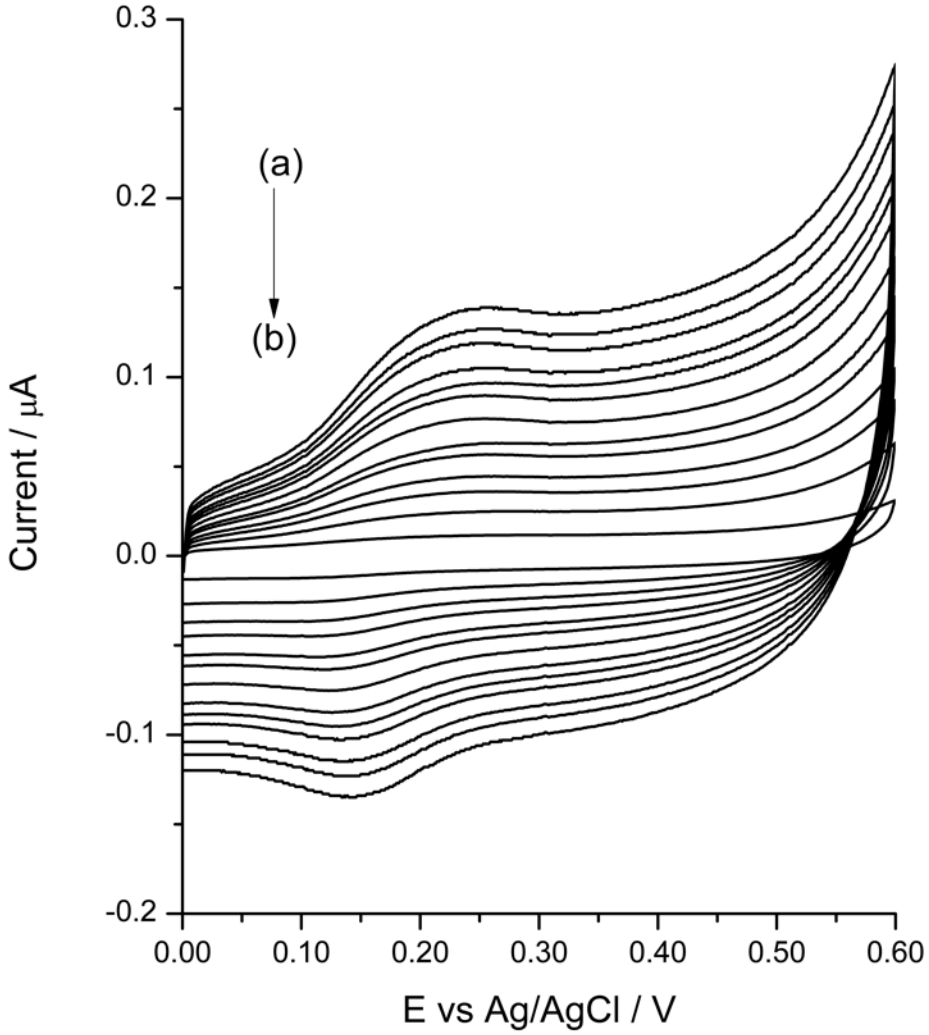

Figure 5.8. Voltammetric response of the rHbI/Ni^{2+}/3-MPA/Au upon successive additions of Na_2S 20 μM at 0.1M phosphate buffer solution at pH 6.70, producing H_2S concentrations of (a) 0, 50, 100, 150, 200, 250, 300, 350, 400, 450, 500, 550, (b) 600 nM."

Structural studies of the hemoglobin I active site have shown that this protein has a glutamine residue at the distal ligand binding site, instead of the equivalent histidine typically found in many invertebrate and vertebrate organisms (Kraus *et al.*, 1990; Pietri *et al.*, 2011). In addition to glutamine, hemoglobin I has a phenylalanine residues near the heme, generating what is known as the "Phe-cage". This unusual amino acid composition of the rHbI distal ligand-binding site is believed to be responsible for the high H_2S affinity. Furthermore, the amperometric response of (a) rHbI/Ni^{2+}/3-MPA/Au and (b) 3-MPA/Au with successive additions of Na_2S to 0.1M phosphate buffer solution at pH 6.70 and an applied potential of 230 mV vs. Ag/AgCl is shown in Fig. 9. As expected, the current response for the electrode rHbI-electrode was higher than for the 3-MPA/Au electrode due to the high affinity of the protein for hydrogen sulfide. The linear response range of H_2S concentration was from 40 nM to 600 nM with a correlation coefficient of 0.998 (n = 16). From the slope of -0.1166 nA/nM, the lower limit of detection was estimated to be 13 nM at a signal to noise ratio of 3, and the lower limit of quantification of 43 nM. The H_2S concentrations were calculated based on the H_2S dissolved in the solution, which is only one component of the total sulfide equilibrium. The equation involved in the calculation corresponding to the total sulfide equilibrium system is $[H_2S] = [Na_2S] /\{1+(K_1/[H^+])+(K_1K_2/[H^+])\}$, where pK_1 = 6.89 and pK_2 = 19.[65-67] In our case, the equilibrium of H_2S system from sodium sulfide is shifted toward the formation of H_2S because the pH of solution is less than pK_1.

The restoration of the electrode for reuse was performed leaving it at a constant potential of 0.0 V vs. Ag/AgCl for 1 h or until observe constant current, favoring an appropriate reducing environment and to induce the hemoglobin to release the bonded H_2S

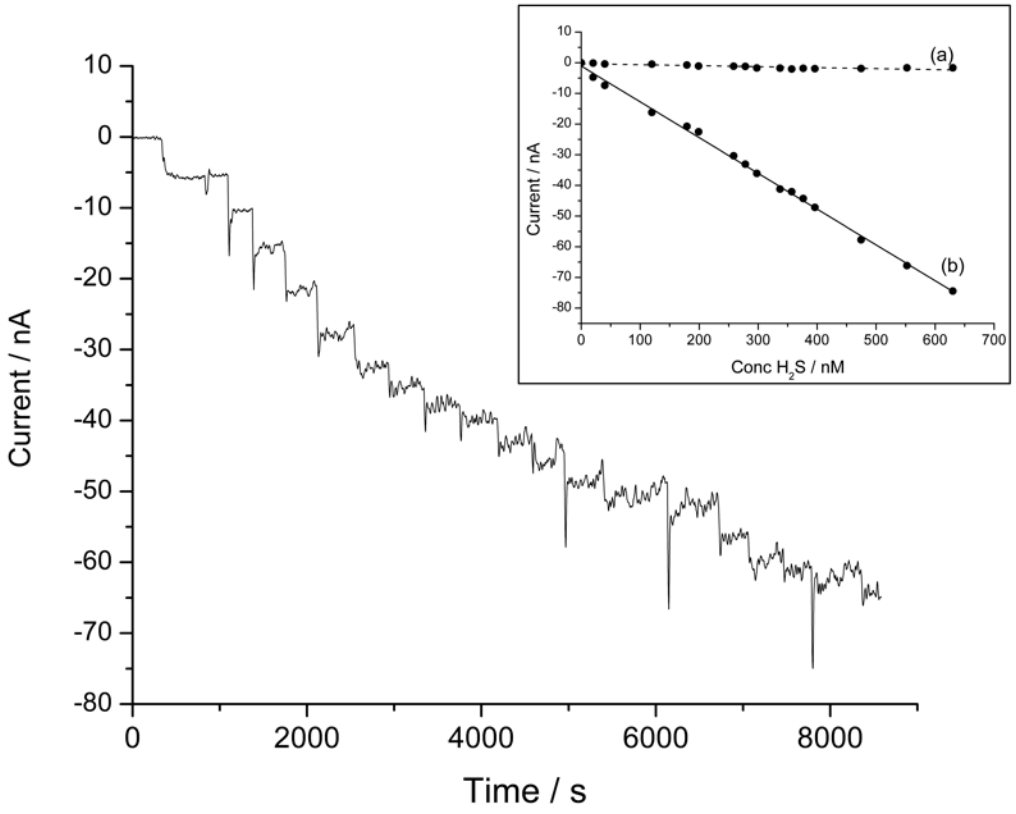

Figure 5.9. Amperometric plot of rHbI/Ni^{2+}/3-MPA/Au electrode in 0.1 M phosphate buffer at pH 6.70. Inset: Current peaks vs. Concentration of H_2S of (a) 3-MPA/Au and (b) rHbI/Ni^{2+}/3-MPA/Au electrodes.

A previous work reported that when the concentration of H_2S increases considerably, (more than 3-10 times the concentration of rHbI) it generates a reducing environment induced by H_2S itself, favoring the reduction of rHbI(III) to rHbIFe(II), and subsequently H_2S is released (Pietri et al., 2009). Therefore, a reducing environment is generated at the electrode leaving a potential of 0 V and promoting the release of the gas. This electrode lost only 7% of its initial activity after more than four successive measurements, and it was stored in 0.1M phosphate buffer solution at pH 6.70 and 4 °C, when not in use. Moreover, the rHbI electrode was tested in a buffer solution containing various common ions to evaluate their response. The electrode holds good response to a mixture of ions; 1 mM Ca^{2+}, Na^{+}, K^{+}, NH_4^{+}, NO_3^{-}, SO_4^{2-}, Cl^{-}, Br^{-}, I^{-} and 100 mM PO_4^{-3} (from buffer). It should be emphasized that higher ions concentration leads to a loss of response, possibly due to hemoglobin denaturation by a salinity effect. In addition, an erratic response is observed when a small aliquot of a solution 1 mM CN^{-} was added to the buffer solution. Cyanide is a ligand that binds strongly to the ferric ion forming a very stable complex with hemoglobin, and that cannot be displaced by ligands such as O_2, NO or H_2S. Some publications in hemeproteins functionality and dynamic confirm this fact (Kraus *et al.*, 1990). On the other hand, when a small aliquot of 1 mM H_2O_2 is added to a phosphate buffer solution, a similar behavior is observed. Several recent studies demonstrate that monomeric hemeproteins similar to rHbI, may be associated with ferric ion of the porphyrin (Griebenow *et al.*, 2011) but as the peroxide concentration increases, it can interact with any part of the assembly structure observing an erratic response of the electrode. In conclusion, for H_2S analysis is recommended that hydrogen peroxide and cyanide are removed. The problem is that iron from the porphyrin in these hemeproteins binds to these ligands in the ferric state, and the oxidation state does not change. The

effective nuclear charge of ferric ion may change slightly when it forms bonds with such substrates, but potential changes are not so extreme as to be detected with the conditions employed in this study. Finally, The relative response current of rHbI-electrode was examined by checking periodically the current generated at 230 mV when it was exposed to a standard solution of Na_2S in 0.1 M phosphate buffer solution at pH 6.70. The modified electrode retained 95% of activity within a storage period of 30 days under these conditions, but after a storage period of 2 months, the electrode showed total loss of activity for H_2S.

6. Conclusions

The immobilization of the recombinant hemoglobin I from *Lucina pectinata* was necessary in order to study it electrochemically and to quantify amperometrically hydrogen sulfide. Apparently, the immobilization of the recombined hemoglobin I using the "histidine-tag" does not affect the function or stability of the protein on the surface. This was demonstrated by the electrokinetic information obtained from the modified electrode rHbI/Ni^{2+}/3-MPA/Au in buffer solution. It was possible to characterize the entire immobilization process using as evidence the potential shifts in the appearance or disappearance of peaks in the voltammograms performed by each step, as well as XPS analysis on the different surfaces of the modification process.

From electrokinetic data it was established that the recombined hemoglobin I generates a redox couple involving one electron, with a transfer constant $\alpha = 0.65$, indicating that it is a single reversible electron transfer process ($n = 1$). The calculated formal potential E°' is 0.213 V vs. Ag/AgCl (0.004 V vs. NHE) for Cys model and 0.190 V vs. Ag/AgCl (–0.029V vs. NHE) for 3-MPA model. The heterogeneous electron transfer constant is low ($k_s = 0.84\ s^{-1}$) compared to the constants obtained for myoglobin immobilized in different surfaces. This suggests that the electronic transfer is slow, resulting in a time-consuming response of the system when hydrogen sulfide was bound. When amperometric analysis was performed with both models, this situation became clear because the electrode response was not instantaneous, having to wait almost a minute for the signal to stabilize.

It was possible to establish calibration curves in phosphate buffer pH 6.70 with both models, resulting the more robust the rHbI/Ni^{2+}/3-MPA/Au because can be analyzed in a

wider range of concentrations for hydrogen sulfide. To regenerate the electrode it is left at 0 V vs. Ag/AgCl (moderate reduction current, E = -0.209 V vs. NHE) governing a reduction ambient and forcing to the hemoglobin release the hydrogen sulfide. Also, the same condition can be achieved submerging the electrode in buffer solution for several hours to induce an autoxidation process. It was also established that common interferences ions such as alkali metals, halides, sulfates and nitrates do not cause significant changes in the behavior of both electrodes, but peroxides or cyanide ions damage the electrodes.

Finally, these models serve as prototypes for future sensors because they allow to determine the electrochemical activity of hemoglobin toward hydrogen sulfide. Interestingly, the possibility of miniaturizing these models should be explored and make and structural changes should be made in recombined hemoglobin I, to favor stronger covalent bonds to a suitable support.

REFERENCES

Abdureyim, A.; Kera, S.; Setoyama, H.; Okudaira, K.K.; Suzuki, R.; Masuda, S.; Ueno, N.; Harada, Y. (1999). Observation of outermost surface layer of 4-mercaptohydrocynnamic acid self-assembled film on Au(111) by Penning ionization electron spectroscopy. *App. Surf. Sci.*, *144*, 430-434

Abe, K. and Kimura, H. (1996). The possible role of hydrogen sulfide as an endogenous neuromodulator. *J. Neurosci.*, *16*, 1066-1071.

Alaejos, M. S. & Garcia, M. F. (2004). Application of amperometric biosensors to the determination of vitamins and alpha-amino acids. *Chem. Rev.*, *104*, 3239-3266.

Aravinda, C. L.; Cosnier, S.; Chen, W.; Myung, N.V.; Mulchandani, A. (2009). Label-free detection of cupric ions and histidine-tagged proteins using single poly(pyrrole)-NTA chelator conducting polymer nanotube chemiresistive sensor. *Biosens. Bioelectron.*, *24*, 1451-1455.

Arnold, F. H. (1991). Metal-affinity separations: a new dimension in protein processing. *Bio/Technology*, *9*, 150-155.

Arrigan, D. and Bihan, L. (1999). A study of L-cysteine adsorption on gold via electrochemical desorption and copper(II) ion complexation. *Analyst*, *124*, 1645-1649.

Aryal, S.; Remant, B. K. C.; Dharmaraj, N.; Bhattarai, N.; Kim, C. H. and Kim, H. Y. (2006). Spectroscopic identification of S-Au interaction in cysteine capped gold nanoparticles. *Spectrochim. Acta Part A*, *63*, 160-163.

Ashok-Kumar, S. and Chen, S. (2007). Direct electrochemistry and electrocatalysis of myoglobin on redox-active self- assembling monolayers derived from nitroaniline modified electrode, *Biosens. Bioelectron.*, *22*, 3042–3050.

Bain, C. D.; Troughton, E. B.; Tao, Y. T.; Evall, J.; Whitesides, G. M.; Nuzzo, R. G. (1989). Formation of monolayer films by the spontaneous assembly of organic thiols from solution onto gold. *J. Am. Chem. Soc.*, *111*, 321–335.

Bakker, E. and Qin, Y. (2006). Electrochemical sensors. *Anal. Chem.*, *78*, 3965-3984.

Baldrich, E.; Laczka, O; Campo, F. J. and Muñoz, F. X. (2008). *Anal. Bioanal. Chem.*, *390*, 1557-1562.

Bard, A.J. and Faulkner, L.R. (2001). Electrochemical Methods: Fundamentals and Applications, 2nd ed.. *John Wiley & Sons, Inc.* Chapters 1, 6, 10 & 14.

Benavides, G. A.; Squadrito, G.L.; Mills, R. W.; Patel, H. D.; Isbell, T. S.; Patel, R. P.; Darley-Usmar, V. M.; Doeller, J. E. and Kraus, D. W. (2007). Hydrogen sulfide mediates the vasoactivity of garlic. *Proc. Natl. Acad. Sci. USA*, *104*, 17977–17982.

Bensebaa, F.; Voicu, R.; Huron, L.; Ellis, T. H.; Kruus, E. (1997). Kinetics of Formation of Long-Chain n-Alkanethiolate Monolayers on Polycrystalline Gold. *Langmuir*, *13*, 5335-5340.

Blunden, J.; Aneja, V.P.; Overton, J.H. (2008). Modeling hydrogen sulfide emissions across the gas–liquid interface of an anaerobic swine waste treatment storage system, *Atmos. Environ.*, *42*, 5602-5611.

Boffi, A.; Rizzi, M.; Monacelli, F. and Ascenzi, P. (2000). Determination of H_2S solubility via the reaction with ferric hemoglobin I from the bivalve mollusc *Lucina pectinata*. *Biochim. Biophys. Acta*, *1523*, 206-208.

Boon Hian Tan, Peter T.-H. Wong, Jin-Song Bian, Hydrogen sulfide: A novel signaling molecule in the central nervous system, Neurochemistry International, Volume 56, Issue 1, January 2010, Pages 3-10.

Bouzaza, A.; Laplanche, A.; Marsteau, S. (2004). Adsorption–oxidation of hydrogen sulfide on activated carbon fibers: effect of the composition and the relative humidity of the gas phase, *Chemosphere*, *54*, 481-488.

Bramanti, E.; D'Ulivo, L.; Lomonte, C.; Onor, M.; Zamboni, R.; Raspi, G.; D'Ulivo, A. (2006). Determination of hydrogen sulfide and volatile thiols in air samples by mercury probe derivatization coupled with liquid chromatography–atomic fluorescence spectrometry, *Anal. Chim. Acta*, *579*, 38-46.

Bush, G. L.; Tassin, A.; Friden, H. and Meyer, D. J. (1991). Secretion in yeast: purification and in vitro translocation of chemical amounts of prepro-alpha-factor. *J. Biol. Chem.*, *266*, 13811-13814.

Carlo, P.; Arienti, G. and Palombaric, R. (2004). Electrochemical assay for determining nitrosyl derivatives of human hemoglobin: nitrosylhemoglobin and S-nitrosylhemoglobin. *Anal. Biochem.*, *330,* 306-310.

Cavalleri, O.; Oliveri, L.; Daccà, A.; Parodi, R. and Rolandi, R. (2001). XPS measurements on L-cysteine and 1-octadecanethiol self-assembled films: a comparative study. *Appl. Surf. Sci.*, *357*, 175-176.

Cerda, J.; Echevarria, Y.; Morales, E. and Lopez-Garriga, J. (1999). Resonance Raman studies of the heme-ligand active site of Hemoglobin I from *Lucina pectinata. Biospectroscopy, 5*, 289-301.

Chaudhari, G. N.; Alvi, M.; Wankhade, H. G.; Bodade, A. B.; Manorama, S. V. (2012). Nanocrystalline chemically modified CdIn2O4 thick films for H_2S gas sensor. *Thin Solid Films*, *520*, 4057–4062.

Chen, S.; Chen, Z.; Ren, W. and Ai, H. (2012). Reaction-based genetically encoded fluorescent hydrogen sulfide sensors, *J. Am. Chem. Soc.*, *134*, 9589-9592.

Choi, M.F. and Hawkins, P. (1997). Development of sulphide-selective optode membranes based on fluorescence quenching, *Anal. Chim. Acta*, *344*, 105-110.

Choi, M.F. and Hawkins, P. (2003). Development of an optical hydrogen sulphide sensor, *Sens. Actuators B*, 90, 211-215.

Ciara, O.; O'Regan, T. M.; O'Riordan, L. J.; Pravda, M. and Guilbault, G. G. (2002). Direct detection of myoglobin in whole blood using a disposable amperometric immunosensor. *Anal. Chim. Acta*, *460*, 141-150.

Colon, M.; Todolí, J.L.; Hidalgo, M. and Iglesias, M. (2008). Development of novel and sensitive methods for the determination of sulfide in aqueous samples by hydrogen sulfide generation-inductively coupled plasma-atomic emission spectroscopy, *Anal. Chim. Acta*, *609*, 160-168.

Crowley, K.; Morrin, A.; Shepherd, R. L.; Panhuis, M.; Wallace, G. G.; Smyth, M. R and Killard, A. J. (2010). Fabrication of polyaniline-based gas sensors using piezoelectric inkjet and screen printing for the detection of hydrogen sulfide, *IEEE J. Sens.*, *10*, 1419-1426.

Das, A; Trammell, S. A. and Hecht, M. (2006). Electrochemical and ligand binding studies of a *de novo* heme protein. *Biophys. Chem.*, *123*, 102-112.

Dodero, G.; De Michieli, L.; Cavalleri, O.; Rolandi, R.; Oliveri, L.; Daccà, A. and Parodi, R. (2000). L-Cysteine chemisorption on gold: an XPS and STM study. *Colloids Surfaces A*, *175*, 121-128.

Doeller, J.; Isbell, T.; Benavides, G.; Koenitzer, J.; Patela, H.; Patel, R.; Lancaster Jr, J.; Darley-Usmar, V. M. and Kraus, D. (2005). Polarographic measurement of hydrogen sulWde production and consumption by mammalian tissues. *Anal. Biochem.*, *341*, 40-51.

Doeller, J.E.; Isbell, T.S.; Benavides, G.; Koenitzer, J.; Patel, H.; Patel, R.P.; Lancaster Jr., J.R.; Darley-Usmar, V.M.; Kraus, D.W. (2005). Polarographic measurement of hydrogen sulfide production and consumption by mammalian tissues. *Anal. Biochem.*, *341*, 40-51.

E. Distrutti, L. Sediari, A. Mencarelli, B. Renga, S. Orlandi, E. Antonelli, F. Roviezzo, A. Morelli, G. Cirino, J.L. Wallace, S. Fiorucci Evidence that hydrogen sulfide exerts antinociceptive effects in the gastrointestinal tract by activating KATP channels J. Pharmacol. Exp. Ther., 316 (2006), p. 325.

Enokido, Y.; Suzuki, E.; Iwasawa, K.; Namekata, K.; Okazawa, H. and Kimura, H. Cystathionine beta-synthase, a key enzyme for homocysteine metabolism, is preferentially expressed in the radial glia/astrocyte lineage of developing mouse CNS FASEB J., 19 (2005), p. 1854.

Erickson, P. F.; Maxwell, I. H.; Su, L. J.; Baumann, M. and Glode, L. M. (1990). Sequence of cDNA for rat cystathionine gamma-lyase and comparison of deduced amino acid sequence with related Escherichia coli enzymes. *Biochem. J.*, *269*, 335-340.

Esfandyarpour, B.; Mohajerzadeh, S.; Khodadadi, A. A. and Robertson, M. D. (2004). Ultrahigh-sensitive tin-oxide microsensors for H_2S detection. *IEEE J. Sensors*, *4*, 449-454.

Eto, K.; Asada, T.; Arima, K.; Makifuchi, T. and Kimura, H. (2002). Brain hydrogen sulfide is severely decreased in Alzheimer's disease. *Biochem. Biophys. Res. Commun.*, *293*, 1485-1488.

Ferreira, A. A. P.; Colli W.; da Costa, P. I.; Yamanaka, H. (2005). Immunosensor for the diagnosis of Chagas' disease. *Biosens. Bioelectron.*, *21*, 175-181.

Font, J.; Gutiérrez, J.; Lalueza, J.; Pérez, X. (1996). Determination of sulfide in the leather industry by capillary electrophoresis, *J. Chromatogr. A*, *740*, (1996) 125-132.

Ganjali, M. R; Moghaddam, A. B.; Dinarvand, R.; Ahadi, S. and Saboury, A. A. (2008). *Biophys. Chem.*, *134*, 25.

Gavira, J.A.; Cámara-Artigas, A.; De Jesús-Bonilla, W.; López-Garriga, J.; Lewis, A.; Pietri, R.; Yeh, S.R.; *et al.* (2008). Structure and ligand selection of hemoglobin II from Lucina pectinata. *J. Biol. Chem., 283*, 9414-9423.

Gavira, J.A.; De Jesús-Bonilla, W.; Cámara-Artigas, A.; López- Garriga, J. and García-Ruiz, J.M. (2006). Capillary crystallization and molecular replacement solution of hemoglobin II from the clam Lucina pectinata. *Acta Crystallograph. Sect. F Struct. Biol. Cryst. Commun.*, *62*, 196-199.

Ge Zhao, G.; Jing-Juan Xu, J. J. and Hong-Yuan Chen, H. Y. (2006). Interfacing myoglobin to graphite electrode with an electrodeposited nanoporous ZnO film. *Anal. Biochem.*, *350*, 145-150.

Geng, B.; Yang, J.; Qi, Y.; Zhao, J.; Pang, Y.; Du, J. and Tang, C. (2004). H_2S generated by heart in rat and its effects on cardiac function. *Biochem. Biophys. Res. Commun.*, *313*, 362-368.

Giggenbach, W. (1971). Optical spectra of highly alkaline sulfide solutions and the second dissociation constant of hydrogen sulfide. *Inorg. Chem.*, *10*, 1333-1338.

Gong, J.; Chen, Q.; Lian, M.; Liu, N.; Stevenson, R. G. and Adami, F. Micromachined nanocrystalline silver doped SnO_2 H_2S sensor, Sensors and Actuators B: Chemical, Volume 114, Issue 1, 30 March 2006, Pages 32-39.

Gongxuan, L.; Wang, Q. and Yang, B. (2004). Myoglobin/Sol−Gel Film Modified Electrode: Direct Electrochemistry and Electrochemical Catalysis. *Langmuir, 20*, 1342-1347.

Gorton, L.; Lindgren, A.; Larsson, T.; Munteanu, F. D.; Ruzgas, T. and Gazaryan, I. (1999). Direct electron transfer between heme-containing enzymes and electrodes as basis for third generation biosensors. *Anal. Chim. Acta., 400*, 91-108.

Gosser, D.K. (1993). Cyclic Voltammetry, Simulation and Analysis of Reaction Mechanisms. *VCH Publishers, Inc.* pp 1-103.

Grant, J. T. and Briggs D. (2003). Surface Analysis by Auger and X-ray Photoelectron Spectroscopy. Eds. *IM Publications*: Chichester, UK.

Griffith, O. W. (1987). Mammalian sulfur amino acid metabolism: an overview. *Methods Enzymol.*, *143*, 366-376.

Griffiths, P. And De Hasseth. (2007). Fourier Transform Infrared Spectrometry (Chemical Analysis: A Series of Monographs on Analytical Chemistry and Its Applications). *Wiley-Interscience*. New Jersey, USA.

Griebenow K.; Santiago-Rodríguez, L.; Méndez, J.; Flores-Fernandez, G; Pagán, M.; Rodríguez-Martínez, J.; Cabrera, C. (2011). Enhanced stability of a nanostructured cytochrome c biosensor by PEGylation, *J. Electroanal. Chem*., *663*, 1-7.

Gu, H.; Yu, A. and Chen, H. (2001). Direct electron transfer and characterization of hemoglobin immobilized on a Au colloid–cysteamine-modified gold electrode. *J. Electroanal. Chem.*, *516*, 119-126.

Hager, G. and Brolo, A. G. (2003). Adsorption/desorption behaviour of cysteine and cystine in neutral and basic media: electrochemical evidence for differing thiol and disulfide adsorption to a Au(111) single crystal electrode. *J. Electroanal. Chem.*, *550*, 291-301.

Hart, J. P.; Crew, A.; Crouch, E.; Honeychurch, K. C.; Pemberton, R. M. (2004). Some recent designs and developments of screen-printed carbon electrochemical sensors/biosensors for biomedical, environmental, and Industrial analyses. *Anal. Lett.*, *37*, 789-830.

Hawkins, S.J.; Ratcliffe, N.M.; Sagastizabal, A. (1998). The use of thin silver films for the detection of low concentrations of hydrogen sulphide, *Anal. Chim. Acta, 359*, 125-132.

Hemdan, E. and Porath, J. (1985). Development of immobilized metal affinity chromatography II. Interaction of amino acids with immobilized nickel iminodiacetate. *J. Chromatogr. A*, *323*, 255-264.

Hongyun, L. & Hu, N. (2003). Heme protein-gluten films: voltammetric studies and their electrocatalytic properties. *Anal. Chim. Acta*, *481*, 91-99.

Hu, N. and Rusling, J.F. (1997). Electrochemistry and catalysis with myoglobin in hydrated poly(ester sulfonic acid) ionomer films, Langmuir, *13*, 4119–4125.

Ichinohe, T. Kanaumi, S. Takashima, Y. Enokido, Y. Nagai, H. Kimura Cystathionine beta-synthase is enriched in the brains of Down's patients Biochem. Biophys. Res. Commun., 338 (2005), p. 1547.

Jagtap, S. V.; Kadu, A. V.; Sangawar, V. S.; Manorama, S. V.; Chaudhari, G. N. (2008). H_2S sensing characteristics of $La_{0.7}Pb_{0.3}Fe_{0.4}Ni_{0.6}O_3$ based nanocrystalline thick film gas sensor. *Sens. Actuators B*, *131*, 290–294.

Jiuhong, Y. & Huangxian, J. (2003). Amperometric biosensor for hydrogen peroxide based on hemoglobin entrapped in titania sol–gel film. *Anal. Chim. Acta*, *486,* 209-216.

Johnson, D.L.; Martin, L.L. (2005). Controlling Protein Orientation at Interfaces Using Histidine Tags: An Alternative to Ni/NTA. *J. Am. Chem. Soc.*, *127*, 2018-2019.

Kabil, O. and Banerjee, R. (2010). The redox biochemistry of hydrogen sulfide. *J. Biol. Chem., 285*, 21903–21907.

Karlberg, T.; Collins, R.; Arrowsmith, C.H.; Berglund, H.; Bountra, C.; Edwards, A.M.; Flodin, S.; Flores, A.; Graslund, S.; Hammarstrom, M.; Johansson, I.; Kotenyova, T.; Kouznetsova, E.; Moche, M.; Nordlund, P.; Nyman, T.; Persson, C.; Sehic, A.; Schutz, P.; Siponen, M.I.; Thorsell, A.G.; Tresaugues, L.; Van Den Berg, S.; Wahlberg, E.; Weigelt, J.; Welin, M. and Schuler, H. (2010). Human 3-mercaptopyruvate sulfurtransferase. PDB ID: 3OHL.

Kida, K.; Yamada, M.; Tokuda, K.; Marutani, E.; Kakinohana, M.; Kaneki, M. and Ichinose, F. (2011). Inhaled hydrogen sulfide prevents neurodegeneration and movement disorder in a mouse model of Parkinson's disease. *Antioxid. Redox Signal.*, *15*, 343–352.

Kimura, H.; Nagai, Y.; Umemura, K.; Kimura, Y. (2005). Physiological roles of hydrogen sulfide: synaptic modulation, neuroprotection, and smooth muscle relaxation. *Antioxid. Redox Signal, 7*, 795-803.

Kraus D.; Wittenberg, J.; Lu, J. and Peisach, J. (1990). Hemoglobins of the Lucina pectinata/bacteria symbiosis II, J. *Biol. Chem., 265,* 16054-16059.

L.F. Hu, P.T. Wong, P.K. Moore, J.S. Bian Hydrogen sulfide attenuates lipopolysaccharide-induced inflammation by inhibition of p38 mitogen-activated protein kinase in microglia J. Neurochem., 100 (2007), p. 1121.

Lawrence, N. S.; Jiang, L.; Jones, T. and Compton, R. (2003). A thin-layer amperometric sensor for hydrogen sulfide: the use of microelectrodes to achieve a membrane-independent response for Clark-type sensors. *Anal. Chem.*, *75*, 2499-2503.

Lawrence, N.; Deo, R. and Wang, J. (2004). Electrochemical determination of hydrogen sulfide at carbon nanotube modified electrodes. *Anal. Chim. Acta*, *517,* 131-137.

Lee, J. M.; Moon, B. U.; Shim, C. H.; Kim, B. C.; Lee, M. B.; Lee, D. D. and Lee, J. H. (2005). H_2S microgas sensor fabricated by thermal oxidation of Cu/Sn double layer. *Sens. Actuators B*, *108*, 84-88.

Lee, M., Schwab, C., Yu, S., McGeer, E., McGeer, P.L., 2009. Astrocytes produce the antiinflammatory and neuroprotective agent hydrogen sulfide. Neurobiol. Aging, Oct;30(10):1523-1534.

Li, G.; Zhub, J.; Zhua, D. and Fan, C. (2000). A reagentless nitric oxide biosensor based on hemoglobin–DNA films. *Anal. Chim. Acta*, *423*, 95-100.

Li, Z. & Hu, N. (2003). Direct electrochemistry of heme proteins in their layer-by-layer films with clay nanoparticles. *J. Electroanal. Chem.*, *558*, 155-165.

Liu, H.; Tian, Z.; Lu, Z.; Zhang, Z.; Zhang, M. and Pang, D. (2004). Direct electrochemistry and electro-catalysis of heme-proteins entrapped in agarose hydrogel films, *Biosensens. Bioelectron.*, *20*, 294–304.

M.A. Garcia-Bereguiain, A.K. Samhan-Arias, F.J. Martin-Romero, C. Gutierrez-Merino Hydrogen sulfide raises cytosolic calcium in neurons through activation of L-type Ca2+ channels Antioxid. Redox Signal., 10 (2008), p. 31.

Ma, F. and Lennox, R. B. (2000). Potential-Assisted Deposition of Alkanethiols on Au: Controlled Preparation of Single- and Mixed-Component SAMs. *Langmuir*, *16*, 6188-6190.

Manorama, S.; Devi, G. S. and Rao, V. J. (1994). Hydrogen sulfide sensor based on tin oxide deposited by spray pyrolysis and microwave plasma chemical vapor deposition. *Appl. Phys. Lett.*, *64,* 3163-3165.

Matsunaga, M.; Nakanishi, T.; Asahi, T. and Osaka, T. (2007). Effect of surface coverage of gold (111) electrode with cysteine on the chiral discrimination of DOPA. *Chirality*, *19*, 295-299.

Mehrvar, M. & Abdi, M. (2004). Recent developments, characteristics, and potential applications of electrochemical biosensors. *Anal. Sci.*, *20*, 1113-1126.

Milan, F.; Augustynskia, J.; Indiani, C.; Smulevich, G.; Antalíkc, M.; Bánó, M.; Sedlák, E.; Glascocke, M. C. and Dawson, J. H. (2004). The heme iron coordination of unfolded ferric and ferrous cytochrome c in neutral and acidic urea solutions. Spectroscopic and electrochemical studies. *Biochim. Biophys. Acta*, *1703*, 31-41.

Mirabella, F. M. Jr. (1993). Practical Spectroscopy Series; Internal reflection spectroscopy: Theory and applications, *Marcel Dekker, Inc*. pp 17-52.

Nesbitt, H.W.; Legrand, D.; Bancroft, G.M. (2000). *Physics and Chemistry of Minerals*, *27*, 357-366.

Nicholls, P.; Kim, J.K. (1982). Sulphide as an inhibitor and electron donor for the cytochrome c oxidase system. *Can. J. Biochem*. *60*, 613-23.

Niranjan, R.S.; Chaudhary, V.A.; Mulla, I.S.; Vijayamohanan, K. (2002). A novel hydrogen sulfide room temperature sensor based on copper nanocluster functionalized tin oxide thin films, *Sens. Actuators B*, *85*, 26-32.

Norio Miura, Yongtie Yan, Geyu Lu, Noboru Yamazo, Sensing characteristics and mechanisms of hydrogen sulfide sensor using stabilized zirconia and oxide sensing electrode, Sensors and Actuators B: Chemical Volume 34, Issues 1–3, August 1996, Pages 367–372.

Nuzzo, R.G.; Zegarski, B. R.; Dubois L. H. (1987). Fundamental studies of the chemisorption of organosulfur compounds on gold(111). Implications for molecular self-assembly on gold surfaces. *J. Am. Chem. Soc., 109*, 733–740.

Pandey, S. K.; Kim, K.; Tang, K. (2012). A review of sensor-based methods for monitoring hydrogen sulfide. *Trends Anal. Chem.*, *32*, 87-99.

Patil, L. A. and Patil, D. R. (2006). Heterocontact type CuO-modified SnO_2 sensor for the detection of a ppm level H_2S gas at room temperature. *Sens. Actuators B*,*120*, 316-323.

Paulo, T.; Diogenes, I. and Abruña, H. D. (2011). Direct electrochemistry and electrocatalysis of myoglobin immobilized on L-cysteine self-assembled gold electrode, *Langmuir*, *27*, 2052-2057.

Pietri, R.; Lewis, A.; León, R.; Casabona, G.; Kiger, L; Yeh, S; Fernandez-Alberti, S.; Marden, M.; Cadilla, C and López-Garriga, J. (2009). Factors controlling the reactivity of hydrogen sulfide with hemeproteins, Biochemistry 48 (2009) 4881-4894.

Pietri, R.; Roman, E. and López-Garriga, J. (2011). Hydrogen sulfide and hemeproteins: knowledge and mysteries, *Antioxid. Redox Signal., 15*, 393–404.

Porter, M. D.; Bright, T. B.; Allara, D. L.; Chidsey, C.E.D. (1987). Spontaneously organized molecular assemblies. 4. Structural characterization of n-alkyl thiol monolayers on gold by optical ellipsometry, infrared spectroscopy, and electrochemistry. *J. Am. Chem. Soc.*, *109*, 3559-3568.

Qian, W.; Zhuang, J. H.; Wang, Y. H. and Huang, Z. X. (1998). The effect of magnesium ion on the electrochemistry of cytochrome c and cytochrome b5 at a gold electrode modified with cysteine. *J. Electroanal. Chem.*, *447*, 187-199.

Ratner, B. D. and Castner, D. G. (1997). Electron Spectroscopy for Chemical Analysis, in: J.C. Vickerman (Ed.), *Wiley*, New York, Ch. 3.

Rodríguez-Fernández, J.; Pereiro, R.; Sanz-Medel, A. (2002). Optical fiber sensor for hydrogen sulphide monitoring in mouth air. *Anal. Chim. Acta, 471*, 13-23.

Roth Mark (2007). Hydrogen sulfide and long life. http://www.fhcrc.org/en/news/center-news/2007/12/hydrogen-sulfide-and-long-life.html Fred Hutchinson Cancer Research Center (accessed Nov. 2011).

Runge, A. F. and Saavedra, S. (2003). Comparison of Microcontact-Printed and Solution-Adsorbed Cytochrome c Films on Indium Tin Oxide Electrodes. *Langmuir, 19*, 9418-9424.

S.W. Lee, Y.S. Hu, L.F. Hu, Q. Lu, G.S. Dawe, P.K. Moore, P.T. Wong, J.S. Bian Hydrogen sulphide regulates calcium homeostasis in microglial cells Glia, 54 (2006), p. 116.

Sánchez, G. And Cabrera, C. (2007). Vertical attachment of DNA–CNT hybrids on gold. *J. Electroanal. Chem.*, *606*, 47–54.

Scheller, F. W.; Bistolas, N.; Liu, S.; Jänchen, M.; Katterl, M. and Wollenberger, U. (2005). Thirty years of haemoglobin electrochemistry. *Adv. Colloid Interface Sci.*, *116*, 111-120.

Shaojun, D.; Zhu, Y.; Cheng, G. (2002). Structural electrochemical study of hemoglobin by in situ circular dichroism thin layer spectroelectrochemistry. *Biophys. Chem.*, *97*, 129-138.

Shen, L.; R. Huang, R.; N. Hu, N. (2002). Myoglobin in polyacrylamide hydrogel films: direct electrochemistry and electrochemical catalysis, *Talanta*, 56, 1131–1139.

Shervedani, R. K.; Mehrjardi, A. H.; Zamiri, N. (2006). A novel method for glucose determination based on electrochemical impedance spectroscopy using glucose oxidase self-assembled biosensor. *Bioelectrochem.*, *69*, 201-208.

Shibuya, N.; Tanaka, M.; Yoshida, M.; Ogasawara, Y.; Togawa, T.; Ishii, K. and Kimura, H. (2009). 3-Mercaptopyruvate sulfurtransferase produces hydrogen sulfide and bound sulfane sulfur in the brain. *Antioxid. Redox Signal.*, *11*, 703-714.

Shirsat, M.; Bangar, M. A.; Deshusses, M.; Myung, N. and Mulchandani, A. (2009). Polyaniline nanowires-gold nanoparticles hybrid network based chemiresistive hydrogen sulfide sensor. *Appl. Phys. Lett.*, *94*, 083502-1–083502-3.

Stipanuk, M. H. and Beck, P. W. (1982). Characterization of the enzymic capacity for cysteine desulphhydration in liver and kidney of the rat. *Biochem. J.*, *206*, 267-277.

Strianese, M.; De Martino, F.; Pellecchia, C.; Ruggiero, G. and D'Auria, S. (2011). Myoglobin as a New Fluorescence Probe to Sense H_2S. *Protein Pept. Lett.*, *18*, 282-286.

Sulkowski, E. (1989). The saga of IMAC and MIT. *Bioessays*, *10*, 170-175.

Sun, H. & Hu, N. (2004). Voltammetric studies of hemoglobin-coated polystyrene latex bead films on pyrolytic graphite electrodes. *Biophys. Chem.*, *110*, 297–308.

Sun, Q; Collins, R; Huang, S; Holmberg-Schiavone, L; Anand, GS; Tan, C. H.; van-den-Berg, S; Deng, L. W.; Moore, P. K.; Karlberg, T and Sivaraman, J. (2009). Structural basis for the inhibition mechanism of human cystathionine gamma-lyase, an enzyme responsible for the production of H(2)S. *J Biol Chem.*, *30*, 3076-3085.

Swaroop, M.; Bradley, K.; Ohura, T.; Tahara, T.; Roper, M.D.; Rosenberg, L. E. and Kraus, J. P. (1992). Rat cystathionine beta-synthase. Gene organization and alternative splicing. *J. Biol. Chem.*, *267*, 11455-11461.

Tangerman, A. (2009). Measurement and biological significance of the volatile sulfur compounds hydrogen sulfide, methanethiol and dimethyl sulfide in various biological matrices, *J. Chromatogr. B*, *877*, 3366-3377.

Ubuka, T.; Abe, T.; Kajikawa, R. and Morino, K. (2001). Determination of hydrogen sulfide and acid-labile sulfur in animal tissues by gas chromatography and ion chromatography, *J. Chromatogr. B*, *757*, 31-37.

Vladka Gaberc-Porekar, Viktor Menart, Perspectives of immobilized-metal affinity chromatography, Journal of Biochemical and Biophysical Methods, Volume 49, Issues 1–3, 30 October 2001, Pages 335-360.

Wallace, K.J.; Cordero, S.R.; Tan, C.P.; Lynch, V.M.; Anslyn, E.V. (2007). A colorimetric response to hydrogen sulfide, *Sens. Actuators B, 120*, 362-367.

Warenycia, M. W.; Goodwin, L. R.; Benishin, C. G.; Reiffenstein, R. J.; Francom, D. M.; Taylor, J. D. and Dieken, F. P. (1989). Acute hydrogen sulfide poisoning. Demonstration of selective uptake of sulfide by the brainstem by measurement of brain sulfide levels. *Biochem. Pharmacol.*, *38*, 973-981.

Watts, J. F.; Wolstenholme, J. (2003). An Introduction to Surface analysis by XPS and AES, 2nd ed.; *Wiley*, England.

Whelan, C.M.; Smyth, M.R.; Barnes, C.J. (1999). HREELS, XPS, and Electrochemical Study of Benzenethiol Adsorption on Au(111). *Langmuir*, *15*, 116-126.

Whiteman, M.; Armstrong, J.S.; Chu, S. H.; Jia-Ling, S.; Wong, B.; Cheung, N. S.; Halliwell, B. and Moore, P. K. (2004). The novel neuromodulator hydrogen sulfide: an endogenous peroxynitrite 'scavenger'?. *Journal of Neurochemistry*, *90*, 765–768.

Whiteman, M.; Le Trionnaire, S.; Chopra, M.; Fox, B.; Whatmore, J. (2011). Emerging role of hydrogen sulfide in health and disease: critical appraisal of biomarkers and pharmacological tools. *Clin. Sci.*, *121*, 459-488.

Wolfbeis, O.S.; Trettnak, W. (1987). Fluorescence quenching of acridinium and 6-methoxyquinolinium ions by Pb^{2+}, Hg^{2+}, Cu^{2+}, Ag^{+} and hydrogen sulphide, *Spectrochim. Acta, Part A*, *43*, 405-408.

Xu, H.; Wu, J.; Chen, C; Zhang, L. and Yang, K. (2010). Detecting hydrogen sulfide by using transparent polymer with embedded CdSe/CdS quantum dots. *Sens. Actuators B*, *143*, 535-538.

Xu, H.; Wu, J.; Chen, C.; Zhang, L.; Ling, K. (2010). Detecting Hydrogen Sulfide by Using Transparent Polymer with Embedded CdSe/CdS Quantum Dots, *Sens. Actuators B*, *143*, 535-538.

Yanez-Sedeno, P. & Pingarron, J. M. (2005). Surface modification of amine-functionalized graphite for preparation of cobalt hexacyanoferrate (CoHCF)-modified electrode: an amperometric sensor for determination of butylated hydroxyanisole (BHA). *Anal. Bioanal. Chem.*, *382*, 884-886.

Yang, W.; Li, Y.; Bai, Y. and Sun, C. (2006). *Sens. Actuators B*, *115*,42.

Yang, Y. W. and Fan, L. J. (2002). High Resolution XPS study of decanethiol on Au (111): single sulfur-gold bonding interaction, *Langmuir*, *18*, 1157-1164.

Zen, J. M.; Kumar, A. S. and Chen, J. C. (2001). Electrocatalytic Oxidation and Sensitive Detection of Cysteine on a Lead Ruthenate Pyrochlore Modified Electrode. *Anal. Chem.*, *73*, 1169-1175.

Zhang, J. and Oyama, M. (2005). Gold nanoparticle-attached ITO as a biocompatible matrix for myoglobin immobilization: direct electrochemistry and catalysis to hydrogen peroxide. *J. Electroanal. Chem.*, *577*, 273-279.

Zhang, J.; Christensen, H. E. M.; Ooi, B. L. and Ulstrup, J. (2004). In situ STM Imaging and Direct Electrochemistry of *Pyrococcus furiosus* Ferredoxin Assembled on Thiolate-Modified Au(111) Surfaces. *Langmuir*, *20*, 10200-10207.

Zhang, S.; Wright, G. and Yang, Y. (2000). Materials and techniques for electrochemical biosensor design and construction. *Biosensors & Bioelectronics, 15*, 273-282.

Zhang, W. & Li, G. (2004). Third-generation biosensors based on the direct electron transfer of proteins. *Anal. Sci.*, *20*, 603-609.

Zhang, W. and Li, G. (2004). Third-Generation Biosensors Based on the Direct Electron Transfer of Proteins. *Anal. Sci., 20*, 603-609.

Zhao, W.; Zhang, J.; Lu, Y. and Wang, R. (2001). The vasorelaxant effect of H_2S as a novel endogenous gaseous K(ATP) channel opener. *EMBO J.*, *20*, 6008-6016.

Zhao, G. C.; Zhang, L.; Wei, Q. W. and Yang, Z. S. (2003). Myoglobin on multi-walled carbon nanotubes modified electrode: direct electrochemistry and electro-catalysis, *Electrochem. Commun.*, *5*, 825–829.

Zhao, G.; Xu, J.; Chen, H. (2006). Interfacing myoglobin to graphite electrode with an electrodeposited nanoporous ZnO film, *Anal. Biochem.*, *350*,145-150.